UNIVERSIDADE FEDERAL DO PARANÁ

VELEDA ASTARTE PAIVA MULLER

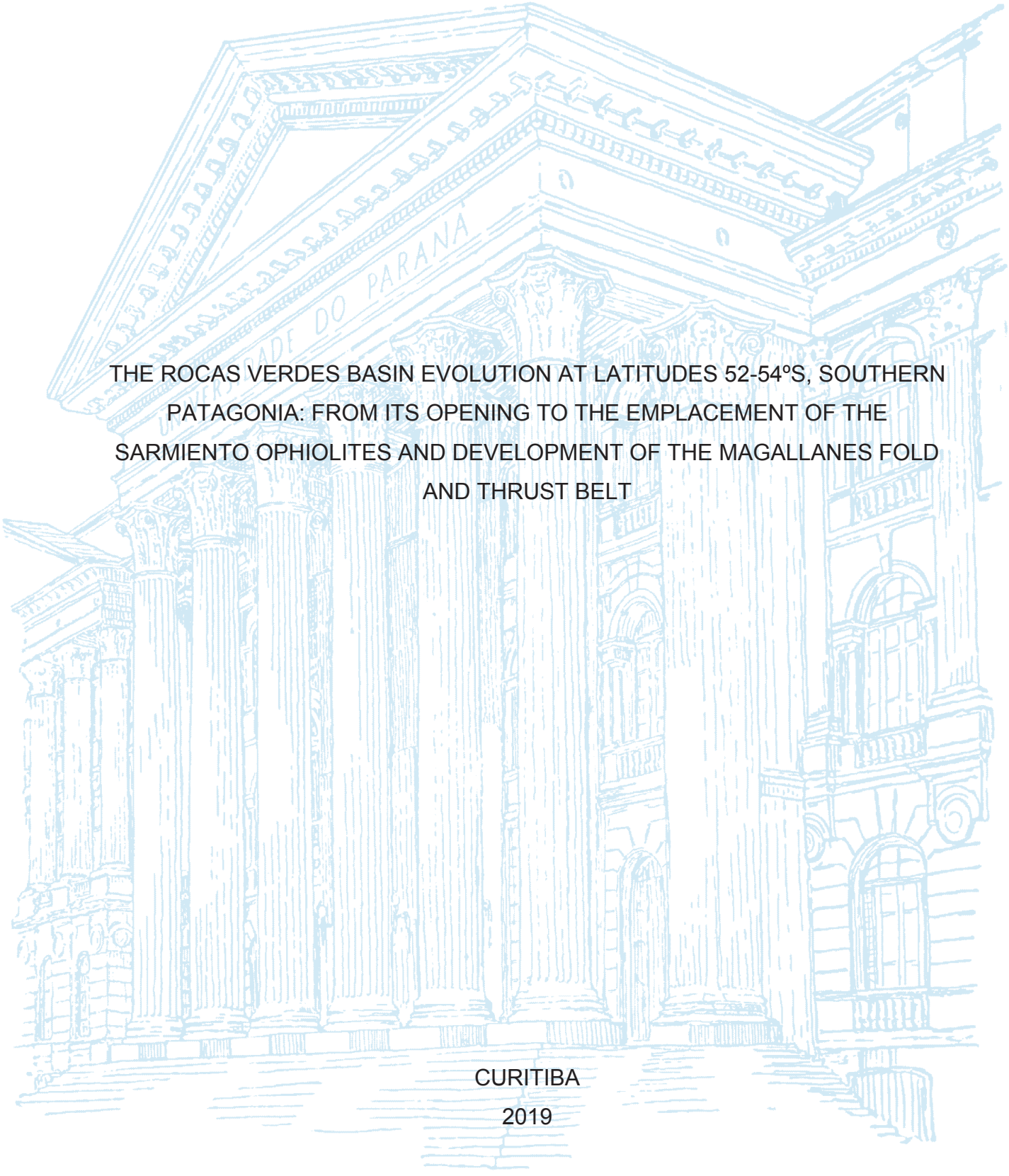

THE ROCAS VERDES BASIN EVOLUTION AT LATITUDES 52-54ºS, SOUTHERN PATAGONIA: FROM ITS OPENING TO THE EMPLACEMENT OF THE SARMIENTO OPHIOLITES AND DEVELOPMENT OF THE MAGALLANES FOLD AND THRUST BELT

CURITIBA

2019

VELEDA ASTARTE PAIVA MULLER

THE ROCAS VERDES BASIN EVOLUTION AT LATITUDES 52-54ºS, SOUTHERN PATAGONIA: FROM ITS OPENING TO THE EMPLACEMENT OF THE SARMIENTO OPHIOLITES AND DEVELOPMENT OF THE MAGALLANES FOLD AND THRUST BELT

Dissertação de Mestrado apresentada como requisito à obtenção do título de Mestre, Programa de Pós-Graduação em Geologia, Área de Concentração Geologia Exploratória, Linha de Pesquisa Evolução Crustal, Setor de Ciências da Terra, Universidade Federal do Paraná.

Orientador: Prof. Dr. Leonardo Fadel Cury
Coorientador: Prof. Dr. Mauricio Calderón

CURITIBA

2019

Catalogação na Fonte: Sistema de Bibliotecas, UFPR
Biblioteca de Ciência e Tecnologia

M958r Muller, Veleda Astarte Paiva
The rocas verdes basin evolution at latitudes 52-54°S, southern patagonia: from its opening to the emplacement of the sarmiento ophiolites and development of the magallanes fold and thrust belt [recurso eletrônico] / Veleda Astarte Paiva Muller – Curitiba, 2019

Dissertação - Universidade Federal do Paraná, Setor de Ciências da Terra, Programa de Pós-Graduação em Geologia,
Orientador: Prof. Dr. Leonardo Fadel Cury
Coorientador: Prof. Dr. Mauricio Calderón

1. Bacias (Geologia). 2. Bacias - Andes Patagônicos. 3. Ofiolito (rocha). I. Universidade Federal do Paraná. II. Cury, Leonardo Fadel. III. Calderón, Mauricio. IV. Título.

CDD: 551.87

Bibliotecária: Roseny Rivelini Morciani CRB-9/1585

MINISTÉRIO DA EDUCAÇÃO
SETOR SETOR DE CIENCIAS DA TERRA
UNIVERSIDADE FEDERAL DO PARANÁ
PRÓ-REITORIA DE PESQUISA E PÓS-GRADUAÇÃO
PROGRAMA DE PÓS-GRADUAÇÃO GEOLOGIA - 40001016028P5

TERMO DE APROVAÇÃO

Os membros da Banca Examinadora designada pelo Colegiado do Programa de Pós-Graduação em GEOLOGIA da Universidade Federal do Paraná foram convocados para realizar a arguição da dissertação de Mestrado de **VELEDA ASTARTE PAIVA MÜLLER** intitulada: **The Rocas Verdes Basin evolution at latitudes 52-54°S, Southern Patagonia: from its opening to the accretionary emplacement of the Sarmiento ophiolites and hinternland development of the Magallanes fold and thrust belt**, após terem inquirido a aluna e realizado a avaliação do trabalho, são de parecer pela sua APROVAÇÃO no rito de defesa.

A outorga do título de mestre está sujeita à homologação pelo colegiado, ao atendimento de todas as indicações e correções solicitadas pela banca e ao pleno atendimento das demandas regimentais do Programa de Pós-Graduação.

CURITIBA, 22 de Abril de 2019.

LEONARDO FADEL CURY
Presidente da Banca Examinadora (UFPR)

MAURICIO CALDERON NETTLE
Coorientador - Avaliador Interno (UNAB)

OSSAMA MOHAMED MILAD HARARA
Avaliador Externo (UFPR)

MIGUEL ANGELO STIPP BASEI
Avaliador Externo (USP)

Ministério da Educação
UNIVERSIDADE FEDERAL DO PARANÁ
Setor de Ciências da Terra
Programa de Pós-Graduação em Geologia

D E C L A R A Ç Ã O

Declaramos para os devidos fins que **Veleda Astarte Paiva Muller** realizou sua defesa de dissertação intitulada "*The Rocas Verdes Basin evolution at latitudes 52-54ºS, Southern Patagonia: from its opening to the accretionary emplacement of the Sarmiento ophiolites and hinternland development of the Magallanes fold and thrust belt*" em 22 de abril de 2019, no Programa de Pós-Graduação em Geologia da Universidade Federal do Paraná, área Geologia Exploratória, nível Mestrado, e que por sugestão da banca examinadora, o título foi alterado para "*The Rocas Verdes Basin evolution at latitudes 52-54ºS, Southern Patagonia: from its opening to the emplacement of the Sarmiento ophiolites and development of the Magallanes fold and thrust belt".*

Curitiba, 03 de setembro de 2019

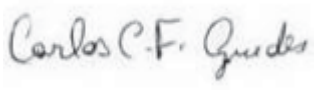

Carlos Conforti Ferreira Guedes
Coordenador do Programa
Pós-Graduação em Geologia

Aos amantes da ciência que a praticam por filosofia e pela busca incansável por entender o funcionamento da natureza. Também dedico aos exploradores do Planeta Terra que não se limitam por seus medos nem pelas intempéries do ambiente, se motivam pela curiosidade e pela paixão por mergulhar no desconhecido.

ACKNOWLEDGMENTS

This work was supported by the Fondecyt research project nº 1161818 Projeto “Tectonic evolution of Middle Jurassic to Early Cretaceous oceanic basins related to the drift of Antarctic Peninsula away from South America and generation of Chilean ophiolitic complexes” in Chile, and by LAMIR/UFPR/PETROBRAS research project n. 2016/00141-1 “Projeto Microbial: geoquímica de carbonatos microbiais continentais associados a precipitação de argilominerais” in Brazil.

I acknowledge the geologists Mauricio Calderón, Julie Fosdick, Andrea Goddard, Cristobal Ramírez de Arellano, Matías Ghiglione, Fernanda Torres and Diego Rojo who were in the field work and helped me in many moments with the collection of samples, measurements, explanations, and also reflections about nature, life and our mission as researchers. Special thanks to the Capitan Hugo Cárdenas and his crew of the Marypaz II, who made possible the campaign through the Patagonian fjords on October, 2017.

My main acknowledgements are to Prof. Leonardo Cury and Prof. Mauricio Calderón who advise me with excited discussions and revisions of the work, they gave me the opportunity of going to Patagonia twice, and provide me good moments of friendship in field, laboratory and also during leisure moments matching ideas about the immensity of the planet Earth and the universe. I am also grateful to Prof. Anelize Bahniuk, Eleonora Vasconcellos and Cadu Barros for additional assistantship during the work. Thanks to all LAMIR team, by the technical, financial and intellectual attendance to this research.

Finally, I acknowledge my family and all my friends, specially Ana Cecília Sowinski, Fernanda Avelar, Isis Armstrong Dias, Bruno Titon, Daniel Patias, Herick Daufenbach, and Victor Dorneles, who ever accompanied my progress during the work and stresses that I passed with comprehension and moments for coffee and laughing. My friends in Chile Fernanda Torres., Carolina Valenzuela and Tomaz Reyes also were the best people in the world receiving me as a long time friend in Chile.

RESUMO

A Bacia de Rochas Verdes (BRV) foi uma bacia marginal da margem sudoeste do Supercontinente Gondwana, sua abertura é associada à quebra inicial do Supercontinente Gondwana durante o Jurassico Superior ao Cretáceo Inferior. A bacia foi preenchida por rochas vulcânicas félsicas durante a fase rifte, e desenvolveu espalhamento de assoalho oceânico com magmatismo bimodal e sedimentação marinha hemipelágica na regiãode *backarc* da margem convergente inicial do Gondwana Oeste. No Cretáceo Superior a BRV começou a se fechar e as unidades empilhadas formam o Cinturão de dobras e cavalgamentos de Magalhães, nos Andes Patagônicos, e o *front* dos cavalgamentos migrou em direção ao foreland para leste durante o Cenozoico. A história da BRV é correlativa com a formação do arco magmático dos Andes Patagônicos, o que é atestado pelo arco cálcio-alcalino desenvolvido do Jurássico Superior ao Cretáceo Inferior na microplaca separada à oeste da margem cratônica Sul Americana, que evouiu para leste até o Cenozoico. Este trabalho descreve as principais unidades dos Andes Patagônicos ocorrendo na região dos Senos Otway e Skyring (52°-54°S), a partir de observações estratigráficas e estruturais, análises petrográficas e geoquímicas para restringir idades de abertura e fechamento da BRV, e as condições de fechamento da bacia envolvendo a colocação dos ofiolitos. As análises U-Pb em zircão nos metatufos riolíticos da fase rifte restringem a abertura da BRV ao Oxfordiano. As análises geoquímicas de rocha total mostram diferentes assinaturas das rochas máficas descritas anteriormente como ofiolitos, implicando em diferentes gêneses para os metabasaltos da região. Análises metamórficas usando pseudosseções de pressão e temperatura e dados de química mineral revelam metamorfismo fácies xisto azul a fácies xisto verde em rochas metavulcânicas e metassedimentares, sugerindo a formação de uma cunha acrescionária na zona de subducção responsável pela colocação dos ofiolitos. Os indicadores cinemáticos mostram vergência para nordeste das zonas de cavalgamento levando o *front* do cinturão de dobras e cavalgamentos, e idades U-Pb em zircão de um diorito intrusive às unidades deformadas da BRV restringe o limite superior da deformação para o Campaniano.

Palavras-chave: Bacia de Rochas Verdes. Andes Patagônicos. Ofiolito. Cinturão de dobras e cavalgamentos.

ABSTRACT

The Rocas Verdes Basin (RVB) was a marginal basin of the Southwesternmost margin of Gondwana, its opening is associated to the early break-up of Gondwana during Late Jurassic to Early Cretaceous. The basin was filled by felsic volcanic rocks during the rifting phase, and developed seafloor spreading, with bimodal magmatism and hemipelagic marine sedimentation, in the backarc region of the early convergent margin of Western Gondwana. During the Late Cretaceous, the RVB starts to close and the stacked units form the hinterland of the Magallanes fold and thrust belt, in the Patagonian Andes, and the thrust front migrates to the foreland in the east during Cenozoic. The RVB history was correlative with the formation of the Patagonian Andes, testified by the calc-alkaline magmatic arc developed in the Late Jurassic-Early Cretaceous in the drifted microplate to the west of the South American cratonic margin, which evolved to the east until Cenozoic times. This work describes the main units of the Patagonian Andes occurring in the region of Otway and Skyring Sounds (52°-54°S) from field stratigraphic and structural observations, to petrographic and geochemical analysis, to constrain ages of opening and closure of RVB, and the pressure-temperature conditions of closure involving ophiolite emplacement. The zircon U-Pb analysis in the rhyolitic metatuffs of the rift phase constrains the opening of RVB to the Oxfordian. The geochemical whole rock analyses show different signatures to the mafic rocks described before as ophiolites, implying different genesis for metabasalts of the region. Metamorphic analyses using pressure-temperature pseudosections and mineral chemistry data reveal blueschist to greenschist metamorphism in felsic volcanic rocks and metasedimentary rocks, suggesting the formation of an accretionary wedge in the subduction zone responsible by the emplacement of the ophiolites. The structural kinematic indicators point out to northeast vergence of the thrust zones leading the fold and thrust belt deformation, and zircon U-Pb ages of a diorite intrusive to the deformed RVB units constrain the upper age limit to the deformation at Campanian.

Key-words**:** Rocas Verdes Basin. Patagonian Andes. Ophiolite. Fold and Thrust Belt.

LIST OF FIGURES

Figures of the article: The Rocas Verdes basin closure and early tectonothermal evolution of the Magallanes fold thrust belt in southern Patagonian Andes (52-54ºS)

Figures of the Complementary Results:

LIST OF TABLES

Tables of the article: The Rocas Verdes basin closure and early tectonothermal evolution of the Magallanes fold thrust belt in southern Patagonian Andes (52-54ºS)

Tables of Complementary Results:

LIST OF MINERAL ABBREVIATIONS

Ab: albite
Am: amphibole
Act: actinolite
An: annite
Bio: biotite
Cbt: carbonate
Cp: clinopyroxene
Fe: carpholite
Chl/Ch: chlorite
Clay m.: clay minerals
Crd: cordierite
Ct: chlorithoid
Czoi: clinozoisite
Ep: epidote
Gt: garnet
Hm: hematite
Hb: hornblende
Ilm: ilmenite
Kao: kaolinite
Kf: alkali-feldspar
Lw: lawsonite
Lmt: laumontite
Mic: microcline
Ms: muscovite
Mt: magnetite
Omph: omphacite
Op: opaques
Pa: paragonite
Pheng: phengite
Pl: plagioclase
Pnt: pyrophanite
Pxmn: Pyroxmangite
Py: pyrite
Qz: quartz
Ru: rutile
Sps: spessartine
Stb: stilbite
St: stilpnomelane
Ta: Talc
TiBio: Ti-biotite
Tt: titanite = Sph: sphene
Tre: tremolite
Wm: white mica
Zoi: zoisite

SUMMARY

1 INTRODUCTION

In Southern Patagonia the Rocas Verdes Basin (RVB) developed as a rift marginal basin of the western South American platform during Late Jurassic to Early Cretaceous, when was filled by explosive and effusive felsic volcanic rocks, had the spreading of an oceanic floor by a mid-ocean ridge, and was capped by marine sedimentation (Dalziel, 1981; Stern and De Wit, 2003; Calderón et al., 2007a). At the same time, the magmatic arc starts to develop with calc-alkaline magmatism of the South Patagonian Batholith (SPB). In the Middle Cretaceous the RVB started to close and the oceanic crust was emplaced over the continental margin to the east, currently preserved as upper parts of ophiolitic complexes, the progression of the inversion of the basin during Late Cretaceous formed the Magallanes fold and thrust belt at the western South Amercian margin (Dalziel, 1981; Harambour, 2002; Calderón et al., 2007a; Fosdick et al., 2011; Calderón et al., 2012; Betka et al., 2015). This study is focused on the mechanisms of emplacement of the ophiolites, searching for vestiges of an accretionary wedge developed during subduction of the oceanic lithosphere below the magmatic arc of the Patagonian Andes, trying to estimate the depths of subduction by the metamorphic conditions recorded on mylonitic rocks, and understood how they were exhumed by the study of the deformational phases at the fold and thrust belt.

The geology near the Otway and Skyring sounds at Southern Patagonia (Fig. 1.1) reveals the current structuring of the Rocas Verdes Basin, where the bimodal magmatic rocks of the Sarmiento Ophiolitic Complex are juxtaposed to volcaniclastic rhyolitic rocks of Tobífera Fm. and sedimentary rocks of Zapata Fm. by eastward thrusts, they have zones of brittle-ductile deformation with protomylonites and low grade metamorphism, a zone of high-pressure and low temperature (14 kbar, 270°C) indicate a paleo-subduction environment. These stratigrahic units are regionally folded, and metasedimentary rocks of the Pre-Jurassic basement are also exposed juxtaposedly to the stacked units of the Rocas Verdes Basin. Some authors relate the juxtaposition of the RVB rocks with the Pre-Jurassic basement rocks to out-of-sequence thrust faults during the later phases of deformation in the fold and thrust belt, which may be responsible by the exhumation of the hinterland units (Fosdick et al., 2011; Betka et al., 2015). The Magallanes foreland basin developed to the east, firstly filled by Cretaceous deep marine sediments provenants from the RVB units,

the magmatic arc (SPB) and the Pre-Jurassic basement (Fildani and Hessler, 2005). Therefore, the sedimentary rocks in the foreland record the exhumation of the hinterland units, which were source of sediments, and it is associated to the transition of the RVB from backarc to retroarc in a convergent environment since Cenomanian (Fosdick et al., 2011).

Mineral and whole rock geochemical data of metamorphic rocks, coupled to the structural study of deformational phases and zircon U-Pb geochronology of RVB units and intrusive bodies, are tools used in this work to constrain the regional conditions and times of ophiolite emplacement and fold and thrust belt construction. Additional whole rock geochemical data of igneous rocks provided a secondary study about magmatic generation and opening of the basin, and a chemostratigraphic study of the units of RVB.

Figure 1.1: Geological map of Chilean Patagonia, the study area is in the square.

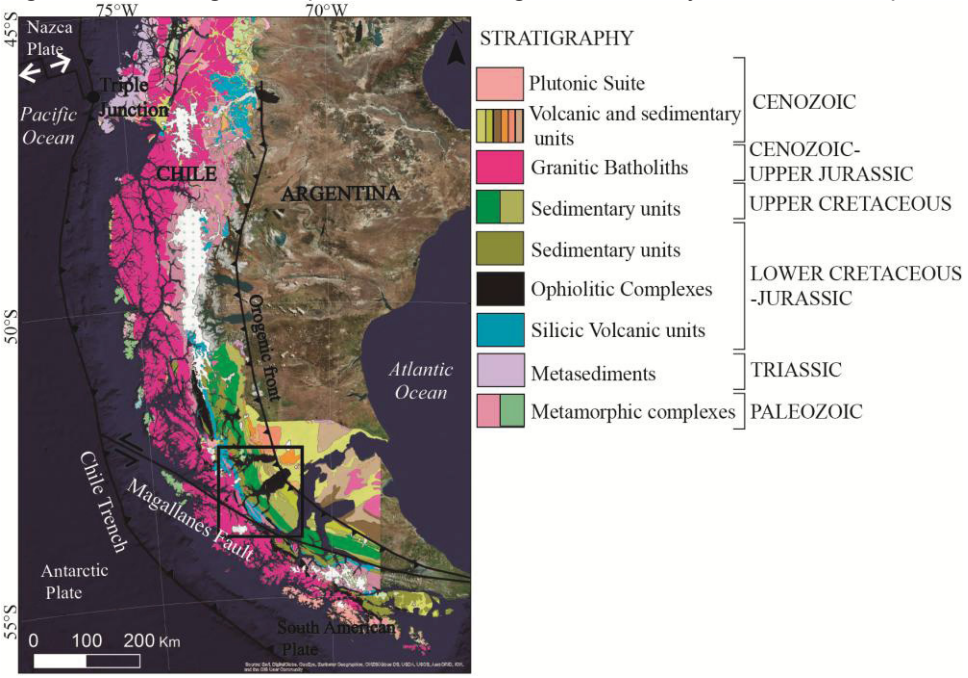

Source of Geological Map: SERNAGEOMIN (2003).

1.1 HYPOTHESIS

The central hypothesis is that metamorphic metatuffs of Tobífera Fm. and metapsamopelites of Zapata Fm. are remnants of the sole thrust of the subduction of the Sarmiento Ophiolitic Complex below the magmatic arc at the drifted continental microplate to the west, which were subducted at least 15 km and may have reached

33 km of depth, recording greenschist to blueschist facies metamorphism. One progressive compressional phase of non-coaxial deformation seems to have accommodated the deformation during the closure of the basin, forming thrusts verging to the east and the northeast. A late second phase of deformation associated to disjunctive foliations, verging to northeast and to the southwest, may have accounted for the exhumation of the belt and juxtaposition with the Pre-Jurassic basement. According to intrusive magmatic bodies, the hinterland development of the fold and thrust belt must have ended prior to Campanian.

1.2 AIMS

1.2.1 General Aim

The main goal of this work is understand the nature of SOC emplacement (accretionary or collisional) and its mechanisms by the temperature and pressure conditions of metamorphism and shear zones developed during the early tectonothermal phase of closure of the Rocas Verdes Basin. A major goal is contribute for the geochemical and geochronologic constraints from the RVB opening to the suture formation and Magallanes fold and thrust belt culmination.

1.2.2 Specific Aims

- Definition of shear zones: It is important to understand the stratigraphic distribution of the units in the fold and thrust belt, and to define the sole thrust and main detachment levels related to ophiolite emplacement and its kinematics.
- Rank deformational phases in the RVB cover and basement: It is important to explain the diachronous deformation in different structural levels during a progressive advancement of the orogenic front, and to understood the exhumation.
- Determine metamorphic P-T conditions: it is the main tool to estimate the depths of burial of the RVB units and correlate to tectonic settings of subduction or collision. Mineral chemistry by electron probe micro analyzer

(EPMA) will enable the construction of pressure-temperature pseudosections for rock samples and determine P-T conditions accurately.

- Identify maximum ages of sedimentation, crystallization and deformation: zircon U-Pb geochronology was used to constrain the maximum age of sedimentation in Zapata Fm. sedimentary fill of the RVB, the crystallization age of the metatuffs of Tobífera Fm. as the fill of the RVB during the rift phase, and the upper age limit of deformation by dating the late intrusions of the RVB units.
- Understand the tectonic environments by geochemical fingerprints: the whole rock geochemistry of rocks of SOC, Tobífera Fm. and Pre-Jurassic basement allow us to understand how the magmatic units evolved during the basin history, and are an important tool for stratigraphic correlations.

1.3 JUSTIFICATION

The study of ophiolitic complexes is important in many tectonic ways, from the origin of ancient oceans to orogenic constructions and continental suture zones. The Patagonian Ophiolites present an important context of transition from marginal to backarc basin opening, suprasubduction environment, and inversion by an initial subduction and lately a collision between ancient terranes of South American plate. This study provides a better comprehension about short-life basins in convergent environments that result in orogenic belts.

2 THEORETICAL BASIS

2.1 OPHIOLITE CONCEPTS AND ITS IMPORTANCE

Ophiolites are tectonic fragments of oceanic lithosphere found in orogenic zones (Coleman, 2014). With the consolidation of the theory of tectonic plates, during the 60´s and 70´s decades they started to be seen as important tectonic elements which provide information about generation and recycling of oceans. They record complete cycles from rifts to orogens that can be found in land, marking plate sutures (Dilek and Furnes, 2014).

The complete stratigraphy of ophiolites includes – from the basis to the top – ultramafic rocks from the superior depleted mantle; ultramafic and mafic rocks from the inferior crust originated by partial mantle melt; mafic rocks on sheeted dyke complexes; and a coverage of pillow lavas, pillow breccias and massive lavas, eventually intercalated with sedimentary and volcaniclastic layers (Anonymous, 1972). About their origin, they can be related or not to subduction, but for their emplacement over the continental crust, are always related to subduction in some instance. Their internal structure, geochemical fingerprint and emplacement mechanisms vary according to plume and trench proximity; nature, geometry and rate of opening of the ridge; composition, temperature and fertility of the mantle; and fluid availability (Dilek and Furnes, 2014).

Ophiolites related with subduction in their generation are called suprasubduction zone ophiolites (SSZ) (Fig. 2.1.1) (Dilek and Polat, 2008). They are always on the upper plate of subduction zones, and the oceanic crust is formed on tectonic settings of forearc, backarc or incipient arc (Dilek and Furnes, 2014). The Patagonian ophiolites are related to the proto-Pacific subduction zone of the Pacific oceanic plate below the South American continental Plate, since Jurassic times, which evolved to the current convergent margin of subduction of the Nazca and the Antarctic oceanic plates below the South American Plate. The seafloor spreading at the RVB occurred in a marginal basin that progressed to a backarc environment by extension in the continental plate by slab rollback (Dalziel, 1981; Stern and De Wit, 2003).

Figure 2.1.1: General development of upper plate basins with spreading centers, induced by slab rollback cycles, and the stratigraphy of the SSZ oceanic crust in that environment.

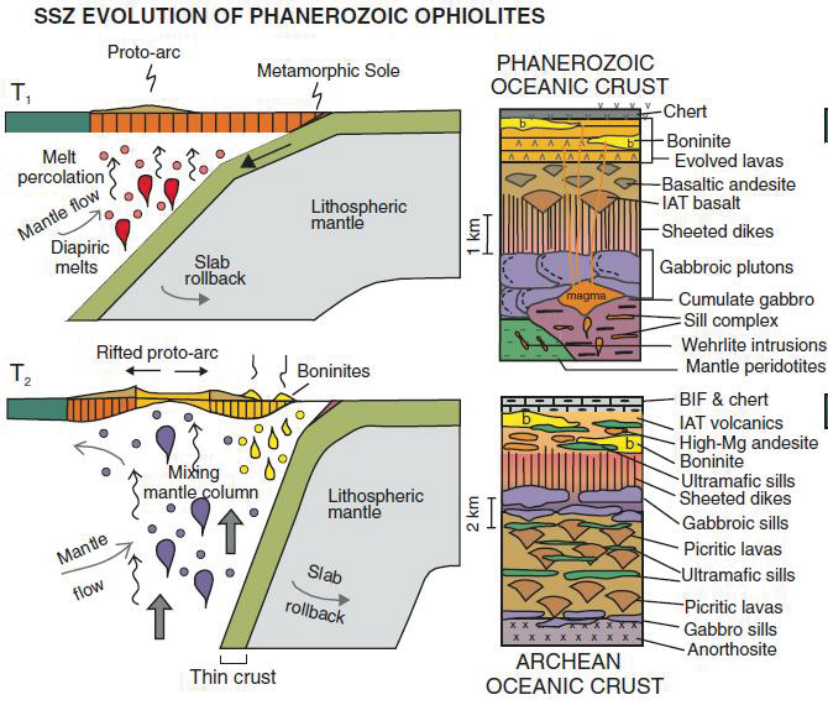

Source: Dilek and Polat (2008).

Backarc environments can evolve by slab rollback, a mechanism when the oceanic slab sinking down into the mantle retraits due to density contrast, the dip angle of subduction becomes higher, causing a collapse in the upper plate, that extends by normal faults, parallel to the convergent margin (Fig. 2.1.2) (Jolivet et al., 1999; Schellart and Lister, 2005). Other stresses on the upper plate, related to backarc extension, are strike slip faults oblique to the convergent margin, and collapse of the thickened crust (Jolivet et al., 1999; Schellart and Lister, 2005). Mantle flow in the wedge accelerates the extension and induces oceanic spreading at the backarc basin (Fig. 2.1.1) (Jolivet et al., 1999; Dilek and Polat, 2008). In this context, spreading centers can be trench-proximal or trench-distal, changing the grade of influence of subduction in the oceanic magmas generation (Dilek and Furnes, 2014). SSZ ophiolites in Patagonia are in trench-proximal setting (Dalziel, 1981; Calderón et al., 2007b; Stern and De Wit, 2003).

Figure 2.1.2: Backarc extension mechanisms,

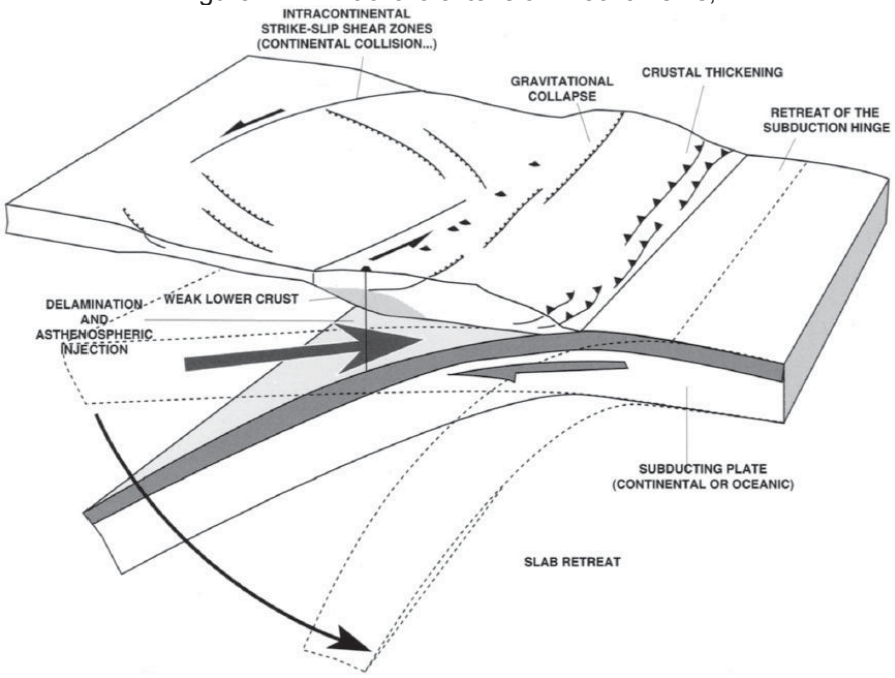

Source: Jolivet et al. (1999).

SSZ ophiolites magmatic and geochemical evolution is controlled by the nature of partial melting on the mantle wedge and the element flux generated by the dehydratation of the subducting slab (Dilek and Furnes, 2014). Their stratigraphy is detailed by Dilek and Furnes (2014), presented on figure 2.1.3. Geochemical fingerprints vary from mid-ocean ridge basalts (MORB) to island arc tholeits (IAT) and boninitic. The progressive partial melting of the mantle results in a source and derived magmas depleted in incompatible elements. The conservative elements as Nb, Ti, Y and heavy rare earth elements (HREEs) are largely unaffected, but during longer processes of mantle extraction, the source becomes depleted in these. At the same time, the oceanic subducting slab is dehydrated and carry oceanic sediments that are melted in depth, enriching the mantle wedge with light rare earth elements (LREEs) and other mobile elements as Cs, Pb, Ba, Th and U (Dilek and Furnes, 2014). A MORB signature is high-Ti e Fe, high HFSE (high-field-strength elements) and HREE distribution and depletion in LREEs. An IAT signature is low-Ti, low HFSE and HREE distribution, rather depletion in LREEs, high contents of Co, Ni and Cr (more primitive mantle). Boninitic magmas include high grade of partial melting in forearc zones, resulting in high Mg and low Ti, high depletion in HREEs, and enrichment in LREEs and incompatible elements (Dilek et al., 2007).

Figure 2.1.3: General stratigraphy of suprasubduction zone ophiolites: banded and folded harzburgite (ol+cpx) (a, b); layered cumulates of dunite (ol) and wehrlite (ol+cpx) (c); layered and folded gabbro (d); varitextured gabbro (e); gabbro cut by basaltic and felsic intrusions (f); sheeted dyke complex (g); volcanic breccias with a hyaloclastic matrix (h); pillow lava (i); massive andesitic lava flow (j); folded chert layers (k).

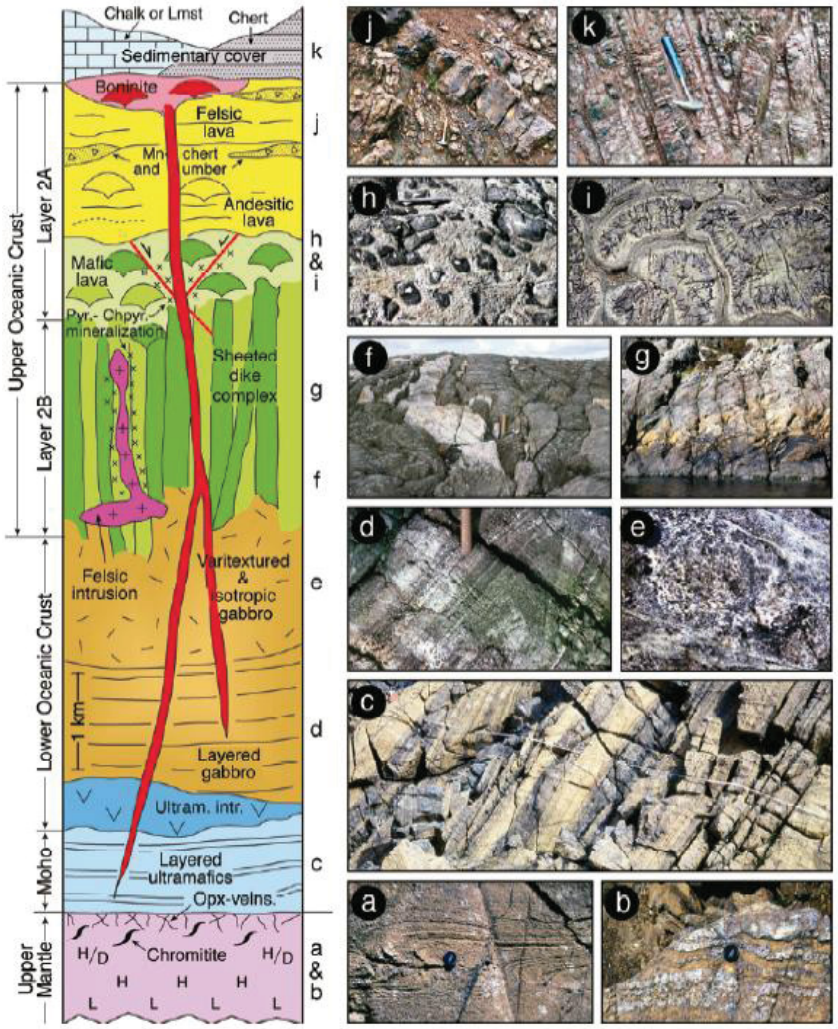

Source: Dilek and Furnes (2014).

The Patagonian ophiolites found in Rocas Verdes Basin are incomplete in stratigraphy, without mantelic ultramafic rocks, but are represented by a general sequence of gabbro, sheeted dykes and pillow lavas (Dalziel, 1981; Calderón et al., 2007b; Calderón et al., 2012). They were generated on the southwestern Gondwanaland, during Late Jurassic to Early Cretaceous seafloor spreading (Dalziel, 1981). Geochemical fingerprints show MORB affinity for these mafic rocks, but trace and REE patterns are also similar to IAT, showing subduction influence and SSZ setting of generation (Stern and De Wit, 2003; Calderón et al. 2007b). Interactions between mantelic magmas with the crust resulted in silicic volcanism in the transition from continental rifting to initial seafloor spreading (Calderón et al. 2007b).

Emplacement mechanisms are responsible for drive the oceanic lithosphere to continental environments, when the compression ratio is higher than extension ratio, and subduction are often the main driver. The factors that control emplacement are: age, thickness and thermal state of the oceanic lithosphere; geometry and size of plate boundaries, and type of interaction between plates (e.j. oceanic x continental) (Dilek and Furnes, 2014; Wakabayashi and Dilek, 2003). Oceanic lithosphere of subducting slabs are tectonically transferred to the upper plate by subduction-accretion, creating accretionary complexes, while oceanic lithosphere spreaded on upper plates are emplaced in continental margins by collisional mechanism, that often include trench-continent or continent-continent collision (Dilek et al., 2007; Dilek and Furnes, 2014). The emplacement of oceanic lithosphere often generate greenschist to blueschist facies metamorphism on the surroundings of the sole thrusts, the main detachment fault that drives ophiolites upon the continental margin (Dilek et al, 2007). The units that “receive” the ophiolites above are most affected by high pressure, low temperature metamorphism (Jolivet et al., 1999; Wakabayashi and Dilek, 2003).

2.2 REGIONAL GEOLOGY

The Rocas Verdes Basin is interpreted as a marginal basin created by rifting of Paleozoic basement complexes at Southern Patagonia, which originated explosive and effusive silicic magmatism of the Tobífera Formation and El Quemado Complex during Late Jurassic to Early Cretaceous (Dalziel, 1981; Pankhurst et al., 2000; Stern and De Wit, 2003; Calderón et al., 2007a; Calderón et al., 2007b; Calderón et al., 2012). The progressive opening of the basin during Late Jurassic-Early Cretaceous generated the seafloor spreading recorded on the ophiolitic complexes Sarmiento, to the north of the Magallanes Strait, and Capitán Aracena, Carlos III, and Tortuga to the south of Magallanes Strait around the Cordillera Darwin (Fig. 2.2.1). It was capped by shales, turbidites and cherts of the Zapata Formation, during Late Jurassic to Early Cretaceous (Fuenzalida and Covacevich, 1988; Fildani and Hessler, 2005; Calderón et al., 2007a).

Figure 2.2.1: Geological sketch map showing the ophiolitic complexes of Southernmost Patagonia and the main units of Rocas Verdes Basin: volcanic felsic Tobífera Fm. and sedimentary Zapata Fm. or their equivalents, besides the metamorphic complexes and the South Patagonian Batholith and main tectonic structures. Abbreviations: CM - Canal de las Montañas; CB - Canal Beagle; CD - Cordillera Darwin, EM - Estrecho de Magallanes; ICT - Isla Carlos III; ICA - Isla Capitán Aracena; IN - Isla Navarino; MFTF - Magallanes-Fagnano transform fault.

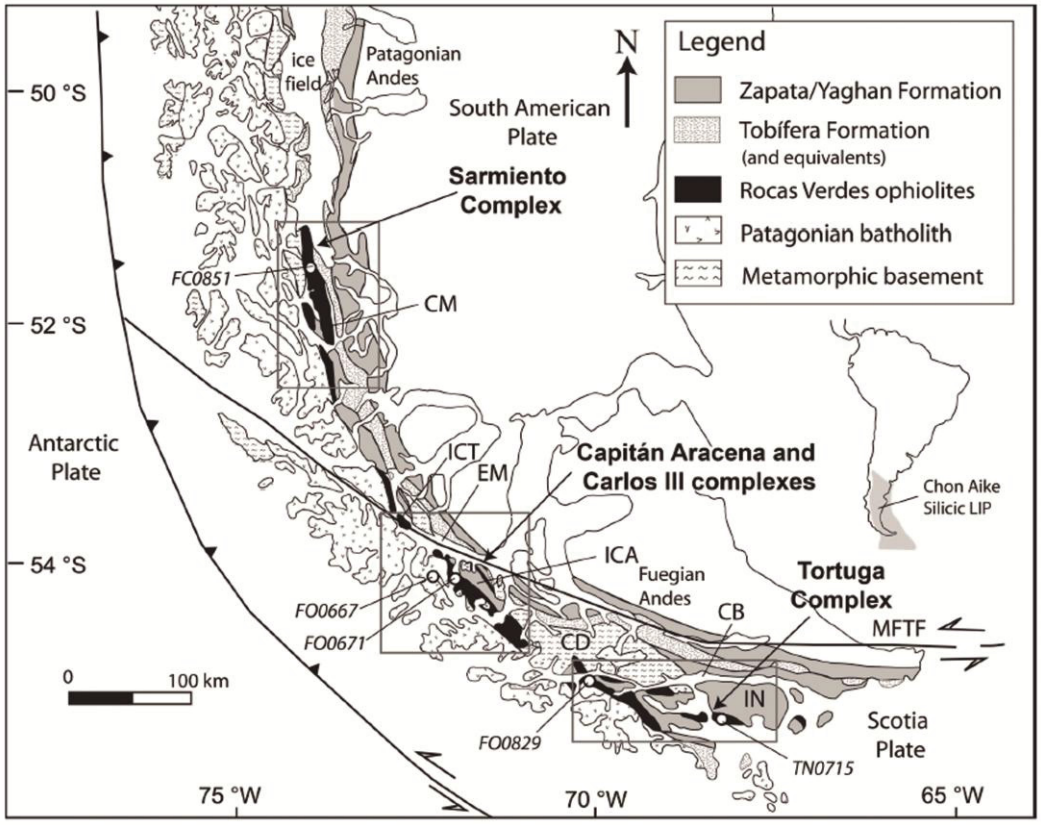

Source: Calderón et al. (2013).

The extensional regime of opening of RVB, as an initial marginal basin, was related to the separation of western Gondwana from the eastern Gondwana when the break-up between South America and Africa was incipient (Dalziel, 1981). The subduction of the Nazca Plate and Antarctic plate below the South American Plate seems to have started after 155 Ma, prior to the westwards migration of Antarctic Peninsula. The subduction resulted in magmatism of the South Patagonian Batholith, contemporaneous to the basin opening and changed the RVB tectonic context to a backarc basin (Hervé et al., 2007b). Subduction influenced the extension rates and slab roll-back can have induced backarc extension (Dalziel, 1981; Calderón et al., 2012).

The basement of RVB is different metamorphic complexes mainly constituted by low grade metasedimentary rocks and metabasites with detrital zircon ages from Mesoproterozoic to Late Triassic (Hervé et al., 2003b). To the study area the first phase of regional metamorphism is accredited to Late Permian (Hervé et al., 2003b),

but recent studies (Hervé et al., 2010; Klepeis et al., 2010; Betka et al., 2015) propose that the Andean orogeny has caused metamorphism and deformation during Cretaceous.

Plutonism in the South Patagonian Batholith resulted from the subduction of oceanic slabs below the South American plate at the western margin of Gondwana. Leucogranites to gabbros are coeval with the felsic volcanic rocks of Tobífera Fm. and the seafloor spreading of RVB during Late Jurassic and Early Cretaceous. Crustal signatures are found in both Late Jurassic SPB and Tobífera Fm., suggesting a common petrogenesis in the lower to middle crust (Calderón et al., 2007b; Hervé et al., 2007b). Subsequent magmatic episodes on SPB occurred during Cretaceous and Neogene, intruding the deformed units of the fold and thrust belt (Hervé et al., 2007b).

Felsic volcanic rocks of the Tobífera Formation and correlative units constitute the *Chon Aike* Large Igneous Province. Pankhurst et al. (2000) related the *Chon Aike* volcanism with the *Karoo-Ferrar* mantle plume magmatism and rifting during the break-up of Southern Gondwana, which migrated westwards from South Africa, Antarctica and Tasmania ancient territories to the proto-Pacific margin of Gondwana during Jurassic (Fig. 2.2.2).

Figure 2.2.2: Location and timing of the silicic volcanism in Chon Aike Large Igneous Province on Patagonia, and its relationship with Karoo magmatic Province and Ferrar magamatic Province. Abbreviations: EWM: Ellworth-Whitmore mountains; SG: South Georgia; FI: Falkland Islands. TI: Thurston Island; MBL: Marie Byrd Land.

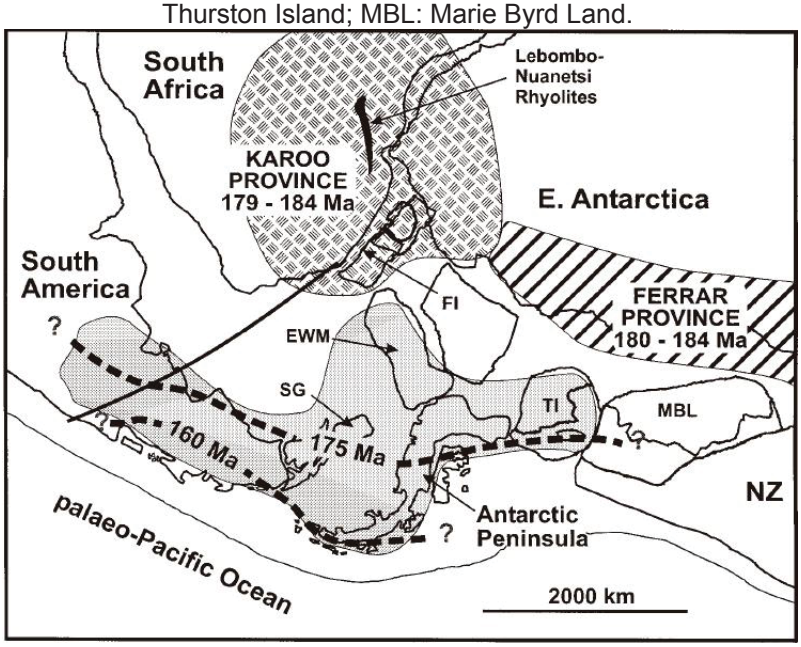

Source: Pankhurst et al. (2000).

Jurassic-Cretaceous rifting on Southwestern Gondwana was accompanied by bimodal oceanic magmatism forming the seafloor of RVB by mid ocean ridges-type spreading centers. Nowadays the SOC represent the remnants of oceanic lithosphere and have three main layers: (1) a mafic-felsic intrusive layer of granophyres and dykes of gabbro and plagiogranites; (2) a mafic-felsic extrusive and intrusive layer of pillow basalts, silicic tuffs, hyaloclastites and dykes of dacite an rhyolite; (3) a mafic extrusive layer of pillow basalts, pillow breccias, cherts and siltstones (Calderón et al., 2007a). Intrusive dacites and plagiogranites cross-cutting pillow basalts of SOC presented zircon ages of 150 Ma, reported as a maximum age for seafloor spreading (Calderón et al., 2007a). Figure 2.2.3 is a synthesis of marginal to backarc evolution of RVB during Mid Jurassic to Early Cretaceous suggested by Stern and De Wit (2003). Despite several modifications in this model in the latest years, it represents well the rifting phase related to Tobífera Fm. silicic magmatism and the general stratigraphy of Sarmiento Ophiolitic Complex, capped by sediments of Zapata Fm.

Figure 2.2.3: Marginal to backarc RVB evolution by rifting with silicic magmatism, oceanic spreading and sediment suplly.

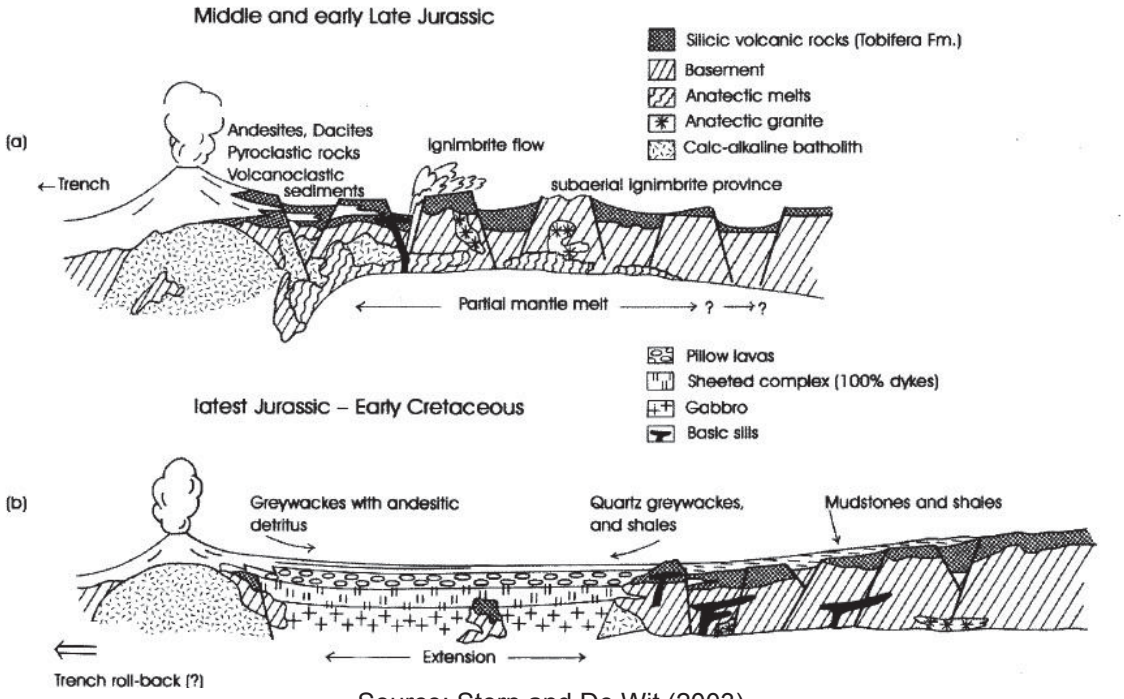

Source: Stern and De Wit (2003).

The Zapata Fm. is constituted essentially by shales deposited in a deep marine hemipelagic environment during Tithonian to Cenomanian (Fildani and

Hessler, 2005; Fosdick et al., 2011). Its upper part has sandstone and graywacke layers deposited by detritic flows triggered by tectonic activity when the RVB started to close (Fildani and Hessler, 2005). The source for sediments was Tobífera highs, the juvenile magmatic arc (SPB) and exhumed oceanic crust (COS) (Fildani and Hessler, 2005). Figure 2.2.4 presents the stratigraphic and tectonic evolution of RVB.

Fig. 2.2.4: Sythesis of RVB stratigraphic and tectonic evolution. Abbreviations: TFm – Tobífera Fm.; ZFm – Zapata Fm.; PBFm – Punta Barrosa Fm.; CTFm – Cerro Toro Fm; TPFM – Tres Pasos Fm.; DFm – Dorotea Fm.

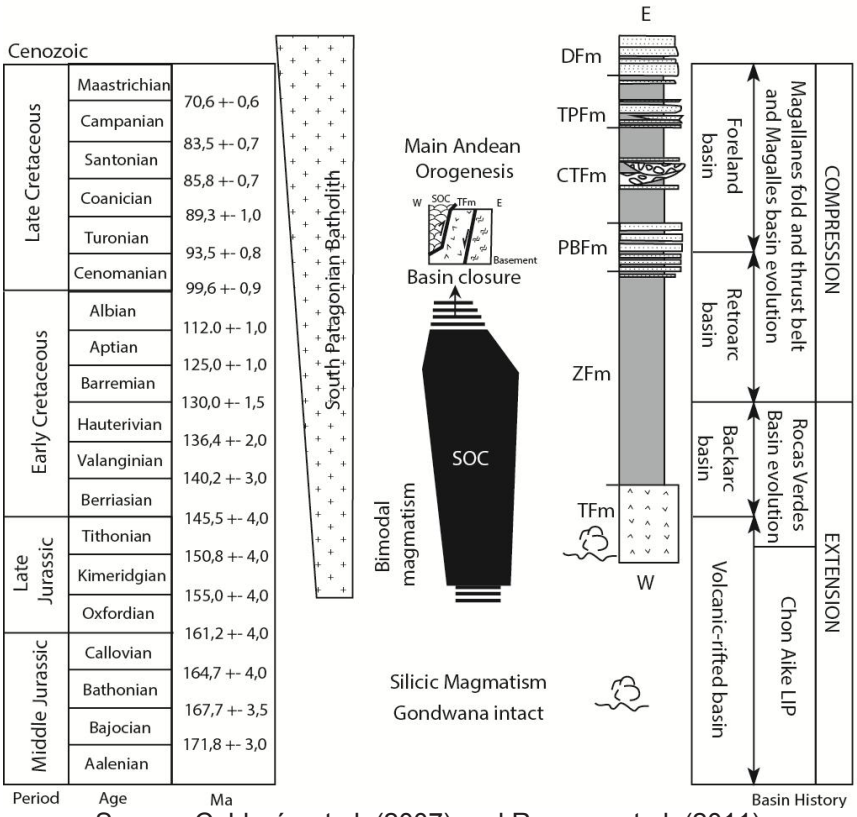

Source: Calderón et al. (2007) and Romans et al. (2011).

The inversion of RVB is related to changes in plate motions between Nazca, Antarctic and South American plates when the opening of Atlantic Ocean consolidates at 130 Ma (Calderón et al., 2007a). The extensional regimen on the western margin became compressive, culminating in collision between the arc and the South American cratonic margin (Dalziel, 1981; Stern and De Wit, 2003; Fosdick et al., 2011; Calderón et al., 2012). The RVB seafloor was partially underthrusted westwards beneath the arc, and partially obducted eastwards onto the craton (Dalziel, 1981; Stern and De Wit, 2003; Calderón et al., 2007a; Fosdick et al., 2011; Calderón et al., 2012). The emplacement of the SOC is considered the first stage of RVB closure (Fosdick et al., 2011). At Sarmiento Cordillera SOC is thrusted upon

Tobífera Fm. by the Canal de las Montañas Shear Zone, assigned as the sole thrust of the obduction with an eastwards tectonic transport, and west vergent backthrusts (Fig. 2.2.5, Calderón et al., 2012). The main compressive deformational event is dated 85 Ma (Ar^{40}/Ar^{39} in phengites from Tobífera Fm.), and 79 Ma is the maximum age for emplacement of ophiolites at Cordillera Sarmiento region (Calderón et al., 2012).

Figure 2.2.5: Schematic E-W cross-section of RVB near Cordillera Sarmiento. Abbreviation: CMSZ – *Canal de las Montañas* Shear Zone.

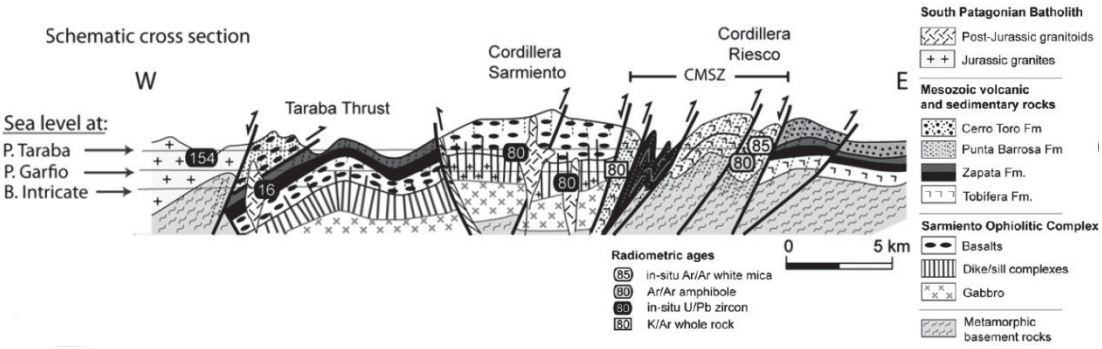

Source: Calderón et al. (2012).

Progressive extrusion of the RVB units occurred by eastward imbrications of thrust sheets, forming the Magallanes fold and thrust belt (Fosdick et al., 2011; Calderón et al., 2012). Inherited normal faults from the rift phase might be reactivated and converted in thrust faults of high dip angle, what accounts for broad uplift of the belt. A transitional thin-skinned to thick-skinned tectonics is interpreted due to incorporation of basement thrust sheets by out-of-sequence reverse faults (Fosdick et al., 2011; Betka et al., 2015). A cross-section summarizes tectonic evolution for the Andean margin in figure 2.2.6.

Figure 2.2.6: Schematic cross-section of the Andean margin at 51°30´S, showing the forearc region, the SPB, uplifted Paleozoic metamorphic basement, SOC, Magallanes fold and thrust belt and Magallanes Basin.

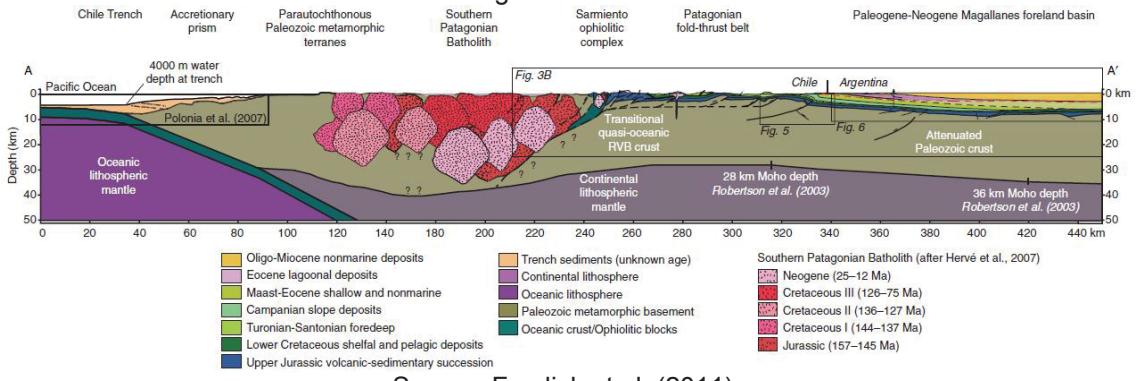

Source: Fosdick et al. (2011).

3 METHODS

During October, 2nd to 14th, a field work was made in the XII Region of Chile, near the Magallanes Strait, Seno Otway and Seno Skyring regions (Fig. 3.1.1). The geologists Mauricio Calderón, Cristóbal Ramírez de Arellano, Julie Fosdick, Matías Ghiglione, Andrea Goddard, Veleda Muller, Diego Rojo and Fernanda Torres, on board of Marypaz II, made up the team that collected geological information, structural data, and seventy rock samples by the thirty six outcrops visited, aiming petrographic, geochemical and geocronological analysis. The methods used to this research are presented on the figure 3.1.2. The article attached at the section 6 of results has the description of the structural and petrographic analysis, the conditions of performance of the X-ray fluorescence of the samples selected for P-T pseudosections, electron probe micro analyser, SHRIMP zircon U-Pb and $^{40}Ar/^{39}Ar$ geochronology, and the description of the thermodynamic modelling of the metamorphic rocks. Because of this, these methods will not be repeated in this section; however, the X-ray fluorescence is repeated because twenty five rock samples were analyzed at a different laboratory and for a different purpose of that first four samples for P-T pseudosections. The additional method of ICP-MS performed at the same twenty five samples of X-Ray Fluorescence is explained in the following text and the results are presented as complementary. SEM analyses in five samples were carried out for a first mineral characterization and are presented as complementary results as well.

Figure 3.1.1: field work navigation route, on board of Marypaz II, on October, 2017.

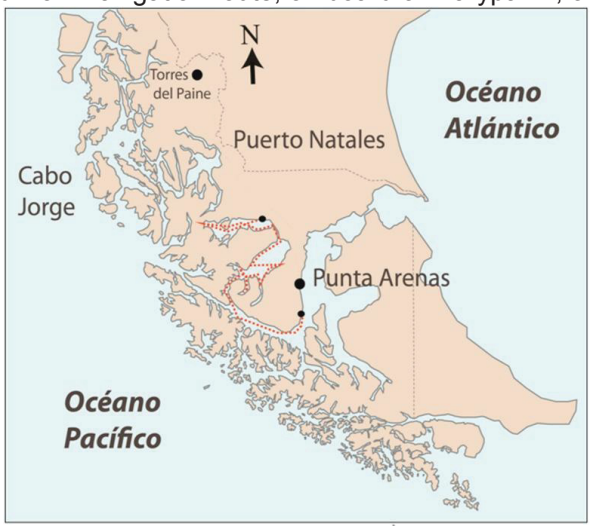

Source: Informe de terreno Proyecto Fondecyt nº 1161818 (2017).

Figure 3.1.2: Flowchart with methods, analytical techniques and results obtained.

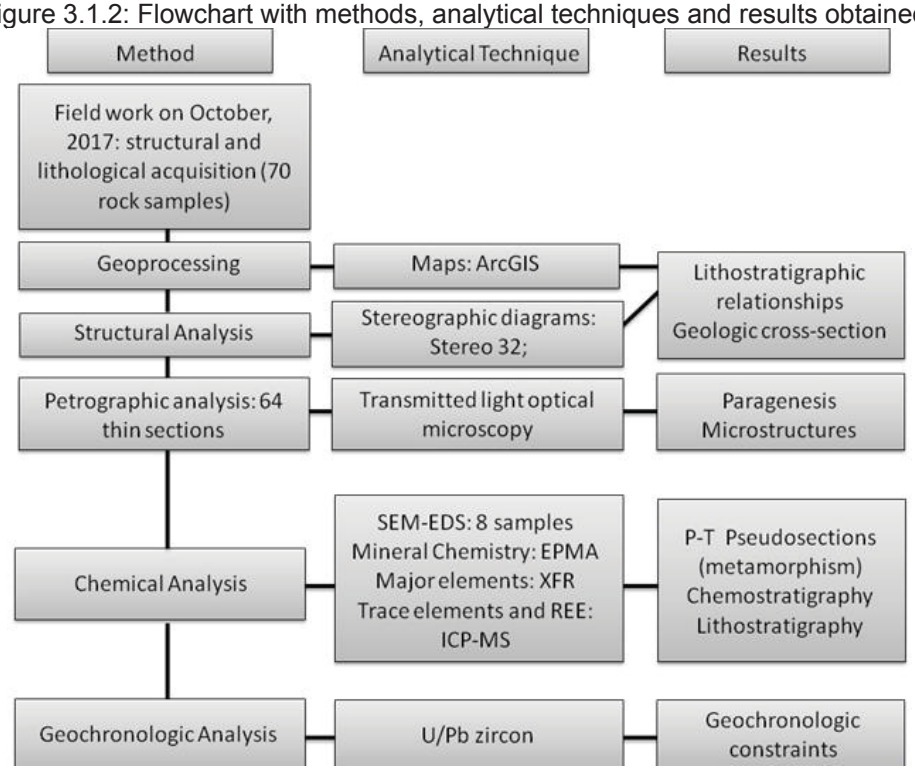

3.1 SCANNING ELECTRON MICROSCOPY

A first semi-quantitative determination of chemical composition and imaging of 8 rock samples of Tobífera Fm., COS and Zapata Fm. and their minerals were obtained using the Scanning Electron Microscopy (SEM) *JEOL* model 6010LA, with energy dispersive x-ray spectrometer (EDS) coupled, of LAMIR. The samples were coated with gold. The SEM operated with 20 kV of tension and amperage of 0,85 μA. The live-time EDS operation was 30 seconds by spot.

3.2 X-RAY FLUORESCENCE

The X-ray fluorescence (XRF) analysis was used to determine the quantitative chemical composition of major elements (Z>12) of the twenty five whole rock samples of Tobífera Fm., COS, Zapata Fm. and the pre-Jurassic basement, at the Bureau Veritas Minerals Laboratory, in Vancouver, Canada. This data must have been used for chemostratigraphic correlations and lithogeochemistry.

The XRF technique consists in the incidence of primary short-wavelength X-rays on a sample, which is a compressed glass bead made from the powdered rock fusion with lithium borate (Rollinson, 1993). The sample is ionized and produces

secondary X-rays (fluorescent X-rays) with wavelengths characteristic of the elements present in the sample (Rollinson, 1993). Different angles of reflection and intensity of radiation permit quantifying the concentration of chemical minerals, converted in percentage (Gomes and Dutra, 1984).

3.3 ICP-MS

The same twenty five samples that were analyzed by XRF were analyzed by inductively coupled plasma mass spectrometer (ICP-MS) of Bureau Veritas Minerals, which results in a quantitative analysis of trace elements and rare earth elements (REE). Multielementar diagrams for REE and trace elements provide a better geochemical classification and discrimination of geotectonic environments, as well as chemostratigraphic relations (Rollinson, 1993).

ICP-MS is also made for a bulk rock sample of powdered material fusion with solution, and standard silicate dissolution is employed. From a nebulizer, the sample solution is passed as an aerosol into an argon plasma (Rollinson, 1993). The inductively coupled plasma is a stream of argon atoms heated by radio-frequency coil and ignited by high-frequency Tesla spark. Sample solution dissociates in the plasma and atomic and spectral lines are excited and detected by photomultipliers, these lines are compared with calibration lines and converted into concentrations (Rollinson, 1993). The mass spectrometry is a vacuum system that receives the ions extracted from the plasma, they are focused with ion lens into the curved electromagnet mass spectrometer, which splits up the atoms according to their mass. Isotope ratios can be read by the differences of deflection of radius curvature of the ions (Rollinson, 1993).

4 RESULTS

The main results of this study are attached to the following text in the form of a scientific article. The figures are numbered according to the article order and the references were done separately for the article and for the dissertation document, some of them are repeated. A section of complementary results are following the article and a broader discussion section finalizes this study.

THE ROCAS VERDES BASIN CLOSURE AND EARLY TECTONOTHERMAL EVOLUTION OF THE MAGALLANES FOLD THRUST BELT IN SOUTHERN PATAGONIAN ANDES (52-54ºS)

Muller, Veleda A.P.[a,b], Calderón, Mauricio[c], Cury, Leonardo F.[a,b], Fosdick, Julie C.[d], Ghiglione, MatiasC.[e], Massonne, Hans-Joachim[f], Fanning, Christopher M.[g], Warren, Clare[h], Ramírez de Arellano, Cristobal[c]

[a] Departmento de Geologia da Universidade Federal do Paraná, Av. Cel. Francisco H. dos Santos 210, 81531-980 Curitiba, Brazil.

[b] Laboratório de Análise de Minerais e Rochas, Av. Cel. Francisco H. dos Santos 100, 81531-980 Curitiba, Brazil.

[c] Carrera de Geología, Facultad de Ingeniería, Universidad Andres Bello, Sazié 2212, Santiago, Chile.

[d] Department of Geosciences, University of Connecticut, 354 Mansfield Road, Storrs, Connecticut 06269, USA.

[e] Instituto de Estudios Andinos “Don Pablo Groeber”, Universidad de Buenos Aires, CONICET, Buenos Aires, Argentina.

[f] Institut für Mineralogie und Kristallchemie, Universität Stuttgart,Azenbergstr. 18, D-70174 Stuttgart, Germany.

[g] Research School of Earth Sciences, Australian National University, Canberra, Australia.

[h] Faculty of Science, Technology, Engineering and Mathematics, School of Environment, Earth and Ecosystem Sciences,The Open University, United Kingdom

ABSTRACT:

The western domain of the Magallanes fold-and-thrust belt (MFTB) consist mainly of N-S and NW-SE trending tectonic slices of pre-Jurassic basement rocks, ophiolitic complexes and volcaniclastic and sedimentary successions of the Late Jurassic-Early Cretaceous Rocas Verdes Basin (RVB). New field and available seismic reflection data near Skyring and Otway sounds (52-54ºS) reveal the architecture of the MFTB dominated by an east-prograding and internally deformed thrust pile structurally above the sedimentary in-fill of the Upper Cretaceous Magallanes foreland basin. The volcaniclastic and hemipelagic sedimentary rocks of the RVB (Tobífera and Zapata formations) are the main lithological units of the western thrust pile and show variable intensities of dynamic recrystallization and development of NW-SE-trending and SW-diping foliations with with top to the northeast vergence. Igneous and detrital U-Pb zircon dating constrain an Upper Jurassic age of felsic metatuffs (ca. 160 Ma; Tobífera Fm.) and an Aptian maximum depositional age of metasedimentary rocks (ca. 124 Ma; Zapata Fm.), indicating a period of ca. 40 myr of sedimentation in depocenters of the Rocas Verdes Basin. Phase diagram modelling on phengite-chlorite bearing metamorphic rocks allow constrain pressure-temperature (P-T) conditions during dynamic recrystallization. The P-T condition of ~14 kbar and ~270ºC was determined in a phyllonite of the westernmost thrust sheet, in which $^{40}Ar/^{39}Ar$ syntectonic phengite dating yielded ca. 71 Ma. In protomylonites from the eastern thrust sheets the P-T conditions varie between 3-5 kbar and 300-320ºC. A biotite-bearing metapelite of the Zapata Formation, located in the central domain near diorite intrusions of ca. 82 Ma record P-T conditions of ~5.5 kbar and 510ºC. The new data indicate that the tectonothermal evolution of the RVB closure involved tectonic burial to 15-35 km depths in a fast subduction environment with stacking and progressive deformation at the base of an accretionary wedge, lately thermally overprined in the Campanian.

KEY-WORDS: RocasVerdes Basin. Patagonian Andes. Fold and thrust belt. Ophiolite. Subduction. Accretionary Wedge.

1 INTRODUCTION

In Mariana-type convergent margins back-arc basins with seafloor spreading might be inverted during orogenic events. Basin closure could be related to the development of subduction zones within the oceanic-type crust ending with the collision between the drifted continental fragments and emplacement of oceanic lithosphere over continental margins, what can be find later as ophiolites in mountain ranges (Wakabayashi and Dilek, 2003; Dilek et al., 2007; Dilek and Furnes, 2014, 2011). Ophiolites could be considered as “structural roofs” of paleosubduction zones, which were transported over metamorphic soles – highly strained thin sheets (<500 m thick) of rocks that record greenschist to blueschist metamorphism – contrasting with the ocean floor hydrothermal metamorphism of the ophiolites (Wakabayashi and Dilek, 2003). The thrust soles are often metavolcanic and metasedimentary rocks dragged from the upper oceanic crust to greater depths during the inception of subduction zones, which could be considered the first and main stage of emplacement of ophiolites (Dilek and Whitney, 1997; Wakabayashi and Dilek, 2003; Dilek et al., 2007; Dilek and Furnes, 2011). High pressure peaks affect the units as a result of underthrusting and/or multiple events of thrusting, and progressive cooling is expected when the layers are imbricated at the upper plate (Wakabayashi and Dilek, 2003). Thrusting over a continental margin or microcontinent characterize “collisional or Thetyan ophiolites”, while thrusting over an accretionary wedge of progressive growth characterize “accretionary or Cordilleran ophiolites” (Wakabayashi and Dilek, 2003). The exhumation of the ophiolites is the late stage of emplacement, when they become exposed to the surface, what can be associated with erosion and latter orogenic structural adjustments (Wakabayashi and Dilek, 2003).

In convergent margins, microcontinents are accreted and fore-arc/back-arc basins, that commonly nestle suprasubduction zone ophiolites, are closed when compression took place (Wakabayashi and Dilek, 2003; Schellart and Lister, 2005; Dilek et al., 2007). Subduction accretion is the most important process of ophiolite emplacement, but collisions between microcontinents are the final stages during amalgamation, and the emplacement can be result of a progression from subduction accretion to continental collision. The ophiolite pseudostratigraphy after the classical Penrose definition (Anonymous, 1972) consist of: ultramafic rocks from the upper-mantle; ultramafic and mafic rocks from the lower crust; sheeted dyke complex of

mafic rocks; and an upper section of pillow basalts, pillow breccias and massive lava flows, eventually intercalated with sedimentary and volcaniclastic layers. Shortening and thickening of the deformed layers can evolve to fold and thrust belts, which can be thin or thick-skinned, depending on the crustal depth and complexity of tectonic imbrications (Kley et al., 1999; Fossen, 2010).

In southernmost Patagonia the Rocas Verdes Basin (RVB) was a marginal basin that evolved from rift to back-arc stages with seafloor spreading, developed throughout the early break-up of southernwestern Gondwana margin, since Middle Jurassic to Early Cretaceous times (Dalziel, 1981; Pankhurst et al., 2000; Stern and De Wit, 2003; Hervé and Fanning, 2003; Calderón et al., 2013, 2007). During the early rifting-stage in the Middle to Late Jurassic, the RVB was filled by volcaniclastic and effusive rhyolitic rocks, seafloor spreading took place in the Late Jurassic, generating oceanic-type lithosphere of bimodal magmatism (Calderón et al, 2007). Throughout the Late Jurassic-Early Cretaceous the bimodal magmatism evolves in the western part of the basin and felsic volcanism continues in the eastern part, meanwhile, hemipelagic sedimentation occurs and the mafic and felsic volcanic rocks are intercalled and capped by these sedimentary successions (Dalziel, 1981; Pankhurst et al., 2000; Fildani and Hessler, 2005; Calderón et al., 2007).

During the widespread opening of the southernmost Atlantic Ocean, since mid-Cretaceous times, convergence rates increased along the western margin of South America and the Andean orogeny took place, proceeding until Cenozoic times with east-directed subduction of Pacific oceanic plates. The higher convergence rates triggered the formation of the Magallanes Fold-and-Thrust Belt (MFTB) at the Patagonian Andes (Harambour, 2002; Fosdick et al., 2011), presented on figure 1. At the latitude of the Sarmiento Ophiolitic Complex, (Fig. 1), a west-directed subduction/underthrusting zone is proposed for the consumption of the oceanic-type lithosphere beneath the arc-bearing microcontinent, causing the tectonic emplacement of ophiolites near ca. 85 Ma (Calderón et al., 2012), and this is considered the first phase of the MFTB development (Gealey 1980; Dalziel 1981; Galaz et al., 2005; Hervé et al., 2007a; Calderón et al., 2012). The timing and kinematics constraints of the early tectonic emplacement of ophiolitic complexes in Patagonia have been inferred from petrological and structural studies in foliated rocks from shear zones corridors bounding ophiolites (Calderón et al., 2005; Galaz et

al., 2005; Hervé et al., 2007a; Fosdick et al., 2011; Calderón et al., 2012: Canal de las Montañas Shear Zone).

Figure 1: Regional map of Southern Patagonia highlighting important tectonic features: the Rocas Verdes Basin inside the green lines, the Cretaceous to Paleocene units of the Magallanes foreland Basin, the South Patagonian Batholith, the thrust front of the Magallanes fold and thrust belt, the Magallanes-Fagnano sinistal transform fault zone between South American Plate and Scotia Plate, and the subduction of the Antarctic plate under the Scotia Plate. SOC: Sarmiento Ophiolitic Complex, TOC: Tortuga Ophiolitic Complex. The black square is the area of this work presented in the figure 2.

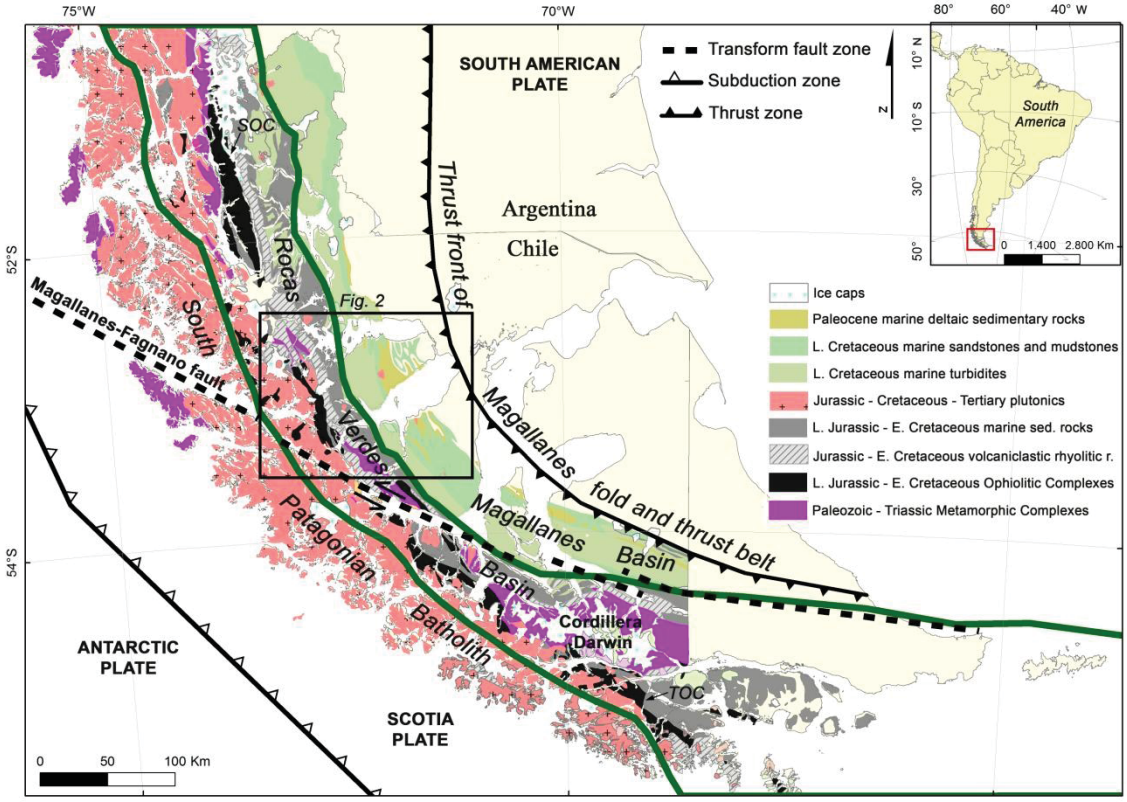

Source: SERNAGEOMIN (2003), Fosdick et al. (2011), and Betka et al. (2015).

The lithostratigraphic units exposed in the Patagonian Andes near Otway and Skyring sounds (52-54ºS) reveals the current structuring of remnants of the RVB, which comprises mainly recrystallized and foliated rhyolitic metatuffs and metapelite-psammite rocks of Tobífera and Zapata formations, respectively, and lesser exposed pillow and massive metabasalts of the Sarmiento Ophiolitic Complex. The metabasalts are thrusted onto the metatuffs and metasedimentary rocks, which underwent brittle-ductile deformation and are imbricated in thrust sheets verging to the east and northeast. Some tectonic slices of metasedimentary schists of the pre-Jurassic continental basement are juxtaposed to the thrust pile. New field data (structural, stratigraphic and petrologic data), mineral composition data, pseudosection modelling of metamorphic rocks and in-situ geochronological

analyses presented in this work and coupled to available seismic reflection data, provide constraints on the tectonothermal evolution of the RVB, specially to the emplacement of the Sarmiento ophiolites. Foliated metapelites and metatuffs record the progressive deformation and evolution of an accretionary wedge.

2 REGIONAL GEOLOGY

The early dispersal of Gondwana in Jurassic times was accompanied by the development of a wide volcanic zone in southwestern South America (Bruhn et al., 1978; Wilson, 1991) and the inception of the Rocas Verdes Basin (Dalziel, 1981; Stern and de Witt, 2003; Calderón et al., 2007). The RVB is interpreted as a marginal basin created by rifting of the pre-Jurassic basement complexes, and filled by volcaniclastic and effusive silicic rocks of Tobífera Fm. and El Quemado Complex (Dalziel, 1981; Pankhurst et al., 2000; Calderón et al., 2007, 2012). The progressive opening of the basin during Late Jurassic-Early Cretaceous generated the seafloor spreading recorded in the Sarmiento and Tortuga ophiolitic complexes, capped by shales, turbidites and cherts of the Zapata and Yaghan formations (Katz et al., 1964; Dalziel, 1981; Fuenzalida and Covacevich, 1988; Fildani and Hessler, 2005; Calderón et al., 2007).

The continental pre-Jurassic basement of the RVB comprises different metamorphic complexes mainly constituted by metasedimentary rocks and metabasites of heterochronous accretionary complexes and ancient passive margins, metamorphosed from lower greenschist to upper amphibolites facies (Nelson et al., 1980; Kohn et al., 1993; Hervé et al., 2003a; Klepeis et al., 2010; Maloney et al., 2011). In the study area near the Skyring and Otway sounds the RVB units overlap and can be interleaved with metapelites of the Eastern Andes Metamorphic Complex, deposited during Late Devonian – Early Carboniferous, and metamorphosed under greenschist facies during the Late Permian Gondwanian orogeny (Thomson et al., 2000; Hervé et al., 2003b, 2008). To the east of the study area, the pre-Jurassic basement is buried below the sedimentary sucession of the Magallanes foreland basin and is constituted by high-grade Cambrian crystalline rocks of the Tierra del Fuego Igneous and Metamorphic Complex, which collided with the Gondwana during Mid-Carboniferous (Hervé et al., 2010b). Other pre-Jurassic basement complexes of Southernmost Patagonia include: to the north of the study area the Staines Complex,

of Upper Paleozoic forearc metavolcanosedimentary rocks (Forsythe and Allen, 1980); to the west of the Patagonian batholiths, the accretionary complexes Denaro, Duque de York, and Diego de Almagro, constituted mainly by Permian–Carboniferous metavolcanosedimentary oceanic rocks (Hervé et al., 2003a, 2008, Sepúlveda et al., 2010); to the south of the study area, at the Scotia Plate: the Cordillera Darwin Metamorphic Complex, of Late Paleozoic to Early Mesozoic metavolcanosedimentary sucessions of passive margins (Hervé et al., 2010a).

The proto-Pacific eastwardly dipping subduction zone at Patagonia seems to have started by Late Permian, recognized by the accretion of Madre de Dios exotic terrane, but is well recorded from Early Jurassic to Cenozoic plutons (Hervé et al., 2007b). The first intrusion phase of the South Patagonian Batholith (SPB) is contemporaneous to the basin opening and bimodal volcanism, and arc inception converted the tectonic context of RVB to backarc (Dalziel, 1981; Hervé et al., 2007; Calderón et al., 2012). Leucogranites and gabbros emplaced near the western boundary of RVB date 157 to 145 Ma (Hervé et al., 2007b), coeval and presenting mutually cross-cutting dyke relationships with pyroclastic rocks of Tobífera Fm. and mafic rocks of the Sarmiento Ophiolitic Complex. The magmatism proceeded episodically until 15 Ma (Hervé et al., 2007b).

At the onset of the RVB the explosive silicic volcanic rocks of Tobífera Formation were deposited in rift-grabens between 170 to 140 Ma, considered later constituents of the *Chon Aike* Large Igneous Province (Pankhurst et al. 2000; Calderón et al. 2007). They are constituted massively by metatuffs and ignimbrites of rhyolitic composition, but on its base may occur syn-tectonic breccias and conglomerates, and the felsic volcanics are commonly intercalled with peperites and fossiliferous sedimentary rocks, which constrain Late Jurassic to Early Cretaceous deposition mainly under submarine conditions (Allen, 1982; Fuenzalida and Covacevich, 1988).

The Rocas Verdes ophiolites contains, from the base upwards, layered and isotropic gabbros, dike complexes, and extrusive successions composed of pillowed and massive basalts with radiolarian chert intercalations, overlain by hemipelagic rocks (Stern and de Witt, 2003). The ophiolitic complexes bear metamorphic assemblages and textures associated to ocean floor-type hydrothermal metamorphism (Elthon and Stern, 1978; Allen, 1982; Avendaño, 2008; Coloma, 2011; Calderón et al, 2013). The Sarmiento Ophiolitic Complex represent an early

magmatic component of the Rocas Verdes ophiolites, comprising Late Jurassic-Early Cretaceous bimodal suite associations (Calderón et al., 2007), with elemental composition of enriched mid-ocean ridge basaltic magmas formed in a suprasubduction environment (Calderón et al., 2013).

The shale-rich Zapata Fm. overlies the ophiolitic complexes and Tobífera Fm, representing the sedimentary infill of the RVB by at least 1000 m of thickness, from Tithonian to Cenomanian (Fildani and Hessler, 2005). The thicker lower part is formed by shales deposited in a deep marine hemipelagic environment, while the upper part of Zapata Fm. present siltstones, sandstones and greywackes layers, interpreted as coarse sedimentation induced by tectonic activity when the RVB started to close (Fildani and Hessler, 2005). Changes in sediment supply reflect the transition from a back-arc basin to a retroarc foreland basin (Wilson, 1991; Fildani and Hessler, 2005).

The initiation of the orogenic deformation, which induced the closure of the RVB and its subsequent emplacement to the east, is interpreted to have occurred since Cenomanian (101 Ma; Fosdick et al., 2011). Orogenic inversion of the RVB caused thrust loading, resulting in flexural subsidence to the east, and turbiditic flows might be triggered by tectonic activity, filling the new deep foreland basin (Fildani and Hessler, 2005). The first unit that ovelies Zapata Fm. is the Punta Barrosa Fm. or the correlative Latorre Fm., with turbidites of low density currents (Fildani and Hessler, 2005; Mpodozis et al., 2007; McAtamney et al., 2011). The subsequent unit is the Cerro Toro Fm or the correlative Escarpada Fm., constituted by shale-rich turbidites and thick conglomerates that filled structurally controled submarine channels (Bernhardt et al., 2011; Romans et al., 2011). Magallanes basin evolved from this deep water environment to shallow marine, deltaic, estuarine, and fluvial environments, by shoaling up and eastwards during Late Cretaceous and Cenozoic (Fosdick et al., 2011; Romans et al, 2011).

The mid-Cretaceous tectonic emplacement of the Rocas Verdes ophiolites upon South America (Dalziel, 1981; Dalziel, 1986) is considered the first stage of Magallanes fold and thrust belt development (Wilson, 1991; Fildani et al., 2003; Fosdick et al., 2011; Calderón et al. 2012; Betka et al. 2015). The Sarmiento Ophiolitic Complex is thrusted upon the Zapata and Tobífera formations through the Canal de las Montañas Shear Zone, with an eastwards tectonic transport and west vergent backthrusts (Calderón et al., 2012), explained by a wedge extrusion model

(Kohn et al., 1993; Harambour, 2002). The sheared parts of the Tobífera Fm. and Sarmiento Ophiolitic Complex experienced pumpellyte-actinolite to greenschist facies metamorphism and mylonitization under 260°C and 5-6 kbar, in a subduction environment (Calderón et al., 2012). The metamorphism was dated ca. 85 Ma and the upper age limit to the ophiolite emplacement was constrained to 79 Ma in the Canal de las Montañas Shear Zone (51-52°S; Calderón et al., 2012).

Two main phases of deformation are proposed to the Magallanes fold and thrust belt, the first, around Campanian, was accommodated in detachment levels within the Zapata and within the pre-Jurassic basement (Betka et al., 2015). The second was an out-of-sequence thrusting phase cutting the early detachments, which occurred by the Maastrichian until Eocene (Betka et al., 2015), responsible by the interleaving of Tobífera and Zapata thrust sheets with the pre-Jurassic rocks by thick-skinned tectonics (Harambour, 2002; Fosdick et al., 2011; Betka et al., 2015). At the latitudes of Cordillera Darwin ophiolite emplacement occurred to the north, accompanied by south-directed subduction of the oceanic floor and underthrusting of the continental margin under the volcanic arc, it has been related to the early stages of the RVB closure near 86 Ma ago (Nelson et al., 1980; Cunningham, 1995; Kraemer, 2003; Klepeis et al., 2010; Maloney et al., 2011).

3 METHODS

3.1 Structural and petrographic analysis

Field descriptions were done in 36 outcrops along Gajardo Channel, Jeronimo Channel and Estero Wickam, to the west of Otway and Seno sounds (52°-54°S; Fig. 2). Petrographic analysis with the optical microscope *Axio Imager* model A2m of the Laboratory of Mineral and Rock Analysis (LAMIR) of the Department of Geology in UFPR, Brazil, were done in 70 thin sections to determine mineral assemblages, textures and microstructures, including samples from the SPB, RVB and Magallanes Basin, which 12 were oriented to determine shear sense.

Structural data of foliations, lineations, bedding and folds were plotted in stereographic diagrams, at equal angle projections, with the software Stereo 32®. The "*Mapa Geologico de Chile, 1:1.000.000*" by SERNAGEOMIN (2003) was used as the basis to geological mapping.

3.2 X-ray fluorescence

The major elements bulk chemical composition of three samples of metatuffs of Tobífera Fm. (FC1723, FC1727, FC1749) and two samples of metapelitic rocks of Zapata Fm. (FC1757, SHP141), were carried out with PHILIPS PW 2400 X-ray fluorescence (XRF) spectrometer at Universität Stuttgart, using glass discs prepared from rock powder and Spectromelt®. The percentage of FeO was calculated using the ratio Fe_2O_3/1.1113 (FeO: Fe_2O_3 = 9:1) and CaO was corrected due to apatite high concentrations using the ratio CaO-(280.4/212.92)*P_2O_5 for the metamorphic modeling. The percentage of oxides was corrected for 100% and is presented for each sample together with the the P-T pseudosection diagrams of the figure 11 to 13.

3.3 Electron probe micro analyser

The chemical composition of minerals was obtained by the electron probe micro analyser (EPMA) CAMECA SX100 with 5 wavelength dispersive spectrometers (WDS) and one EDS, at Universität Stuttgart, Germany. It was carried out in phengite, chlorite, epidote, feldspar and biotite of the same five samples analyzed by XRF. Operating conditions were an acceleration voltage of 15 kV, a beam current of 15 nA, a beam size of 7–10 μm or a focussed beam (for very small crystals), and 20 seconds counting time on the peak and on the background for each element. The standards used were natural wollastonite (Si, Ca), natural orthoclase (K), natural albite (Na), natural rhodonite (Mn), synthetic Cr2O3 (Cr), synthetic TiO2 (Ti), natural hematite (Fe), natural baryte (Ba), synthetic MgO (Mg), synthetic Al2O3 (Al) and synthetic NiO (Ni). The PaP correction procedure provided by Cameca was applied. The mineral composition data are presented in Table 1.

Table 1: Representative electron microprobe analyses (in wt%) of phengite, chlorite, biotite, epidote, feldspar and amphibole in metatuffs of Tobífera Fm. (FC1723, FC1727, FC1749) and metapelites of Zapata Fm. (FC1757, SHP141)

Sample no.	FC1723#53	FC1727#71	FC1749#50	FC1757#16	SHP141#24		FC1723#18	FC1723#40	FC1727#69	FC1749#45	FC1757#9	SHP141#39		FC1757#23		FC1723#32	SHP141#48		FC1723#43	FC1727#57	FC1749#37	FC1757#30	SHP141#18		SHP141#20
Mineral	phengite	phengite	phengite	phengite	phengite		chlorite	chlorite	chlorite	chlorite	chlorite	chlorite		biotite		epidote	epidote		feldspar	feldspar	feldspar	feldspar	feldspar		amphibole
SiO2	49.63	49.76	51.97	49.01	48.61	SiO2	35.61	23.68	25.24	33.73	26.41	27.00	SiO2	35.58	SiO2	38.19	37.68	SiO2	67.79	69.41	68.06	62.28	68.16	SiO2	61.99
TiO2	0.01	0.15	0.05	0.25	0.08	TiO2	0.00	0.02	0.02	0.02	0.01	0.02	TiO2	2.87	TiO2	0.02	0.04	TiO2	0.00	0.00	0.00	0.01	0.13	TiO2	0.07
Al2O3	32.80	25.73	29.64	28.29	27.61	Al2O3	26.70	20.94	18.40	23.13	19.83	19.95	Al2O3	17.44	Al2O3	29.73	29.13	Al2O3	19.78	19.42	19.50	24.57	19.95	Al2O3	2.23
FeO	0.89	3.80	0.81	0.18	1.14	FeO	7.53	31.30	30.91	11.33	26.96	21.01	FeO	21.35	Cr2O3	0.00	0.00	Cr2O3	0.00	0.00	0.00	0.00	0.00	Cr2O3	0.01
Fe2O3	0.00	1.29	0.00	4.89	1.83	MnO	0.04	0.36	0.77	0.36	0.58	0.71	Fe2O3	0.00	Fe2O3	5.68	6.40	Fe2O3	0.13	0.00	0.12	0.24	0.15	FeO	8.68
MnO	0.00	0.05	0.00	0.05	0.07	MgO	21.35	11.33	12.06	21.65	14.55	18.96	MnO	0.27	Mn2O3	0.00	0.30	Mn2O3	0.00	0.00	0.00	0.00	0.00	MnO	0.42
MgO	2.21	3.18	3.59	3.83	3.78	H2O	13.41	10.95	10.93	12.89	11.36	11.63	MgO	8.69	MgO	0.05	0.04	MgO	0.00	0.00	0.01	0.00	0.00	MgO	13.58
CaO	0.05	0.01	0.02	0.03	0.02	Total	104.64	98.58	98.34	103.12	99.71	99.28	CaO	0.02	CaO	24.25	24.37	CaO	0.28	0.12	0.11	5.74	0.22	CaO	10.01
Na2O	0.28	0.08	0.09	0.10	0.04								Na2O	0.01	Na2O	0.00	0.02	Na2O	11.99	11.78	12.03	8.63	11.54	Na2O	0.04
K2O	10.65	10.66	10.81	11.61	10.73	Si	6.3675	5.1883	5.5421	6.2773	5.5753	5.5699	K2O	9.95	H2O	1.94	1.93	K2O	0.04	0.06	0.05	0.13	0.13	K2O	0.27
BaO	0.29	0.14	0.16	0.16	0.00	Al iv	1.6325	2.8117	2.4579	1.7227	2.4247	2.4301	BaO	0.21	Total	99.86	99.90	BaO	0.02	0.02	0.00	0.01	0.00	H2O	2.0700
H2O	4.61	4.42	4.64	4.57	4.42	sum4	8.0000	8.0000	8.0000	8.0000	8.0000	8.0000	H2O	3.92				Total	100.03	100.82	99.89	101.60	100.28	Total	99.3600
Total	101.42	99.27	101.76	102.97	98.33	Al vi	3.9949	2.5967	2.3027	3.3512	2.5085	2.4209	Total	100.30	Si	2.9572	2.9314								
						Ti	0.0000	0.0025	0.0039	0.0033	0.0021	0.0023			Ti	0.0011	0.0021	Si	2.9692	3.0056	2.9823	2.7244	2.9723	Si	8.9981
Si	6.4609	6.7557	6.7189	6.4378	6.5914	Fe2+	1.1259	5.7362	5.6758	1.7641	4.7602	3.6237	Si	2.7218	Al	2.7129	2.6714	Al	1.0211	0.9911	1.0073	1.2667	1.0253	Al_T	0.0000
Al iv	1.5391	1.2443	1.2811	1.5622	1.4086	Mn	0.0057	0.0672	0.1433	0.0562	0.1045	0.1245	Al iv	1.2782	Cr	0.0000	0.0000	Fe3	0.0043	0.0000	0.0039	0.0079	0.0048	sum4	8.9981
sum4	8.0000	8.0000	8.0000	8.0000	8.0000	Mg	5.6924	3.7024	3.9480	6.0076	4.5806	5.8301	Ti	0.1649	Fe3	0.3310	0.3747	Ti	0.0000	0.0000	0.0000	0.0000	0.0042	Ti	0.0071
Al vi	3.4945	2.8729	3.2346	2.8171	3.0045	sum6	10.8188	12.1050	12.0737	11.1824	11.9560	12.0020	Al vi	0.2941	Mg	0.0061	0.0048	su1	3.9947	3.9967	3.9944	3.9992	4.0066	Al_O	0.3814
Ti	0.0011	0.0155	0.0044	0.0242	0.0077	H	16.0000	16.0000	16.0000	16.0000	16.0000	16.0000	Fe2	1.3659	sum6	3.0511	3.0705	Ba	0.0003	0.0003	0.0000	0.0002	0.0000	Cr	0.0015
Fe2+	0.0972	0.4312	0.0873	0.0196	0.1297	Compositions							Fe3	0.0000	Ca	2.0114	2.0315	Ca	0.0130	0.0055	0.0053	0.2692	0.0104	Fe3	0.0000
Fe3+	0.0000	0.1318	0.0000	0.4833	0.1863	xSi	1.1838	0.5942	0.7711	1.1386	0.7876	0.7850	Mn	0.0173	Na	0.0000	0.0000	Na	1.0183	0.9892	1.0220	0.7317	0.9755	Fe2	1.0521
Mn	0.0000	0.0055	0.0000	0.0060	0.0076	xMg	0.8342	0.3895	0.4042	0.7675	0.4850	0.6087	Mg	0.9906	sum8	2.0114	1.8807	K	0.0020	0.0035	0.0028	0.0072	0.0072	Mn	0.0521
Mg	0.4284	0.6430	0.6926	0.7498	0.7643	xFe	0.1650	0.6034	0.5811	0.2254	0.5040	0.3780	sum6	2.8329	H	1.0000	1.0000	su2	1.0336	0.9985	1.0302	1.0084	0.9972	Mg	2.9386
sum6	4.0212	4.1000	4.0189	4.1000	4.1000								Ca	0.0016	Compositions			Components						Ca	1.5562
Ca	0.0070	0.0012	0.0021	0.0049	0.0024								Na	0.0014	Ps [Fe/(Al+Fe)]	0.11	0.12	Anorthite	0.0128	0.0058	0.0052	0.2673	0.0105	Na	0.0114
Ba	0.0149	0.0073	0.0079	0.0084	0.0000								K	0.9713				High Albite	0.9852	0.9907	0.9921	0.7256	0.9822	sum8	6.0019
Na	0.0708	0.0209	0.0223	0.0251	0.0117								Ba	0.0063				K Feldspar	0.0020	0.0035	0.0027	0.0071	0.0073	K	0.0504
K	1.7682	1.8470	1.7833	1.9460	1.8569								sum8	0.9806										H	2.0000
sum8	1.8609	1.8764	1.8156	1.9843	1.8710								H	2.0000										components	
H	4.0000	4.0000	4.0000	4.0000	4.0000								Compositions											xAl	0.0000
Components													xAl	0.1471										xMg	0.7361
Ms	0.6968	0.5112	0.6056	0.5721	0.5950								xMg	0.420											
Wm_Phl	0.0106	0.0500	0.0094	0.0500	0.0500																				
Al_Cel	0.1974	0.2289	0.3241	0.2199	0.2539																				
Fe_Al_Cel	0.0448	0.1535	0.0409	0.0057	0.0431																				
Pg	0.0380	0.0112	0.0123	0.0126	0.0063																				
Ti_Mn_Ca_Wm	0.0123	0.0453	0.0077	0.1396	0.0517																				
xOH	1.0000	1.0000	1.0000	1.0000	1.0000																				

Abbreviations: Ms, Muscovite; Wm, White mica, Phl, Phlogopite; Cel, Celadonite; Pg, Paragonite, Ps: pistacite

Structural formulae and various parameters (mainly molar fractions X of end member components) were calculated using the CALCMIN software (Brandelik, 2009) as follows: biotite O= 11, all Fe is divalent; white mica, valences =42, cations without interlayer cations ≤12.1; chlorite, O= 28, all Fe is divalent; feldspar, O=8; ilmenite, O= 3, cations = 2

3.4 Thermodynamic modelling of metamorphic rocks

The metatuffs and metapelites selected for construction of pressure-temperature (P-T) pseudosections were collected at different structural levels within the thrust wedge. All show dynamic recrystallization and syntectonic growth of very fine white mica and chlorite defining the main foliation. A detailed description of mineral assemblages and textures is provided below.

Whole rock analyses were used to constrain geothermobarometric conditions of metamorphism, constructing phase diagrams with the software package PERPLE_X, which reproduce the stability fields of mineral assemblages from the bulk composition, in function of pressure (P), on the y axis, and temperature (T), on the x axis, calculating the minimum Gibbs energy for stable phases, according to processes and algorithms described by Connolly (1990). Strongly recrystallized rocks were selected and is considered that the whole rock composition is representative of the effective bulk composition during the main stage of dynamic metamorphism.

The thermodynamic model for the five samples considers the TiMNCKMFASH (TiO_2 – MnO – Na2O – CaO - K2O–FeO–MgO–Al2O3–SiO2–H2O–O2) system at a range of pressures between 8 to 18 kbar (SHP141) and between 2 and 7 kbar (FC1723; FC1727; FC1749; FC1757), and temperatures in the interval between 150 to 550°C. The thermodynamic data set was Holland and Powell (1998, updated 2002) for mineral and aqueous fluids. The solid-solution models are from the list given by the Perple_X package, and the models used here are from Massonne and Willner (2008) and take the acronym (M), Holland and Powell (1998) and take the acronym (HP), they were chosen for each sample according to their normative composition: Chl(HP) for chlorite, Pheng(HP) for magnesium-iron white micas, Mica(M) for margarite-muscovite-paragonite white micas, Pa(M) for paragonite, Bio(HP) and TiBio(HP) for biotite, Stlp(M) for stilpnomelane, Carp(M) for carpholite, Ctd(HP) for chloritoid, feldspar for plagioclase or alkaline feldspar, Ep(HP) for epidote, Gt(HP) for garnet, Acm(M) for sodic pyroxene, Act(M) for actinolite, Tre for tremolite, Carb(M) for carbonates, Pu(M) for pumpellyite, Omph(HP) for omphacite, IlGkPy for ilmenite-geikielite-pyrophanite, GlTrTsPg for amphibole and MtUl(A) for ulvospinel and magnetite.

The mineral chemical analysis allows us to choose an appropriate interval for the isopleths, lines of constant composition which constrain the maximum and minimum temperature and pressure for the generation of a specific mineral (Connolly, 1990; Will, 1998), from specified chemical ratios in a solid solution. The isopleths are calculated with PERPLE_X and the intersection between isopleths of more than one solid solution in a sample provide a precise P-T field for chemical equilibrium during metamorphism.

3.5 SHRIMP zircon U-Pb

To constrain the age of different tectonic slices in the fold and thrust belt three samples were analyzed. Igneous zircons from a metatuff of the Tobífera Fm. (FC1727) in Estero Wickam were analyzed to establish a crystallization age of the volcanic pile thrusted onto the easternmost thrust sheet of the Zapata Fm. Detrital zircon populations of a metasedimentary rock of the Zapata Fm. (FC1754) located in the westernmost portion of the belt at Gajardo channel, were analyzed to constrain sedimentary sources and establish a maximum depositional age of the protolith. The dating of igneous zircons from a diorite (FC1759) that intrudes the RVB units in the same channel will provide the age of crystallization and the upper age limit of metamorphism and deformation of RVB rocks in the hinterland of the fold and thrust belt.

The ages were obtained with the Sensitive High Resolution Ion Micro Probe (SHRIMP) at the Research School of Earth Sciences, Australian National University, in Canberra. Analytical techniques followed Williams (1998), processing used the SQUID Excel Macro of Ludwig (2000) (Table 2 a-c), uncertainties are reported at the 1σ level. Corrections for common Pb were made using the measured $^{238}U/^{206}Pb$ and $^{207}Pb/^{206}Pb$ ratios following Tera and Wasserburg (1972) as outlined in Williams (1998). The geological time-scale follow the Chronostratigraphic Chart 2018 by IUGS-ICS (www.stratigraphy.org).

Table 2 a: Summary of SHRIMP U-Pb results for zircon from sample FC1727.

Grain. spot	U (ppm)	Th (ppm)	Th/U	$^{206}Pb^*$ (ppm)	$^{204}Pb/^{206}Pb$	f_{206} %	Total $^{238}U/^{206}Pb$	±	Total $^{207}Pb/^{206}Pb$	±	Radiogenic $^{206}Pb/^{238}U$	±	Age (Ma) $^{206}Pb/^{238}U$	±
1,1	411	249	0,61	8,9	0,000336	0,14	39,80	0,48	0,0504	0,0011	0,0251	0,0003	159,8	1,9
2,1	299	133	0,45	6,5	-	0,35	39,55	0,49	0,0520	0,0012	0,0252	0,0003	160,4	2,0
2,2	3035	1556	0,51	66,1	0,000090	0,68	39,47	0,44	0,0547	0,0030	0,0252	0,0003	160,2	1,9
3,1	154	66	0,43	3,3	0,000270	<0.01	39,87	0,56	0,0489	0,0019	0,0251	0,0004	159,8	2,3
3,2	476	264	0,55	9,9	0,000107	0,01	41,28	0,50	0,0492	0,0009	0,0242	0,0003	~~154,3~~	~~1,9~~
4,1	426	239	0,56	9,4	-	0,31	39,06	0,46	0,0517	0,0010	0,0255	0,0003	162,5	1,9
4,2	1776	922	0,52	38,6	0,000027	0,07	39,49	0,41	0,0498	0,0004	0,0253	0,0003	161,1	1,7
5,1	2689	1582	0,59	60,8	0,000012	<0.01	37,97	0,39	0,0490	0,0004	0,0263	0,0003	~~167,7~~	~~1,7~~
6,1	3119	1607	0,52	70,3	0,000043	<0.01	38,11	0,39	0,0489	0,0003	0,0263	0,0003	~~167,1~~	~~1,7~~
7,1	571	388	0,68	12,3	0,000022	0,11	39,82	0,46	0,0502	0,0008	0,0251	0,0003	159,7	1,8
8,1	262	151	0,58	5,6	0,000478	0,34	40,48	0,51	0,0519	0,0013	0,0246	0,0003	156,8	2,0
8,2	1563	602	0,39	33,0	0,000072	0,03	40,64	0,43	0,0494	0,0005	0,0246	0,0003	156,7	1,7
9,1	332	212	0,64	7,1	-	<0.01	40,16	0,49	0,0492	0,0011	0,0249	0,0003	158,5	1,9
10,1	831	491	0,59	18,4	0,000155	0,34	38,89	0,42	0,0520	0,0007	0,0256	0,0003	163,1	1,8
10,2	2490	1368	0,55	54,8	0,000024	<0.01	39,02	0,41	0,0487	0,0004	0,0256	0,0003	163,3	1,7
11,1	237	133	0,56	5,1	0,000256	0,26	40,22	0,53	0,0513	0,0013	0,0248	0,0003	157,9	2,1
12,1	385	203	0,53	8,5	0,000129	0,12	38,79	0,46	0,0503	0,0010	0,0258	0,0003	163,9	1,9
13,1	420	215	0,51	9,0	0,000180	0,15	40,03	0,50	0,0504	0,0010	0,0249	0,0003	158,8	2,0
14,1	457	250	0,55	9,8	0,000134	0,25	39,94	0,46	0,0513	0,0009	0,0250	0,0003	159,0	1,8
15,1	151	70	0,46	3,8	0,002035	1,08	~~33,64~~	~~0,52~~	~~0,0584~~	~~0,0020~~	0,0294	0,0005	~~186,8~~	~~2,9~~
16,1	190	83	0,44	4,1	0,000334	0,34	39,95	0,54	0,0520	0,0015	0,0249	0,0003	158,8	2,2
17,1	615	387	0,63	13,5	0,000130	<0.01	39,20	0,44	0,0493	0,0008	0,0255	0,0003	162,4	1,8
18,1	609	373	0,61	12,9	0,000156	<0.01	40,62	0,47	0,0482	0,0008	0,0246	0,0003	157,0	1,8
19,1	264	91	0,35	8,4	-	0,01	~~27,03~~	~~0,33~~	~~0,0510~~	~~0,0010~~	0,0370	0,0005	~~234,1~~	~~2,8~~
20,1	1250	1063	0,85	28,5	0,000022	0,03	37,70	0,40	0,0497	0,0005	0,0265	0,0003	~~168,7~~	~~1,8~~
21,1	628	463	0,74	13,6	0,000281	0,17	39,75	0,50	0,0506	0,0008	0,0251	0,0003	159,9	2,0
22,1	297	144	0,48	6,3	0,000257	0,17	40,40	0,51	0,0505	0,0012	0,0247	0,0003	157,4	2,0

Notes: 1. Uncertainties given at the one σ level.

2. Error in Temora reference zircon calibration was 0.31% for the analytical session.
(not included in above errors but required when comparing data from different mounts).

3. f_{206} % denotes the percentage of ^{206}Pb that is common Pb.

4. Correction for common Pb for the U/Pb data has been made using the measured $^{238}U/^{206}Pb$ and $^{207}Pb/^{206}Pb$ ratios following Tera and Wasserburg (1972) as outlined in Williams (1998).

	Age	± internal		**± include std: ie external**	
wtd ave main grouping	**159,9**	1,0	0,70	**1,1**	MSWD = 1.4 for 21 of 26 areas analysed

Table 2 b: Summary of SHRIMP U-Pb results for zircon from sample FC1759.

Grain. spot	U (ppm)	Th (ppm)	Th/U	$^{206}Pb^*$ (ppm)	$^{204}Pb/^{206}Pb$	f_{206} %	Total $^{238}U/^{206}Pb$	±	Total $^{207}Pb/^{206}Pb$	±	Radiogenic $^{206}Pb/^{238}U$	±	Age (Ma) $^{206}Pb/^{238}U$	±
1,1	452	353	0,78	5,1	0,000023	0,27	76,06	0,99	0,0498	0,0013	0,0131	0,0002	84,0	1,1
2,1	1459	1346	0,92	16,3	-	0,09	76,92	0,84	0,0484	0,0007	0,0130	0,0001	83,2	0,9
3,1	454	277	0,61	5,1	-	0,14	76,81	0,96	0,0488	0,0013	0,0130	0,0002	83,3	1,0
4,1	1840	1077	0,59	19,9	0,000113	0,02	79,33	0,85	0,0478	0,0006	0,0126	0,0001	~~80,7~~	~~0,9~~
5,1	293	177	0,60	3,2	-	0,15	77,85	1,07	0,0489	0,0016	0,0128	0,0002	82,2	1,1

Notes: 1. Uncertainties given at the one σ level.

2. Error in Temora reference zircon calibration was 0.31% for the analytical session.
(not included in above errors but required when comparing data from different mounts).

3. f_{206} % denotes the percentage of ^{206}Pb that is common Pb.

4. Correction for common Pb for the U/Pb data has been made using the measured $^{238}U/^{206}Pb$ and $^{207}Pb/^{206}Pb$ ratios following Tera and Wasserburg (1972) as outlined in Williams (1998).

	Age	± internal		**± include std: ie external**
wtd ave all	**82,5**	1,7	2,08	**1,7**
wtd ave less grain 4	**83,2**	1,0	1,24	**1,0**

MSWD = 1.8 for the 5 grains in the heavy min separate
MSWD = 0.45 for 4 of the 5 grains in the heavy min separate

Table 2 c: Summary of SHRIMP U-Pb results for zircon from sample FC1754.

Grain. spot	U (ppm)	Th (ppm)	Th/U	$^{206}Pb^*$ (ppm)	$^{204}Pb/^{206}Pb$	f_{206} %	Total Ratios $^{238}U/^{206}Pb$	±	$^{207}Pb/^{206}Pb$	±	Radiogenic Ratios $^{206}Pb/^{238}U$	±	$^{207}Pb/^{235}U$	±	$^{207}Pb/^{206}Pb$	±	ρ	Age (Ma) $^{206}Pb/^{238}U$	±	$^{207}Pb/^{206}Pb$	±	% Disc
1,1	568	76	0,13	79	0,000041	0,07	6,186	0,068	0,0755	0,0016	0,1615	0,0018	1,669	0,040	0,0749	0,0016	0,460	965	10	1066	43	9
2,1	773	596	0,77	14	0,000138	0,23	46,956	0,558	0,0506	0,0009	0,0212	0,0003						136	2			
3,1	257	75	0,29	28	-	<0.01	7,902	0,096	0,0757	0,0008	0,1266	0,0015	1,321	0,022	0,0757	0,0008	0,740	768	9	1087	22	29
4,1	357	387	1,08	6	0,000457	0,36	48,655	0,676	0,0515	0,0014	0,0205	0,0003						131	2			
5,1	111	72	0,65	2	-	0,12	48,813	0,975	0,0496	0,0025	0,0205	0,0004						131	3			
6,1	207	75	0,36	15	-	0,01	11,495	0,146	0,0583	0,0009	0,0870	0,0011						538	7			
7,1	319	36	0,11	21	-	<0.01	13,196	0,161	0,0548	0,0008	0,0759	0,0009						472	6			
8,1	251	79	0,31	17	0,000042	<0.01	12,658	0,160	0,0564	0,0009	0,0791	0,0010						490	6			
9,1	348	120	0,34	14	0,000139	<0.01	21,841	0,271	0,0520	0,0009	0,0458	0,0006						289	4			
10,1	480	59	0,12	31	-	0,04	13,199	0,151	0,0568	0,0007	0,0757	0,0009						471	5			
11,1	300	326	1,08	130	0,000015	0,02	1,989	0,023	0,1861	0,0007	0,5027	0,0057	12,886	0,154	0,1859	0,0007	0,952	2625	25	2706	6	3
12,1	57	40	0,70	1	0,002984	2,15	51,867	1,424	0,0656	0,0036	0,0189	0,0005						120	3			
13,1	272	241	0,89	8	0,000415	0,04	29,215	0,394	0,0508	0,0012	0,0342	0,0005						217	3			
14,1	139	79	0,57	2	0,001976	0,23	48,675	0,865	0,0505	0,0021	0,0205	0,0004						131	2			
15,1	95	43	0,45	2	0,000831	0,69	50,506	1,051	0,0540	0,0028	0,0197	0,0004						126	3			
16,1	281	88	0,31	49	-	<0.01	4,928	0,058	0,0838	0,0007	0,2030	0,0024	2,354	0,033	0,0841	0,0007	0,828	1191	13	1295	16	8
17,1	409	257	0,63	15	-	<0.01	22,987	0,279	0,0501	0,0009	0,0436	0,0005						275	3			
18,1	138	96	0,69	2	0,000783	<0.01	49,936	0,933	0,0453	0,0021	0,0201	0,0004						128	2			
19,1	114	57	0,50	2	-	0,33	48,319	0,947	0,0513	0,0025	0,0206	0,0004						132	3			
20,1	273	111	0,40	18	0,000107	0,07	13,335	0,166	0,0569	0,0009	0,0749	0,0010						466	6			
21,1	560	216	0,39	22	0,000030	0,24	21,577	0,251	0,0540	0,0008	0,0462	0,0005						291	3			
22,1	292	102	0,35	11	0,000172	0,02	22,738	0,293	0,0520	0,0011	0,0440	0,0006						277	4			
23,1	418	113	0,27	26	0,000043	0,06	13,708	0,159	0,0565	0,0007	0,0729	0,0009						454	5			
24,1	462	81	0,17	52	0,000011	0,02	7,625	0,087	0,0678	0,0006	0,1311	0,0015	1,223	0,018	0,0677	0,0006	0,769	794	8	858	20	7
25,1	429	94	0,22	24	-	0,10	15,304	0,179	0,0557	0,0007	0,0653	0,0008						408	5			
26,1	125	56	0,45	2	0,000568	0,16	49,166	0,918	0,0499	0,0023	0,0203	0,0004						130	2			
27,1	78	75	0,96	3	0,000313	<0.01	22,393	0,414	0,0514	0,0020	0,0447	0,0008						282	5			
28,1	67	36	0,53	3	0,000423	<0.01	23,000	0,444	0,0504	0,0022	0,0436	0,0009						275	5			
29,1	52	22	0,42	1	0,001169	0,30	51,146	1,381	0,0509	0,0039	0,0195	0,0005						124	3			
30,1	269	100	0,37	5	0,000921	0,15	47,963	0,709	0,0499	0,0015	0,0208	0,0003						133	2			
31,1	570	313	0,55	101	-	<0.01	4,850	0,053	0,0844	0,0006	0,2062	0,0022	2,402	0,031	0,0845	0,0006	0,856	1209	12	1303	13	7
32,1	55	29	0,53	1	-	0,13	53,278	1,428	0,0494	0,0037	0,0187	0,0005						120	3			
33,1	108	38	0,35	6	0,000390	0,40	14,735	0,223	0,0585	0,0018	0,0676	0,0010						422	6			
34,1	172	122	0,71	6	-	<0.01	23,342	0,338	0,0516	0,0014	0,0428	0,0006						270	4			
35,1	47	25	0,54	1	0,002269	10,69	46,656	1,295	0,1334	0,0069	0,0191	0,0006						122	4			
36,1	746	309	0,41	29	0,000041	<0.01	22,141	0,248	0,0515	0,0006	0,0452	0,0005						285	3			
37,1	90	39	0,43	1	0,000431	0,45	52,517	1,136	0,0520	0,0028	0,0190	0,0004						121	3			
38,1	122	52	0,43	2	0,000452	<0.01	50,652	0,972	0,0480	0,0023	0,0198	0,0004						126	2			
39,1	391	245	0,63	51	-	<0.01	6,596	0,074	0,0792	0,0006	0,1517	0,0017	1,667	0,024	0,0797	0,0007	0,797	911	10	1189	17	23
40,1	72	37	0,52	1	0,000004	0,19	46,566	1,056	0,0503	0,0030	0,0214	0,0005						137	3			
44,2	1692	29	0,02	95	0,000034	0,04	15,360	0,160	0,0552	0,0004	0,0651	0,0007						406	4			
41,1	929	778	0,84	34	0,000037	0,03	23,328	0,257	0,0519	0,0006	0,0429	0,0005						271	3			
42,1	77	48	0,62	3	0,000644	0,18	21,716	0,400	0,0535	0,0020	0,0460	0,0009						290	5			
43,1	81	30	0,37	6	-	<0.01	11,429	0,185	0,0577	0,0015	0,0876	0,0014						541	9			
44,1	193	42	0,22	22	-	<0.01	7,471	0,094	0,0739	0,0009	0,1338	0,0017	1,364	0,024	0,0739	0,0009	0,714	810	10	1038	25	22
45,1	749	356	0,47	28	0,000040	0,04	23,156	0,259	0,0520	0,0007	0,0432	0,0005						272	3			
46,1	128	62	0,48	2	0,000286	0,07	50,985	0,945	0,0491	0,0023	0,0196	0,0004						125	2			
47,1	169	109	0,64	3	0,000247	0,48	49,656	0,885	0,0524	0,0022	0,0200	0,0004						128	2			
48,1	137	53	0,39	5	0,000156	0,25	23,736	0,374	0,0536	0,0016	0,0420	0,0007						265	4			
49,1	672	38	0,06	44	0,000017	0,04	13,238	0,145	0,0568	0,0005	0,0755	0,0008						469	5			
50,1	782	58	0,07	61	-	0,20	11,051	0,119	0,0604	0,0005	0,0903	0,0010						557	6			
51,1	695	159	0,23	45	-	<0.01	13,276	0,147	0,0559	0,0006	0,0754	0,0008						468	5			
52,1	242	160	0,66	4	0,000314	<0.01	51,601	0,793	0,0479	0,0017	0,0194	0,0003						124	2			
53,1	64	32	0,50	1	0,000710	0,05	51,977	1,306	0,0488	0,0033	0,0192	0,0005						123	3			
54,1	439	264	0,60	8	0,000364	<0.01	47,684	0,628	0,0478	0,0012	0,0210	0,0003						134	2			
55,1	609	501	0,82	21	-	0,09	25,214	0,290	0,0519	0,0008	0,0396	0,0005						251	3			
56,1	99	53	0,54	2	0,000184	0,60	51,418	1,043	0,0533	0,0027	0,0193	0,0004						123	3			
57,1	56	25	0,46	1	0,001789	0,09	49,985	1,326	0,0493	0,0035	0,0200	0,0005						128	3			
58,1	374	222	0,59	6	-	<0.01	52,133	0,718	0,0473	0,0013	0,0192	0,0003						123	2			
59,1	215	107	0,50	38	0,000084	0,14	4,805	0,059	0,0844	0,0008	0,2078	0,0025	2,384	0,039	0,0832	0,0009	0,737	1217	14	1274	22	4
60,1	226	86	0,38	43	0,000004	0,01	4,488	0,054	0,0874	0,0007	0,2228	0,0027	2,683	0,039	0,0874	0,0007	0,827	1297	14	1368	16	5
61,1	157	80	0,51	22	0,000040	0,07	6,082	0,078	0,0812	0,0009	0,1643	0,0021	1,827	0,033	0,0806	0,0010	0,710	981	12	1213	25	19
62,1	440	89	0,20	82	-	<0.01	4,588	0,051	0,0833	0,0006	0,2180	0,0024	2,510	0,033	0,0835	0,0006	0,849	1271	13	1281	13	1
63,1	463	224	0,48	31	-	0,10	12,878	0,147	0,0575	0,0007	0,0776	0,0009						482	5			
64,1	591	369	0,62	20	0,000070	<0.01	24,969	0,292	0,0513	0,0008	0,0401	0,0005						253	3			
65,1	132	64	0,49	2	0,000356	<0.01	50,719	0,929	0,0470	0,0022	0,0198	0,0004						126	2			
66,1	301	198	0,66	5	0,000355	0,16	52,215	0,757	0,0497	0,0015	0,0191	0,0003						122	2			
67,1	144	69	0,48	2	0,000513	0,04	50,052	0,906	0,0489	0,0022	0,0200	0,0004						127	2			
68,1	250	234	0,93	4	-	<0.01	49,160	0,740	0,0479	0,0016	0,0204	0,0003						130	2			
69,1	621	502	0,81	23	0,000158	<0.01	23,175	0,267	0,0513	0,0007	0,0432	0,0005						272	3			
70,1	970	459	0,47	56	0,000010	0,02	14,872	0,160	0,0553	0,0005	0,0672	0,0007						419	4			

Notes :

1. Uncertainties given at the one σ level.
2. Error in Temora reference zircon calibration was 0.28% for the analytical session.
   (not included in above errors but required when comparing $^{206}Pb/^{238}U$ data from different mounts).
3. f_{206} % denotes the percentage of ^{206}Pb that is common Pb.
4. For areas older than ~800 Ma correction for common Pb made using the measured $^{204}Pb/^{206}Pb$ ratio.
5. For areas younger than ~800 Ma correction for common Pb made using the measured $^{238}U/^{206}Pb$ and $^{207}Pb/^{206}Pb$ ratios following Tera and Wasserburg (1972) as outlined in Williams (1998).
6. For % Disc, 0% denotes a concordant analysis.

3.6 $^{40}Ar/^{39}Ar$ dating

One sample of metapelite of Zapata Fm. (SHP141) was analyzed in the Open University $^{40}Ar/^{39}Ar$ Laboratory. Polished thick sections of this sample were broken into 5x5mm2 squares, washed in acetone and distilled water before packing into foil packets. Mica mats were analysed by spot-dating using an SPI SP25C 1090 nm laser focussed through a Leica microscope, coupled to an automated extraction system and a Nu Noblesse mass spectrometer. Neutron fluence was monitored using the GA1550 biotite standard with an age of 98.79±0.54 Ma (Renne et al., 1998). J values were calculated by linear interpolation between two bracketing standards; a standard was included between every 8 and 10 samples in the irradiation tube. Results were corrected for blanks, ^{37}Ar decay and neutron-induced interference reactions. Typical blank measurements are included for each sample and tabled data are blank corrected. Background measurements bracket every 1–2 samples. The correction factors used were: $(^{39}Ar/^{37}Ar)Ca=0.00065$, $(^{36}Ar/^{37}Ar)Ca=0.000265$, $(^{40}Ar/^{39}Ar)K=0.0085$ based on analyses of Ca and K salts. Analyses were also corrected for mass spectrometer discrimination. The branching ratio of Steiger and Jaeger (1977) were used.

4 RESULTS: THE MAGALLANES FOLD-AND-THRUST BELT (52-54ºS)

The Rocas Verdes ophiolites are located ca. 50 km to the west of the present-day front of the MFTB (Figs. 1 and 2). They occur in tectonic slices that share fault bounded contacts in a narrow zone of imbricated thrust sheets consisting of strongly N-S to NW-SE trending and west dipping foliated succession of volcano-sedimentary rocks belonging to the Tobífera and Zapata formations (Fig. 2), which is itself internally thrusted and folded, with east-dipping foliations in the innermost part of the belt, interleaved with pre-Jurassic basement slices by thrusts (Stewart et al., 1971; Allen, 1982; Harambour, 2002; Calderón, 2006, 2012; Betka et al., 2015). The various imbricated tectonic slices of pre-Jurassic and Late Jurassic-Early Cretaceous rocks of the RVB, are cross cutted by meter-wide dikes of lamprophyre and plutonic rocks outside of the limits of the South Patagonian Batholith (Calderón et al. 2012).

Figure 2: Geologic map of the study area and stereographic projections of foliations and lineations measured in the field work.

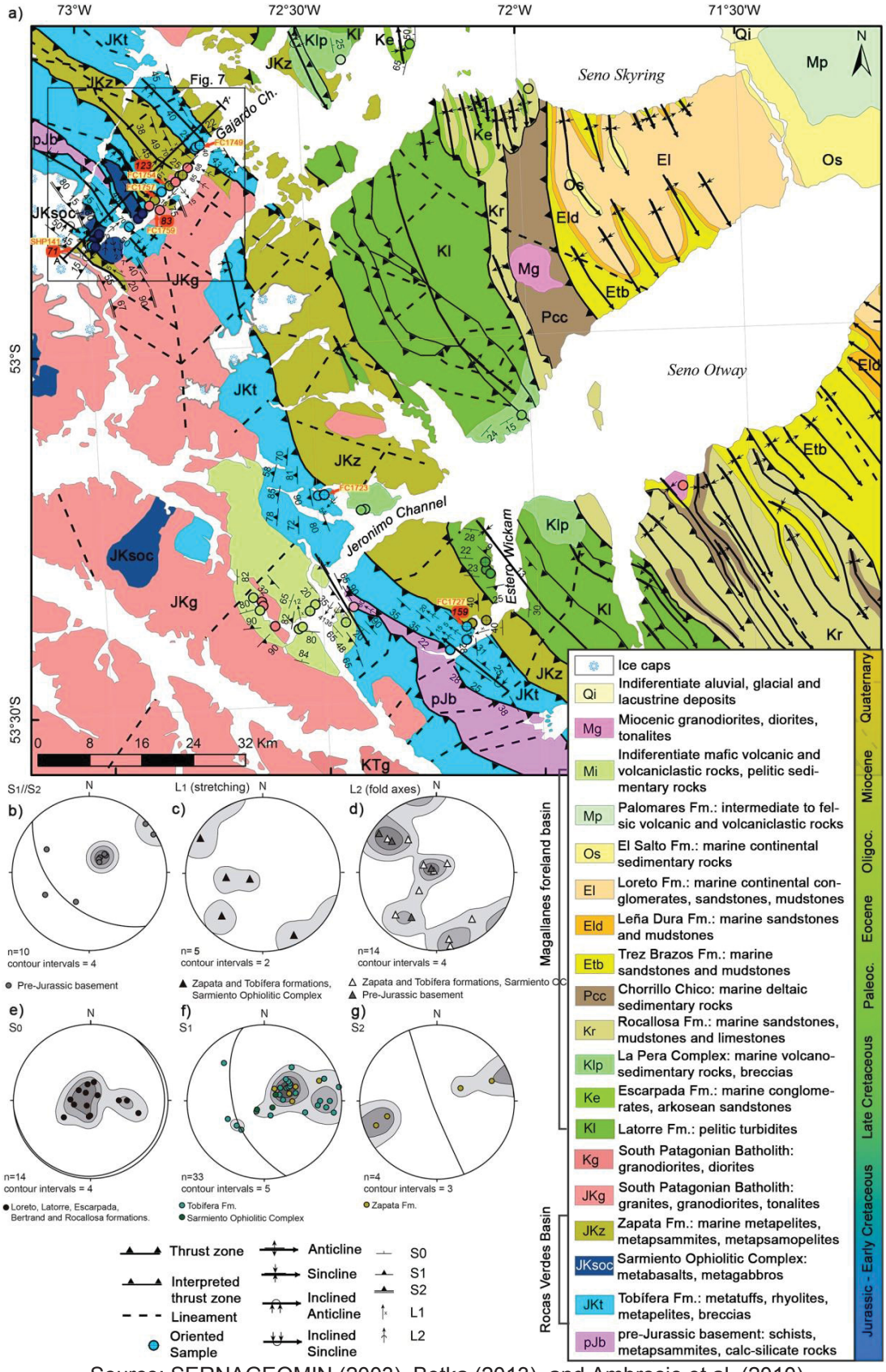

Source: SERNAGEOMIN (2003), Betka (2013), and Ambrosio et al. (2010).

Eastwards to the foreland of the belt, the sedimentary successions of the Zapata Fm. are overlain by Late Cretaceous marine distal turbidites of the

Latorre Fm., marine channel conglomerates of the Escarpada Fm., and shallow marine deposits of the Fuentes and Rocallosa formations (Mpodozis et al., 2007; McAtamney et al., 2011) grading to the to the continental Cenozoic units of the Magallanes Basin, like the metapelites of Loreto Fm. cropping-out in the Estero Wichkam. The foreland is also folded and thrusted internally by a thin-skinned tectonics of open to gentle folds of tens of meters of waveleght and steep thrust faults of N-S trending and dipping to the west (Fig. 2 a; Kley et al., 1999; Hervé et al., 2010b; Fosdick et al., 2011; Betka et al., 2015). In depth, the sedimentary sucessions of Magallanes basin and the underlying Late Jurassic-Early Cretaceous layers of the RVB are unconformably seated over the pre-Jurassic basement, which is constituted by Cambrian high-grade rocks of the Tierra del Fuego Igneous and Metamorphic Complex (Fig. 3; Harambour, 2002; Hervé et al., 2010b).

Figure 3: Seismic cross-section of the Magallanes Basin and interpreted subsurface RVB and pre-Jurassic basement strata and structures.

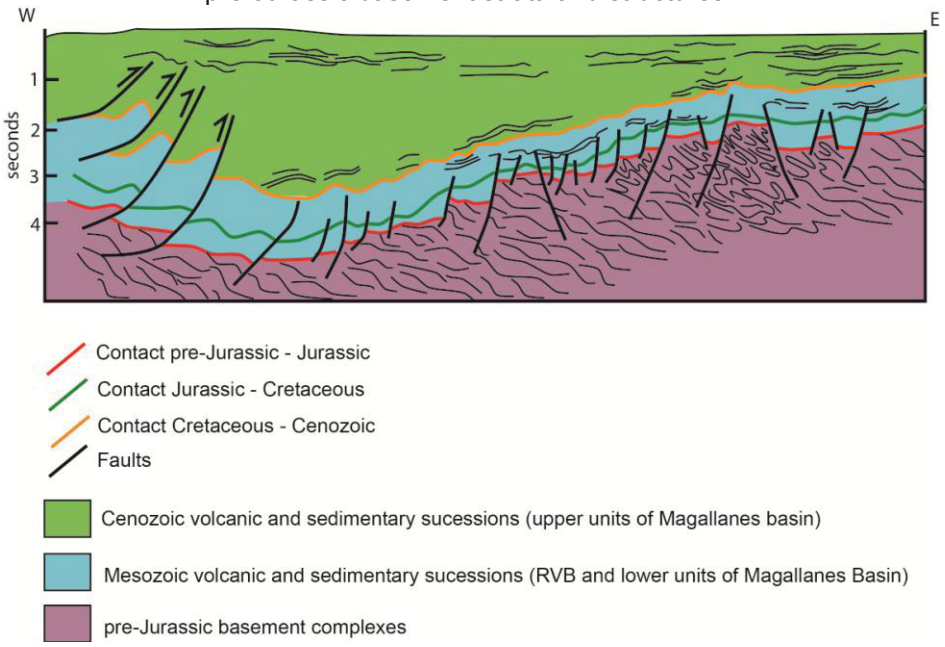

Source: Hervé et al. (2010b).

The figure 3 shows an interpreted seismic cross-section of the eastern domain of the MFTB focused on the Magallanes Basin, sectioning the eastern region between the Otway and Skyring sounds (Harambour, 2002; Hervé et al., 2010b). Analysing this cross-section it is clear the trasition from major thrust faults dipping in intermediate to high angle to the west, in the western domain, affecting the pre-Jurassic basement, the Mesozoic and the Cenozoic layers, to a sequence of steep normal faults dipping to the west, conjugated with some

normal faults dipping to the east, forming a horst-grabben system in the eastern domain. These normal faults affect the pre-Jurassic basement and the Mesozoic units, but cause negligible deformation on the Cenozoic units of the Magallanes Basin, which change from greater to minor thickness. The geometries of Mesozoic reflectors include open to closed fault-propagation-folds above the thrusts on the western domain, related to the shortening of the RVB, and gentle folds above the horsts and grabbens, associated to deposition syn-deformational during the rifting of the pre-Jurassic basement, on Late Jurassic-Early Cretaceous times. The transitional change from thrusts in the west to normal faults in the east, with similar steep dipping to the west, suggest the role of the inherited normal faults of the rift phase as preferred planes of reactivation to the thrust system. At least at the eastern boarder of the RVB, the displacements of pre-Jurassic basement by the thrusts are of few metters to the east, but the contact with the Mesozoic units serves as a detachment level and decoupling of the overlying units that are considerable more shortened.

The following sections describe the lithostratigraphic units observed in field with structural and petrographic remarks, highlighting their main characteristics, and they are presented in the figure 4 as a summary.

Figure 4: Synthesis of the petrographic features of the observed units in this study: a) calc-silicate rock of the pre-Jurassic basement of Jeronimo Channel (FC1721) and b) correspondent photomicrograph showing the S1//S2 pair of foliations; c) metatuff of Tobífera Fm. of Gajardo Channel (FC1749) and d) correspondent photomicrograph showing the stretching of porphyroclasts of quartz and micaceous domains defining the mylonitic foliation S1; e) pillow basalt of the SOC of Gajardo channel (FC1760) and f) correspondent photomicrograph; g) diorite of Western Gajardo channel (FC1759) intrusive to Zapata Fm. and h) correspondent photomicrograph showing phaneritic texture; i) deformed metapsammite of Zapata Fm. of Gajardo Channel (FC1753) with the S1 and S2 foliations, and j) photomicrograph of metapsammite (FC1757) of Zapata Fm. of Gajardo Channel with thermal overprinting near the intrusive diorite (FC1759); k) turbidites of the Escarpada Fm. of Escarpada Island in Skyring sound (FC1744) showing the erosive contact in the top of a normal grading muddy layer; l) correspondent photomicrograph of conglomerates.

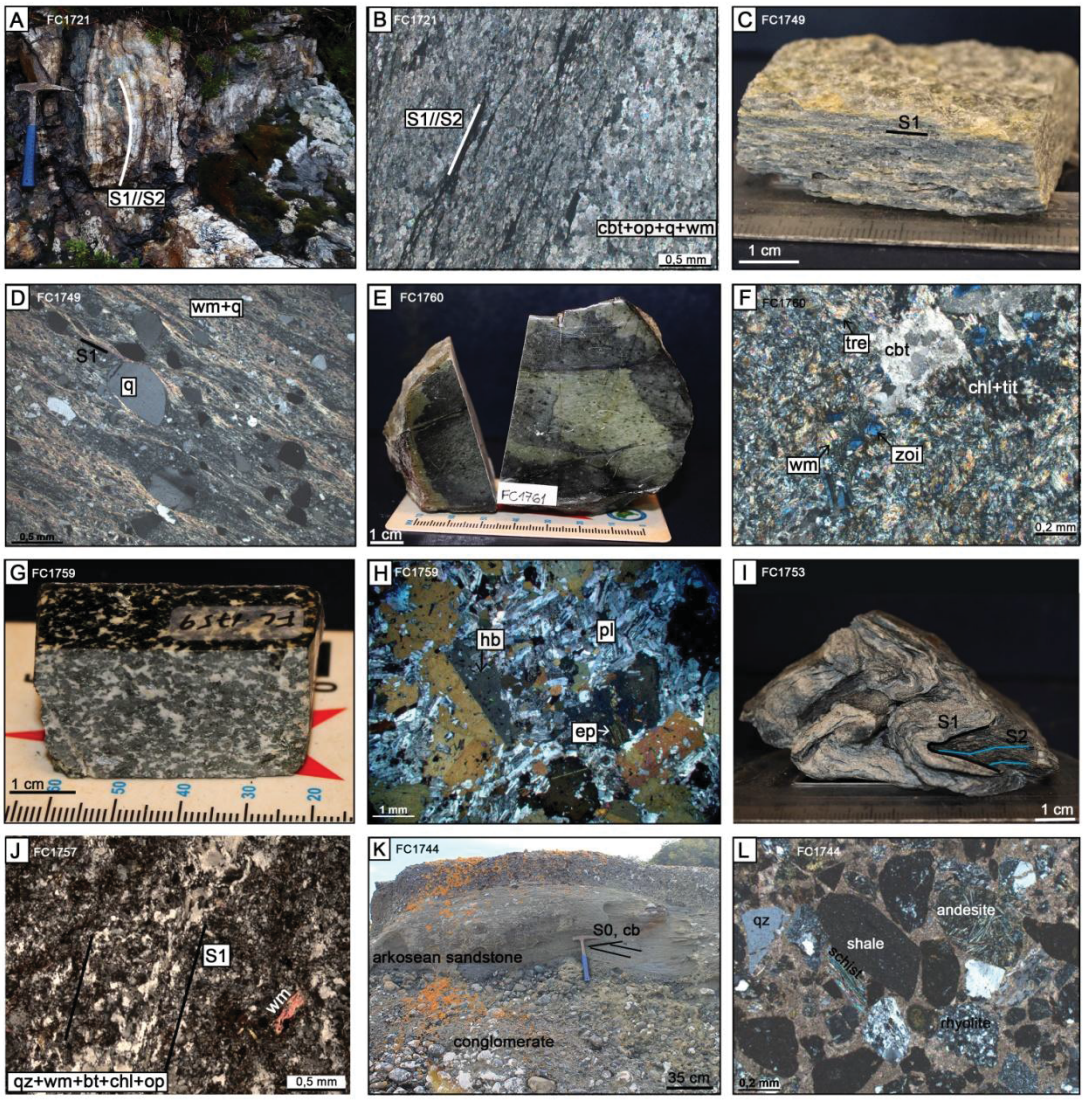

4.1 Pre-Jurassic Basement

The basement of the RVB consists of metapelites, metapsammites and calc-silicate rocks, in layers of meters and tens of meters of thickness, frequently in contact with Tobífera sheets. Metapelites and metapsammites are fine to very fine-grained constituted mainly of quartz, plagioclase, alkali-

feldspar, micaceous minerals as white mica, chlorite and biotite, and opaques, in different proportions (Fig. 4 a, b). The quartz crystals often have planar and polygonal contacts, and undulose extinction, bulging, and subgrain rotation, which are common microstructures attesting dynamic recrystallization. The plagioclase and alkali-feldspar have curvilineous contacts. The micaceous minerals are preferred oriented insterstitial to quartz or concentred in cleavage domains defining a mm-spaced schistosity “S1” formed by solution pressure. The opaque minerals are anhedric, concentred in submilimetric layers parallel to the schistosity. Calc-silicatic rocks are composed of carbonate (up to 80%), white mica, quartz, opaques and epidote. The carbonate has planar contacts and is preferred oriented with sigmoidal geometry, surrounded by preferred oriented white mica, and opaques concentred in submilimetric discontinuous and anastomosed layers.

Thus, the foliation S1 is a schistosity milimetricaly spaced, continuous to discontinuous and anastomosed, trending northwest-southeast and dipping from low to high angles to the southwest and to the northeast (Fig. 2 b). The S1 is often crenulated in milimetric open folds, micaceous minerals and fine layers of opaques also might be preferred oriented in planes oblique to the S1 schistosity, defining a S2 crenulation foliation which has similar spatial orientations with S1 (Fig. 2 b). Centimetric kink bands, and open to tight folds up to 30 cm of wavelength also occur affecting the S1 and S2. Fold axes lineations plunge with low-dip angle to the northeast, or anomalously plunge to the southwest or are subvertical (Fig. 2 d).

4.2 Tobífera Fm.

The Tobífera Fm. is mainly represented by tens of meters-thick tectonic slices of metatuffs (Fig. 4 c, d; Fig. 5 a, c) intercalated with metasiltones in layers up to 2 meter of thickness (Fig. 6 c, d), and local occurrences of rhyolites and breccias. The felsic metatuffs have mm-sized porphyroclasts of quartz, feldspars and rhyolite, placed in a very fine matrix of quartz, white mica, chlorite, epidote and opaques (Fig. 4 c, d). The volcaniclastic stratification might be preserved in outcrop scale and in thin-sections by an anastomosed preferred orientation of undeformed porphyroclasts and very fine-grained quartz-mica in the matrix. Light gray rhyolites are massive with spherulites of 1 to 2 mm which

are placed in a very fine-grained matrix with relic granophyric texture. The volcaniclastic breccias consist of up to 1.5 cm rectangular clasts of schists, probably incorporated in pyroclastic flows during continental rifting.

Figure 5: a) Contact of Tobífera Fm. over Zapata Fm. in Estero Wickam, by a thrust zone with top to the northeast. B) Outcrop of Zapata Fm. with metapelites intercalled with boudinated layers of metapsammites; c) metatuff of Tobífera Fm. with the S-C-type S1 foliation; d) photomicrograph of Zapata metapelite (FC1728) showing the S-C-type S1 foliation that disrupts recrystallized quartz veins; e) photomicrograph of Tobífera metatuff (FC1727) with broken porphyroclasts of feldspars an stretched quartz, truncated by cleavage domains of white mica, chlorite and opaque minerals. Abbreviations: JKz: Zapata Fm.; JKt: Tobífera Fm.

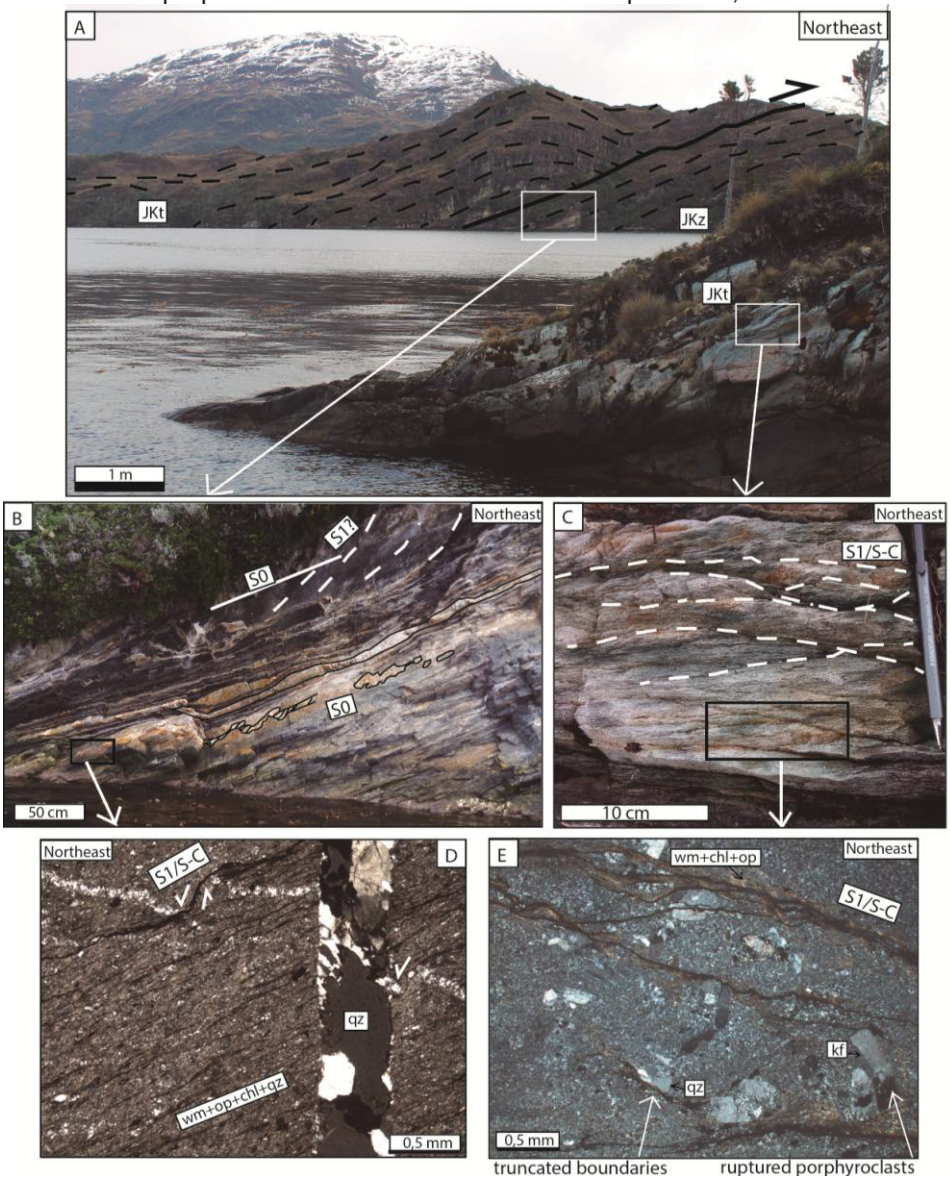

Some corridors of strained metatuffs are protomylonitic, in which porphyroclasts of quartz are stretched, they present trails of fluid inclusions, undulose extinction, subgrains, fish geometries and strain shadows of quartz and white mica, formed by dislocation creep and solution pressure (Fig. 4 d). The feldspars have undulose extinction and are normally broken and disrupted,

showing a more brittle behaviour than quartz. On these corridors the white mica and chlorite are recrystallized, they are preferred oriented and concentred in continuous and discontinuous cleavage domais that surround the porphyroclasts, defining a S-C-type composite foliation thermed “S1”, presented in figure 4 (c, d) and 5 (c, e). The S1 trends north-south to northwest-southeast and has low to high-dip angles to southwest and northeast (Fig. 2 f). Open metric to tens of meters folds have regional expression and crop-out the region, associated to thrust zones, like showed in figure 5 where Tobífera Fm. is thrusted over Zapata Fm (Fig. 5 a). Stretching lineations of quartz are dip-directed and plunge to the south with low-dip angle, or to the west with high-dip anlge (Fig. 2 c). Sets of up to 10 cm-thick parallel quartz veins cut obliquely the stratification, as showed in figure 6, they are sheared and openly to closely folded and the fold axes are subhorizontal plunging to the south, or anomalously subvertical plunging to the southwest or northeast (Fig. 2 d). Some polycrystalline quartz porphyroclasts seems derived from early quartz veins, suggesting progressive deformation (Fig. 6 a).

Dark metapsammites have a slaty cleavage that is also an expression of the S-C-type S1 defined by preferred oriented white mica, chlorite, platy quartz and opaques in one or two composite planes, mm-porphyroclasts of quartz and pyrite show strain fringes and strain shadows of quartz and white mica. These metapelites may present a complex deformation with closed disarmonic and discontinuous closed mm-folds disrupted and strained, transposed by a possible S2 foliation, showed in Fig. 6 b, c.

Figure 6: Different occurrences of the S1 and S2 foliations in Tobífera and Zapata formations: a) Tobífera metatuff of the Jeronimo Channel (FC1723) and interpretation of S1 as the mylonitic foliation folded in tight folds related to straining during mylonitizations (F1), and openly folded by F2; quartz veins are tension gashes resulting from the progressive deformation; b) photomicrograph (natural light) of Tobífera metapsammite of the westernmost Gajardo Channel (FC1770) with complex deformation, the S1 schistosity is tightly folded inside microlithons of the S2 mylonitic foliation, in c) the same thin-section (polarized light) showing portions with dynamic recrystallized quartz parallel to S2 foliation; d) Zapata metapsammite of the Gajardo Channel (FC1753) with complex deformation, the S1 foliation is folded and ruptured by a S2 mylonitic foliation, in d) the S1 foliation is overprinted by the S2, quartz microlithons present grain boundary migration.

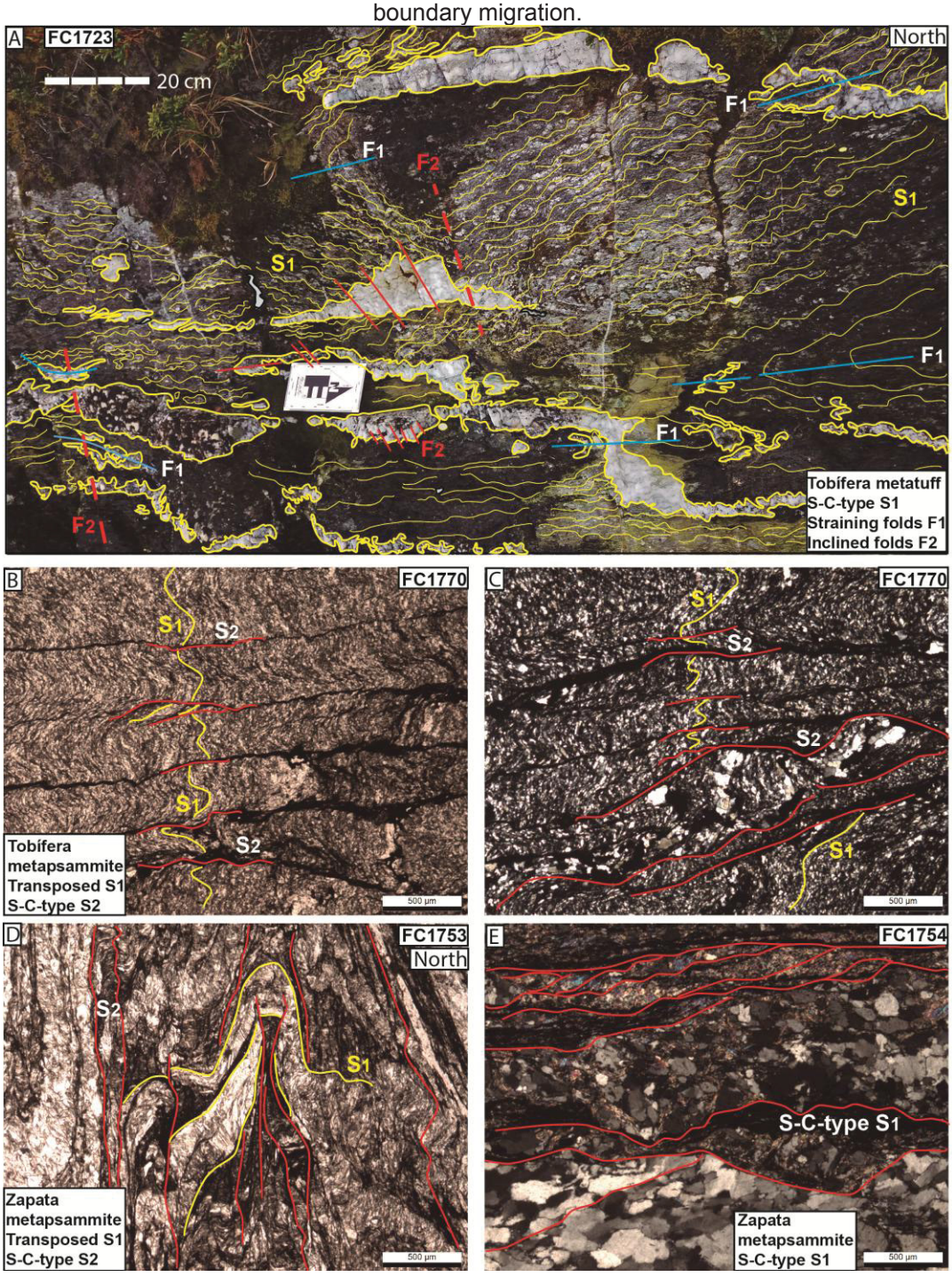

4.3 Sarmiento Ophiolitic Complex

Outcrops of tens of meters in the middle portion of the Gajardo Channel (Fig. 2a) are composed by massive and pillow basalts, interpreted as remnants of the upper section of the Sarmiento Ophiolitic Complex (or eventually interbedded lava flows within the Tobífera Fm) thrusted upon Zapata and Tobífera layers. The primary mineralogy has been erased and is variably constituted by tremolite-actinolite, titanite, epidote, chlorite, plagioclase (albite), carbonate and quartz (Fig. 4 e, f). Carbonate and quartz filling cavities and fractures between pillow structures, indicate their crystallization from CO2-rich fluids after the emplacement of pillow lava flows (Fig. 4 f). In the western portion of the Gajardo Channel, near the boundary with the South Patagonian Batholith (the innermost domain of the MFTB), fine to medium grained foliated metabasalts are composed by plagioclase, stretched and folded actinolite porphyroblasts, and preferred oriented chlorite defines cleavage domains of a disjunctive foliation S1, crenulated in milimetric disarmonic open folds, which is probably associated to ductile shear zones in the boundary of the ophiolites. Metabasalts are also folded in centimeter to meter scale. The S1 foliation on this location trends northwest-southeast and dip to the southwest and northeast due to folding (Fig. 2 f). Microveins of carbonate can be parallel to the main foliation suggesting that CO2-enriched fluids interacted with the rock during the main deformation.

4.4 Zapata Fm.

Zapata Fm. is constituted by dark metapelites and metapsammopelites with intercalations with cm-thick layers (1 to 20 cm) of metapsammites (Fig. 5 a), with variable proportions of quartz, feldspar, micas, and opaque minerals (Fig. 4 I, j). The metapelites and metapsammites often present flattened quartz grains and preferred oriented white mica, chlorite, clays and opaque layers defining an anastomosed slaty cleavage “S1”. In some localities, for example in the middle portion of Gajardo Channel (*e.g.* sample FC1754, Fig. 6 e), the metapsammites are strongly recrystallized and a schistosity is defined by mm-thick microlithons of polygonal quartz with bulging and subgrain rotation, and white mica cleavage domains that present a composite S-C-type preferred

orientation (Fig. 5 d, Fig. 6 e), showing the shearing character of S1. In Gajardo Channel, the S1 show a complex pattern of deformation, the microlithons are folded in mm-to-cm closed folds that are disarmonic and discontinuous, the flanks are broken and displaced by a possible “S2” foliation, the hinges are strained, parallel to a preferential plane where opaque minerals concentrate and the micaceous minerals are oriented in composite S-C-type geometries (Fig. 6 d). This suggest that the sedimentary bedding “S0” is deformed and totally recrystallized to the quartz-microlithons and micaceous-opaque cleavage domains of the foliation thermed “S1”, crenulated and transposed by a S2 crenulation cleavage that also assumes a mylonitic character with straining of S1. The S1 foliation trend north-south to northwest-southeast and dip to southwest in medium to high-dip angle (Fig. 2 f), while the S2 trend NNW-SSE and dips in high angle to the northeast with (Fig. 2 g) The fold axes of crenulations plunge with low-dip angle to southeast or southwest, and some of them anomalously plunge to the northwest (Fig. 2 d).

The lithic sandstone layers have up to 15 cm of thickness are probably part of the turbiditic upper member of the Zapata Fm. (Fig. 5 b). They are deformed and stretched forming boudins, and present an anastomosed disjunctive cleavage S1. Quartz veins cross cut the Zapata outcrops and might be folded, ruptured and displaced by the anastomosed mylonitic foliation (Fig. 5 b, d). These features are well observed in the footwall of the reverse thrust fault between the foliated Tobífera sheet and the underlying folded Zapata Fm presented on the figure 5.

4.5 Satelite Plutons

The RVB units are locally intruded by plutons of diorites, tonalites and granodiorites located outside the limits of the South Patagonian Batholith (Fig. 2 a; Fig. 4 g, h), that are massive to magmatic foliated, medium grained and are constituted by euhedric to subhedric hornblende with inclusions of euhedric plagioclase and epidote, the anfibole is weakly altered to chlorite; euhedric to subhedric plagioclase that is moderately altered to sericite, and might be zoned; and anhedric titanite. These intrusive rocks can present enclaves of metapelitic rocks up to 15 cm of diameter. The outcrops can range from metric intrusions to entire mountains of tens of kilometers, rising from the sea level up to 1400

meters, often covered by ice caps. Straight and milimetric quartz veins are common in preferential directions and high dip angle.

4.6 Cretaceous Units of Magallanes Basin

The Upper Cretaceous sedimentary record of deep to shelf marine environments in the Magallanes Basin is marked by the transition from backarc to retroarc environment on the foreland. On the western part of the MFTB in Seno Otway, low density currents turbidites of the Latorre Fm. are present in three cycles of 1 meter of thickness: poorly sorted sandstones that grade normally to shales on the top. On Seno Skyring, lithic sandstones, shales and clasts sustained conglomerates with carbonatic matrix and many well-preserved fossils of mollusks, foraminifers and ostracods, constitute the Bertrand Fm. Pyroclastic/volcaniclastic sucessions of La Pera Complex are lithic sandstones composed by angular clasts of quartz, plagioclase and mafic lithic clasts in a poor selected fine matrix. At Isla Escarpada turbiditic sucessions of high-density currents of the Escarpada Fm. are represented by layers up to 10 meter of thickness of lithic conglomerates sustained by polimitic rounded clasts of meteplitic rocks, rhyolites and schists, intercalated to coarse lithic sandstones (Fig. 4 k, l). To the east of Seno Skyring, the Rocallosa Fm. are wackstones composed by micritic matrix with calcispheres, oolites, ostracodes, algaes, and other undetermined fossils, and plagioclase angular fragments. On the eastern Estero Wichkam the Loreto Fm. crops-out in metapsamopelites constituted by quartz, clays, white mica, carbonate and opaques, with planar stratification and convolute folds, over planar layers of black shales composed essentially of clays. The sedimentary bedding in the Magallanes Basin rocks is subhorizontal to gently dipping to the southwest (Fig. 2 e).

5 INTEGRATED STRUCTURAL GEOLOGY AND KINEMATIC ANALYSIS

The lithotypes of the three main units of the Rocas Verdes Basin – Tobífera Fm., Zapata Fm., and Sarmiento Ophiolitic Sarmiento – in the study area present in common the occurrence of a metamorphic foliation “S1” characterized by discontinuous and continuous cleavage domains of preferred oriented micaceous minerals, normally white mica and/or chlorite, and stretched

sigma-shaped porphyroclasts and porphyroblasts that often have strain shadows and strain fringes of quartz. The pressure solution is the main recrystallization mechanism, forming the micaceous domains in flat contact with the quartz-feldspatic porphyroclasts and microlithons, as well as the strain shadows and strain fringes. Quartz porphyroclasts often have fluid inclusion trails suggesting twining before pressure solution on its boundaries, because these trails are truncated by the cleavage domains.

Nevertheless, this foliation (S1) also was diagnosed as a mylonitic foliation by the dynamic recrystallization microstructures, as bulging and subgrain rotation in quartz, where dislocation creep is the active recrystallization mechanism, besides fish geometries of strained quartz, white mica, chlorite, and actinolite (metabasalts), and the S-C-type geometry that cleavage domains normally present, sometimes involving a complex disarmonic and discontinuous folding of the primary bedding (*e.g.* Zapata metapsammites, and metapelitic layers of Tobífera Fm., Fig. 6 b-d). It is important to note that feldspars of Tobífera Fm. are deformed with a brittle behavior, normally broken instead of plastically stretched, whereas the quartz is plastically stretched in the same litothypes (metatuffs, Fig. 4 b, c; and 5 e), what testify the deformation in the brittle-ductile transition on metatuffs, characterizing the S1 as protomylonitic in these rocks.

Therefore, the S1 (proto)mylonitic foliation in the RVB lithotypes is considered a result of shearing that occurs widely in Tobífera metatuffs, with brittle-ductile character, widely in Zapata metapelites and metapsammites, with a ductile character, and localized in strained metabasalts of the Sarmiento Ohpiolitic Complex, with a ductile character. The primary structures and minerals of the protoliths are partially recognized. This deformational phase was thermed “D1”, characteristically non-coaxial and decurrent of Andean metamorphism in shear zones associated to the closure of the RVB, involving corridors with complex deformation.

Table 3: Table of oriented samples. The attitudes are at Clar notation (Dip direction/dip angle). The vergence is a suggestion of direction of shearing in accordance with microtectonic indicators.

Locality	Latitude	Longitude	Unit	Lithology	Sample	S0		S1		S2		Thin sect	Vergence
Estero Condor	-53° 22.216'	-72° 31.757'	Miocene Indiferentate	Slate	FC1718			235	32			199	55 NE
West of Cutter cove	-53° 22.446'	-72° 27.532'	Miocene Indiferentate	Slate	FC1720			240	38			187	50 E
Isla Santa Cruz	-53° 12.592'	-72° 28.992'	Tobífera Fm.	Metatuff/mylonite	FC1723			265	85			309	31 NE-sinistral
Estero Wickham	-53° 25.090'	-72° 09.259'	Tobífera Fm.	Metatuff/mylonite	FC1727			230	25			89	90 N-E
Estero Wickham	-53° 23.663'	-72° 07.333'	Zapata Fm.	Metapsammite	FC1729			175	28			119	60 NE
Estero Wickham	-53° 18.979'	-72° 06.379'	Latorre Fm.	Slate	FC1731	170	9	10	22			189	75 NE
Estero Wickham	-53° 18.979'	-72° 06.379'	Latorre Fm.	Slate	FC1732	352	23	145	25			296	85 NE
Canal Gajardo (spot 1)	-52° 43.218'	-72° 43.841'	Tobífera Fm.	Metatuff/mylonite	FC1749			230	25			296	80 NE
Canal Gajardo (spot 3)	-52° 45.421'	-72° 46.252'	Zapata Fm.	Metapsammite	FC1753					230	49	158	90 N
Canal Gajardo (spot 10)	-52° 51.004'	-72° 58.737'	Ophiolite	Metabasalt/mylonite	FC1763			225	20			349	85 N
Canal Gajardo (spot 10)	-52° 51.004'	-72° 58.737'	Ophiolite	Metabasalt/mylonite	FC1765			25	45			159	80 NE
Canal Gajardo (spot 11)	-52° 49.914'	-72° 57.483'	Ophiolite	Metabasalt	FC1768			240	90			349	88 none

The statistical analysis of poles of S1 show a greater concentration in the northeast quadrant (~065/54), reflecting the majority of foliation planes trending northwest-southeast and dipping moderately to southwest (Fig. 2 f). Nevertheless, the dipping angles can be steeper, and to northeast as well. The alignment of poles forms a ~E-W girdle suggesting a fold pattern of horizontal fold axes trending N20W. The stretching lineations on planes dipping to the southwest normally has a dip-direction plunging subhorizontaly or steeply (~70°) to the south or to the west, suggesting thrusting with vergence to the northeast and to the east. Twelve oriented samples of Tobífera and Zapata formations, and Sarmiento ophiolites were collected in the field and they are listed on the Table 4 with their respective kinematic indicators, which were sigma-shaped porphyroclasts and porphyroblasts, and S-C-geometries of the foliation S1. When they could be reconstructed showed top to the north and northeast vergence as well, which are the transportation directions of thrusts and could be associated with the emplacement of Sarmiento ophiolites. The timing of metamorphism and pressure-temperature conditions of formation of S1 will be discussed in the following sections with the geochronologic analysis (section 6) and the P-T pseudosections (section 7).

The foliations S1 and S2 of the pre-Jurassic basement are subparalel and thus, were grouped in the same stereogram due to its poorly representationin outcrops of the study area. The S2 is a crenulation foliation inclined to S1, which is a continuous or discontinuous schistosity, defined by quartz or carbonate microlithons mm-spaced by white mica and biotite cleavage domains. The statistical analysis of the poles of S1 and S2 shows that they are slightly aligned with the poles of the S1 foliation in the RVB units. However, the

pre-Jurassic basement trend more to northwest than the RVB units (Fig. 2 b). The coincidence of orientation between the foliations of the pre-Jurassic basement and the Cretaceous RVB foliations suggest a correlation, implying that the pre-Jurassic basement was also affected by the Cretaceous Andean deformation, instead of persisting totally authochtonous.

Open to gentle horizontal folds of tens of meters affect the RVB rock pile and the pre-Jurassic basement in the western domain (hinterland) of the MFTB, and the Magallanes Basin Cretaceous formations in the eastern domain (foreland) of the MFTB. However, in the foreland the folds are more open and gentle, as presented before in the interpreted seismic cross-section of figure 3. These folds have approximately vertical to inclined axial planes dipping to southwest, and subhorizontal fold axes trending north-south to northwest-southeast. These folds are apparently fault-propagation-folds associated to thrusts, which result from the progressive deformation on the MFTB, and could rotate the lineations L1 and L2, and foliations S1 and S1/S2 (pre-Jurassic). The fold axes of crenulations and cm-folds measured in field are dispersed (Fig. 2 d), but could be grouped in three main zones of concentration. The preferential azimuths 168/6 and 304/15 have low-dip plunging and could express the regional fold pattern slightly tilted. The preferential azimuth 300/79 has a high-dip angle and uncertain origin, but could be a strong tilting of crenulations by the regional folding, or a non-recognized phase of deformation of subvertical fold axes, that could be associated to transcurrences in the MFTB.

A cross-section of Gajardo channel (Fig. 7) summarizes the stratigraphic and structural architecture of the MFTB in the study area, it is interpreted from the outcrops analysed in the field, the Geological Map of SERNAGEOMIN (2003), and observations of Harambour (2002) in Gajardo Channel. From west to east, Zapata Fm. is thrusted upon a Tobífera thrust sheet, thrusted over a slice of ophiolite. On this portion of the belt, the foliation S1 is NW-SE trending and dips to southwest in low to medium angles, and to northeast with high dip angles, suggesting a double vergence of the belt near the Sarmiento ophiolites. To the east, the ophiolite thrusts over another thrust sheet of Tobífera Fm., which is internally folded, and it is thrusting over a Zapata Fm. layer. A thrust cuts the Tobífera Fm. and a pre-Jurassic basement slice is between the Tobífera-Zapata sheets. To the east the stratigraphy of Tobífera Fm. over Zapata Fm. is duplicated, what could be realted to a duplex

structure due to out-of-sequence thrust faults (also reported by Fosdick et al., 2011 and Betka et al., 2015 in the MFTB). The pre-Jurassic basement is internally folded and planes of S2 are truncated by RVB units above a lower detachment fault. Plutonic intrusions are cutting the deformed imbrications of RVB untis, and were dated to provide an upper age limit to deformation, that is presented in the following section.

Figure 7: Geological map and cross-section of Gajardo channel from A to A´ in horizontal scale = 1:150000 and vertical scale = 1:100000, with stereographic diagrams for the main structures.

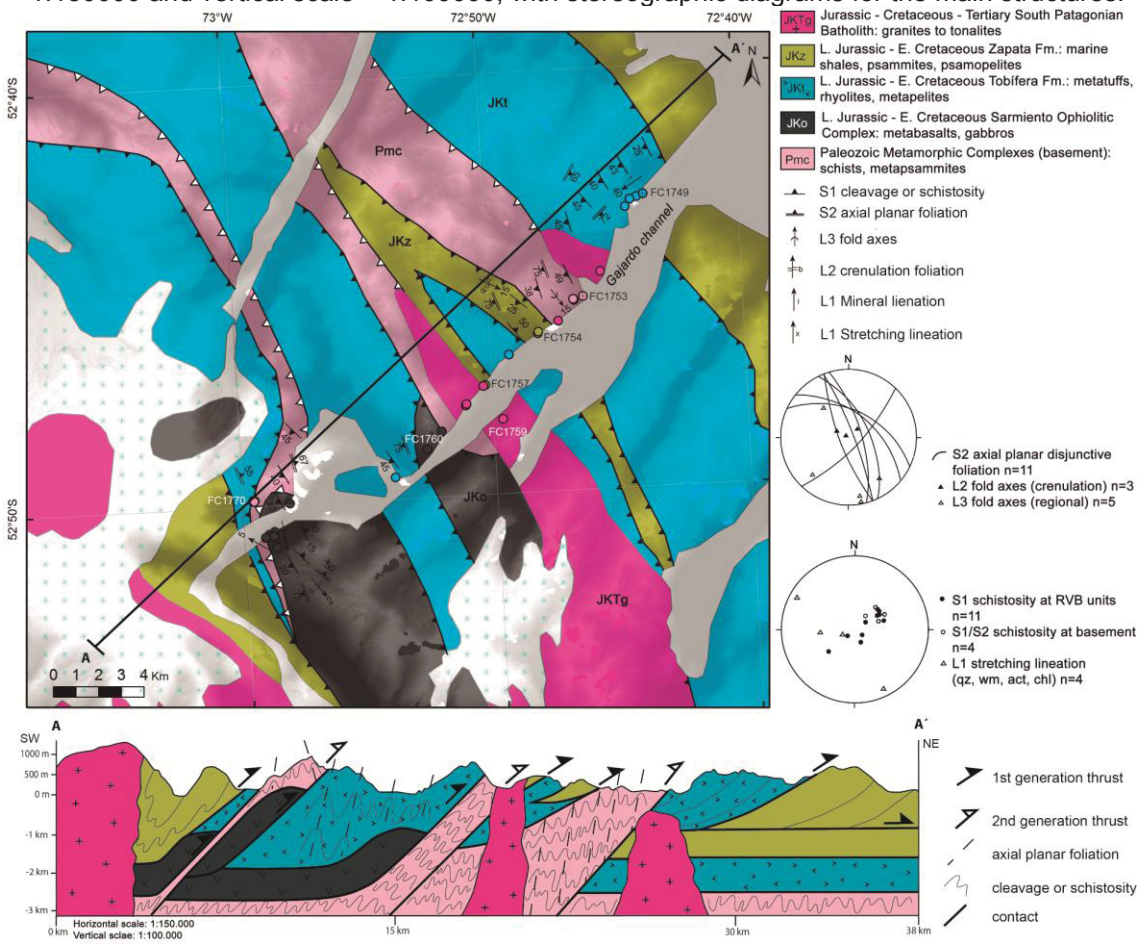

6 GEOCHRONOLOGY

6.1 Zircon U-Pb Geochronology

Three samples were analyzed for SHRIMP Zircon U-Pb geochronology with different purporses, giving us a general idea of sources of sediments and maximum depositional age for the sedimentary units of RVB, crystallization ages of Tobífera Fm. metatuffs, and the upper age limit of deformation in the fold and thrust belt by the crystallization age of a diorite intruding the Tobífera and Zapata thrust sheets. All calculated ages are reported with 95% confidence

limit uncertainties. For close comparison, ages reported from previous literature are quoted with 2 sigma uncertainties.

Sample FC1727 is a metatuff of the Tobífera Fm. from Estero Wickam, composed approximately of 15% of porphyroclasts essentially of alkali feldspars and plagioclase, normally fractured and faulted, in perfect bonding with the matrix, but some of them have a discrete reaction rim (Fig. 5 e). The cleavage domains are rich in white mica (15% of whole rock), chlorite (2% of whole rock) opaques (2% of whole rock) and iron oxides (1% of whole rock). The matrix is composed by very fine grained quartz (45% of whole rock) and feldspar (20%). The zircons have oscillatory zoning of igneous crystallization but a strong clear rim of Uranium loss (Fig. 8a).

The ages of sample FC1727 are concentrated in a Late Jurassic peak, where 21 of 26 analyses are between 153 Ma and 163 Ma, one age of 154.3 ± 1.9 Ma was measured in a diffuse core and it did not fit the statistical mean, because of this it was disconsidered. The mean age calculated is 159.9 ± 1 Ma (MSWD=1.4) (Fig. 8a), and must be the crystallization age of the metatuff. A least significant Middle Jurassic peak is represented by 3 analyses, around 168 Ma. One single grain had its calculated age for Early Jurassic (186.8 ± 2.9 Ma), and another one for Late Triassic (234.1 ± 2.8 Ma), which could be inherited from the continental crust during the petrogenesis of magmas, what occur occasionally at Tobífera Fm. and other units of the Chon Aike Large Igneous Province (Pankhurst et al., 2000).

Sample FC1754 is a metapsammite of Zapata Fm. from the middle portion of Gajardo Channel, it is from the hangingwall of a thrust that puts basement and RVB units over the Tobífera Fm. to the east (Fig. 7). This metapsammite is composed of quartz (70%) in recrystallized microlithons, and white mica (25%), chlorite (2%) and opaques (3%) in cleavage domains with S-C-type geometries. This layer of Zapata Fm. is localized affected by contact metamorphism of plutonic intrusions that was also dated by zircon U-Pb geochronology. The zircons have their habits partially preserved due to breaking, and are little rounded, showing little transportation (Fig. 8c).

Figure 8: Zircon U-Pb geochronological analyses using the SHRIMP. a) Concordia diagram of crystallization ages and the representative zircons of a metatuff of Tobífera Fm. (FC1727); b) Concordia diagram of detrital zircons of a metapsammitic rock of Zapata Fm. (FC1754); c) histogram of the detrital ages of samples FC1754 and FC1727, and representative zircons of sample FC1754; d) Concordia diagram of a diorite intrusive to the Zapata Fm. in Gajardo Channel (FC1759) and the zircons analysed.

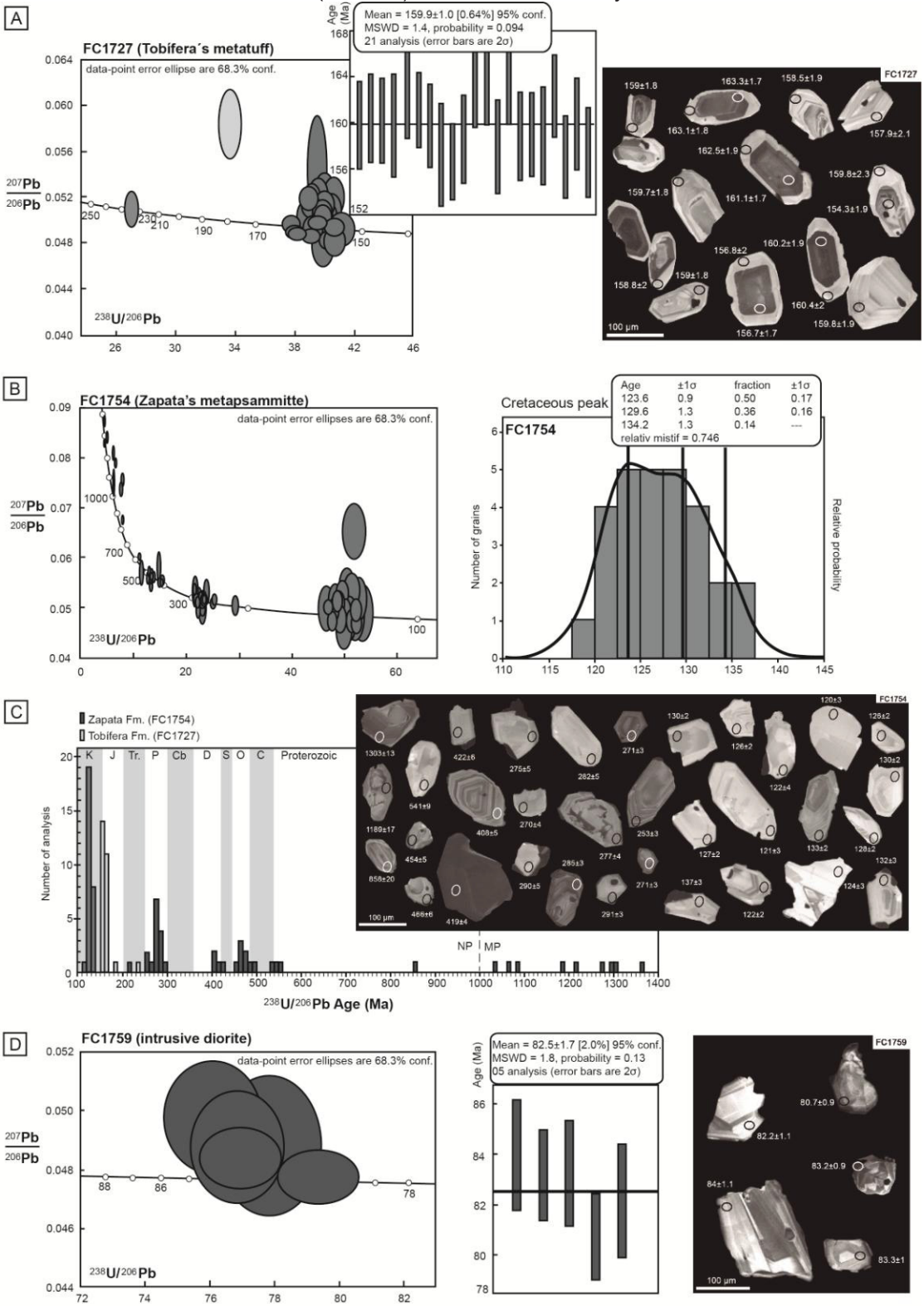

The histogram of figure 8c show a wide range of ages for sample FC1754, from Early Cretaceous (minimum age = 120 ± 3 Ma) to the Mesoproterozoic (maximum age = 1368 ± 16 Ma), and one zircon is Archean (2706 ± 6 Ma). The Early Cretaceous peak between 120 and 134 Ma is narrow and predominant (28 analyses), and were grouped in three classes: 123.6 ± 0.9 Ma; 129.6 ± 1.3 Ma; and 134.2 ± 1.3 Ma (Fig. 8b), which have the greater relative probability patterns of provenance. One zircon presented a Triassic age (217 ± 3 Ma). Scattered ages (15 analyses) between 250 and 290 Ma have a prominent peak at 280 Ma (5 analyses), with a greater asymmetry for older ages, meaning Permian predominance. Lesser significant peaks are around 410 Ma (Devonian-Silurian, 4 analyses), 470 Ma (Ordovician, 7 analyses), and 540 Ma (Cambrian, 3 analyses) (Fig. 8 c). The Neoproterozoic and Mesoproterozoic ages are scattered from single grains with ages closer to 1000 Ma (6 analyses) and 1300 Ma (5 analyses), their range of error is between 10 and 14 Ma (Fig. 8 b).

Sample FC1759 is a medium grained diorite from the middle Gajardo channel, composed of hornblende (60%), saussuritized plagioclase (25%), quartz (10%), and traces of titanite, epidote, and opaque minerals. This is an intrusive pluton that intrudes the Tobífera and Zapata formations and causes a thermal imprinting of the mineral assemblages. The dating of this rock provides an absolute crystallization age and a maximum age for the deformation on the western domain of the MFTB, where the ophiolites are emplaced. Only five zircons were found in this sample and they have a irregular oscillatory zoning. They yielded a dominant peak at Late Cretaceous, the mean age calculated is 82.5 ± 1.7 Ma (MSWD=1.8; Fig. 8d), and the maximum age of crystallization is 80.7 ± 0.9 Ma.

6.2 $^{40}Ar/^{39}Ar$ geochronology

One mylonitic metapelite of Zapata Fm. (SHP141) was dated using the $^{40}Ar/^{39}Ar$ technique in metamorphic phengite *in situ* using an IR laserprob. The metapelite is composed of quartz (40%) and phengite (60%) preferred oriented and strained, defining continuous cleavage domains. Multiple analysis spots on mats of phengite yielded a mean age of 71.4 ± 1.1 Ma (MSWD = 9.6). The spots fit well the isochron analysis (Fig. 9), pointing towards a Maastrichian age

of the metamorphism. One spot has an older age that could be due to incomplete recrystallization.

Figure 9: $^{40}Ar/^{39}Ar$ in a metapelite of Zapata Fm. (SHP141) by multiple analysis spots on mats of phengite yielded a mean age of 71.4 ± 1.1 Ma (MSWD = 9.6).

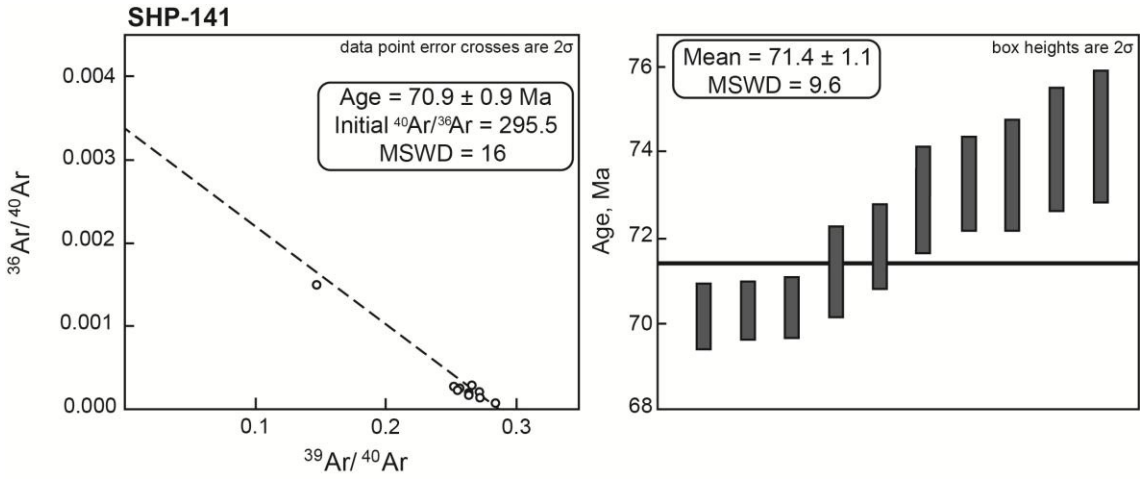

7 P-T CONSTRAINTS

The mineral assemblages and microstructures in strained meatuffs, metapelites and metapsammites of Tobífera and Zapata formations suggest low-grade metamorphism. However, five samples rich in white mica (phengite), chlorite, feldspar, and eventually epidote, biotite, and amphibole could have their mineral chemistry analyzed punctually using the electron probe micro-analyzer, and whole rock geochemistry of these samples using the X-ray fluorescence allows the construction of P-T pseudosections for thermobarometric constraints. This analysis provides a metamorphic modeling, allowing an estimative of depths of burial of these units and, consequently, discussions about the tectonic environment of deformation of the RVB, associated to the emplacement of ophiolites.

7.1 Mineral chemistry

Representative mineral chemistry analyses of white mica, feldspar, chlorite, biotite, epidote and amphibole of two metapelites of Zapata Fm. and three metatuffs of Tobífera Fm. are presented in Table 1, and diagrams are presented in figure 10. The #Mg means the Mg-number [#Mg=

$Mg^{+2}/(Mg^{+2}+Fe^{+2})$], while the X_{Mg} means the molar fraction [Mg= $Mg^{+2}/(Mg^{+2}+Fe^{+2}+Mn^{+2})$]. The X_{Al} is the Al total divided by 2. Minor phases such as rutile, stilpnomelane were identified with the X-ray detector.

Figure 10: Diagrams for mineral chemistry of: a) chlorite classification; b) white mica classification; c) feldspar classification.

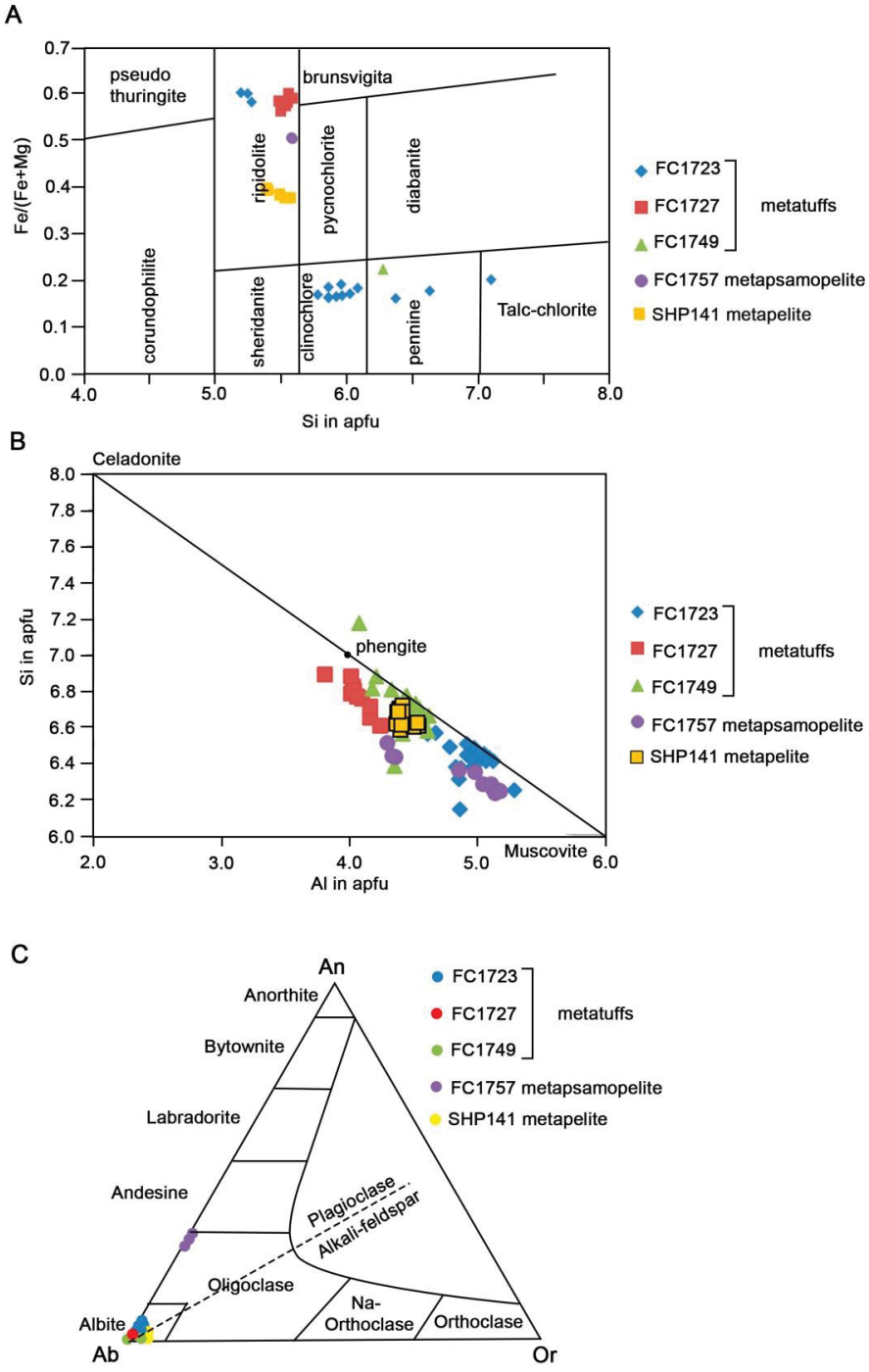

One metapelite of Zapata Fm. from the western portion Gajardo Channel (SHP141) had twelve crystals of white mica analyzed, the tetrahedrally co-ordinate Si is higher than 3.1 but the maximum is 3.35. The dominant

member is muscovite (Fig. 10 b). Two crystals of feldspar were analyzed and are albite (Fig. 10 a). Seven crystals of chlorite were analyzed and have the #Mg of ca. 0.6, the classification is ripidolite (Fig. 10 c). Five crystals of epidote were classified as pistacite, the amount of Fe_2O_3 is between 5.5% and 8.5%. Four crystals of amphibole were analyzed, the #Mg is around 0.72. and the Si is ca. 8, resulting in actinolite.

One metapsamopelite of Zapata Fm. from the middle portion of Gajardo Channel (FC1757) had twelve crystals of white mica analyzed, the tetrahedrally co-ordinate Si is higher than 3.1 but the maximum is 3.3. The dominant member is muscovite (Fig. 10 b). The content of Mg is normally around 0.3 but four crystals have Mg contents around 0.7. Eight crystals of biotite were analyzed and the #Mg is around 0.4 while the X_{Al} is between 0.12 and 0.17. Six crystals of feldspar were analyzed and are oligoclase in composition (Fig. 10 a). Only two crystals of chlorite were analyzed and have the #Mg of 0.48, the classification is ripidolite (Fig. 10 c).

One metatuff of Tobífera Fm. from the eastern portion of Gajardo channel (FC1749) had twenty-four crystals of white mica analyzed, the amount of tetrahedrally co-ordinate Si is higher than 3.3, some crystals reach 3.6, characterizing phengite (Fig. 10 b) and the content of Mg is normally higher than 0.6. Only one crystal of chlorite was analyzed and presented a #Mg of 0.76, classified as pennine (Fig. 10 a). Three crystals of feldspar were analyzed and are albite (Fig. 10 c).

The sample FC1723 is a sheared metatuff of Tobífera Fm. from Jeronimo Channel with abundant white mica. Twenty-four crystals were analyzed, the tetrahedrally co-ordinate Si content varies from 3.07 to 3.28, the majority of the crystals have Si above 3.2 and the average is 3.21, characterizing phengite. The Mg is normally greater than 0.4 with some crystals reaching 0.8. The component that dominates is muscovite, with lesser content of Al-celadonite (Fig. 10 b). Thirteen crystals of chlorite have a #Mg around 0.8 but three crystals have anomalous low #Mg of ca. 0.4. They majority of crystals were classified as clinochlore, but some crystals are pennine, talc-chlorite and ripidolite (Fig. 10a). Six crystals of feldspar were analyzed and the dominant component is albite (almost 100%) with no significant Ca and K content (Fig. 10c). Seven crystals of epidote were characterized as pistacite with a high amount of Fe_2O_3 around 5.5%.

One metatuff of Tobífera Fm. from Estero Wickam (FC1727) had nine crystals of white mica analyzed, the amount of tetrahedrally co-ordinate Si varies from 3.3 to 3.45, characteristic of phengite and the Mg is around 0.6. Nine crystals of chlorite have the #Mg around 0.4 and were classified as ripidolite (Fig. 10 a). Only one crystal of feldspar was analyzed and it is almost pure albite (Fig. 10 c).

7.2 P-T Pseudosection Modelling

The metamorphic modeling using P-T pseudosections were done for: two metapelites of Zapata Fm., one showing a medium pressure – medium temperature (MP-MT) condition of metamorphism, and another showing a high pressure – low temperature (HP-LT) condition of metamorphism, presented on figure 11; three metatuffs of Tobífera Fm. showing a medium pressure – low temperature (MP-LT) condition of metamorphism in this unit, the most representative diagram is presented on figure 13. The diagrams of isopleths of the five samples are presented on figure 12, and considerations are done in the following sections.

7.2.1 P-T pseudosections of metasedimentary rocks (Zapata Fm.)

Sample SHP141 is a phyllonite derived from metapelite from the western end of the Gajardo channel. It is composed essentially of fine grained and preferrentially oriented phengite (40%), quartz (25%), chlorite (15%), plagioclase (15%), epidote (5%) and actinolite (tr.). The best field of metamorphism showed in figure 11 was interpreted from the intersection between the isopleths of #Mg in chlorite (0.58-0.60, average: 0.59) and Si in phengite (3.3-3.6, average: 3.33), which is near 14 kbar and 270°C. At these conditions, the predicted stable mineral assemblage is white mica (39%), quartz (25%), chlorite (20.5%), carpholite (9%), lawsonite (3%), clinopyroxene (1.5%), stilpnomelane (1.8%), rutile (0.1%) and hematite (0.1%). The amount of carpholite is high and characteristic of low grade high-pressure metamorphism, but this mineral was not found in the thin section and must be converted in chlorite during a prograde metamorphism. The lawsonite is characteristic of high pressure metamorphism but also was not found in the thin section, and

must be converted in albite. The omphacite must be converted in chlorite and actinolite. Predicted rutile and hematite can be traces in the rock. The modal actinolite and epidote are traces and not representative.

Figure 11: Calculated P-T pseudosections for the metapelite of Zapata Fm. (sample SHP141). Mineral abbreviations: Wm: white mica; Ch: chlorite; Ct: chlorithoid; Cp: clinopyroxene; Gt: garnet; Am: amphibole; St: stilpnomelane; Tt: titanite; Q: quartz; Fc: carpholite; Ep: epidote; Law: lawsonite; Stb: stilbite; Anl: analcite; Ilm: ilmenite; Mt: magnetite; Hm: hematite; Lmt: laumontite; Ru: rutile; Pa: paragonite.

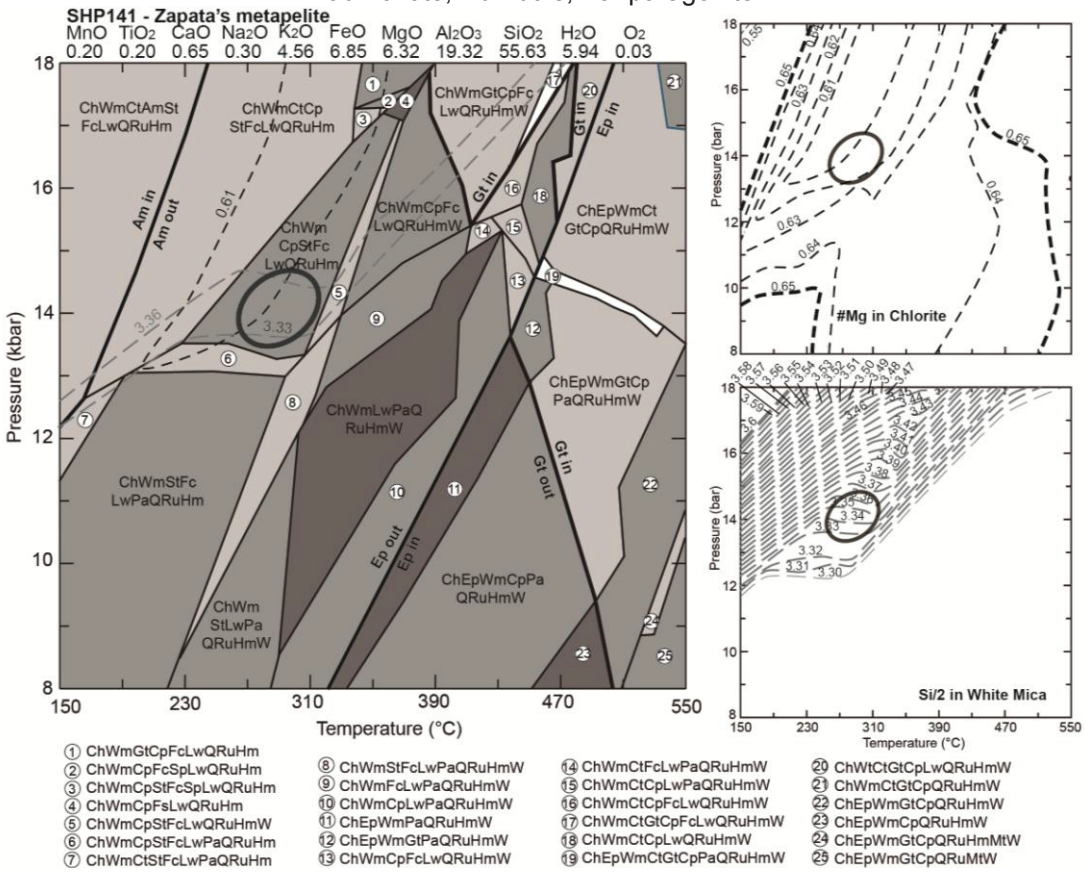

Sample FC1757 is a metapsammopelitic rock of Zapata Fm. from the middle portion of Gajardo channel, with considerable amounts of plagioclase (25% of the whole rock). Besides, a weak inherited stratification is recognizable by thin layers with higher proportions of quartz (55% of the whole rock) with common bulging and subgrain rotation, intercalated with levels rich in biotite (7%), white mica (5%) and chlorite (3%), together with quartz and sericitized plagioclase, opaque minerals are insterstitial (5%). Some of the white mica crystals have a detrital habit weakly deformed, and no preferred orientation. Biotite aggregates have decussate texture, typical of contact metamorphism and, indeed, this outcrop is significantly close to the intrusive diorite (FC1759) dated using zircon U-Pb. The best intersection field is where the isopleths of Si

content in phengite (3.10-3.29, average: 3.18) and X_{Mg} in biotite (0.4-0.44, average 0.42) match, near 4 kbar and and 470°C (Fig. 12 a, d), where the predicted mineral assemblage is quartz (53.7%), plagioclase (26.3%), biotite (4.6%), white mica (3.9%), epidote (0.8%), chlorite (0.8%), rutile (0.1%) and water (9.7%). The isopleths of #Mg in chlorite (0.45-0.49, average: 0.48) is out of the suggested metamorphic field, but the field where the isopleths of the three minerals must match (510°C, 5500 bar) have a composition with garnet, which is not present in the rock. The intermediate temperature is due to contact metamorphism, and the pressure is medium.

However, a second field of intersection (Fig. 12 a, d) between the isopleths of biotite and phengite suggest an inherited first metamorphic event near 310°C and 3.5 kbar, where the predicted mineral assemblage is quartz (54.5%), plagioclase (19.5%), white mica (8%), epidote (5%), chlorite (3.5%), biotite (1%), titanite (0.5%) and water (8%). The predicted epidote and phengite may have been partially decomposed to form plagioclase, and the chlorite to form biotite. The titanite must have been converted in rutile and released Ca to plagioclase reactions.

7.2.2 P-T pseudosections of metatuffs (Tobífera Fm.)

Sample FC1749 is a protomylonite derived from a fine grained metatuff on the eastern portion of Gajardo Chanel, which is on the hangingwall of a shear zone of contact with Zapata Fm. This metatuff is composed of 20% of porphyroclasts essentially of quartz (15% of the whole rock as porphyroclasts), but with sparse feldspars (5% of the whole rock). Here, the porphyroclasts present sigma strain shadows of quartz (35% of the whole rock in the matrix), white mica (40% of the whole rock), chlorite (2%) and opaque minerals (3% of the whole rock) (Fig. 4 d). The best P-T field (Fig. 12 b, e) in a temperature of 310°C and 5 kbar was interpreted mainly from the predicted mineral assemblage in accordance with the model mineral assemblage, in a field that match the average of Si in phengite (3.15-3.48, average: 3.36). Only one crystal of chlorite was found in the rock and thus, the isopleths for chlorite were considered not representatives. The predicted stable mineral assemblage is quartz (48.2%), feldspar (28.3%), white mica (15.9%), rutile (1.2%), clinopyroxene (0.5%), titanite (0.1%) and water (1.8%). The clinopyroxene was

not found in the thin section. The free water is very similar to the LOI of the rock that is 1.6%.

Figure 12: Isopleths of #Mg in chlorite, #Mg in biotite, #Fe in epidote and Si/2 in white mica for the samples FC1757; FC1749 and FC1723.

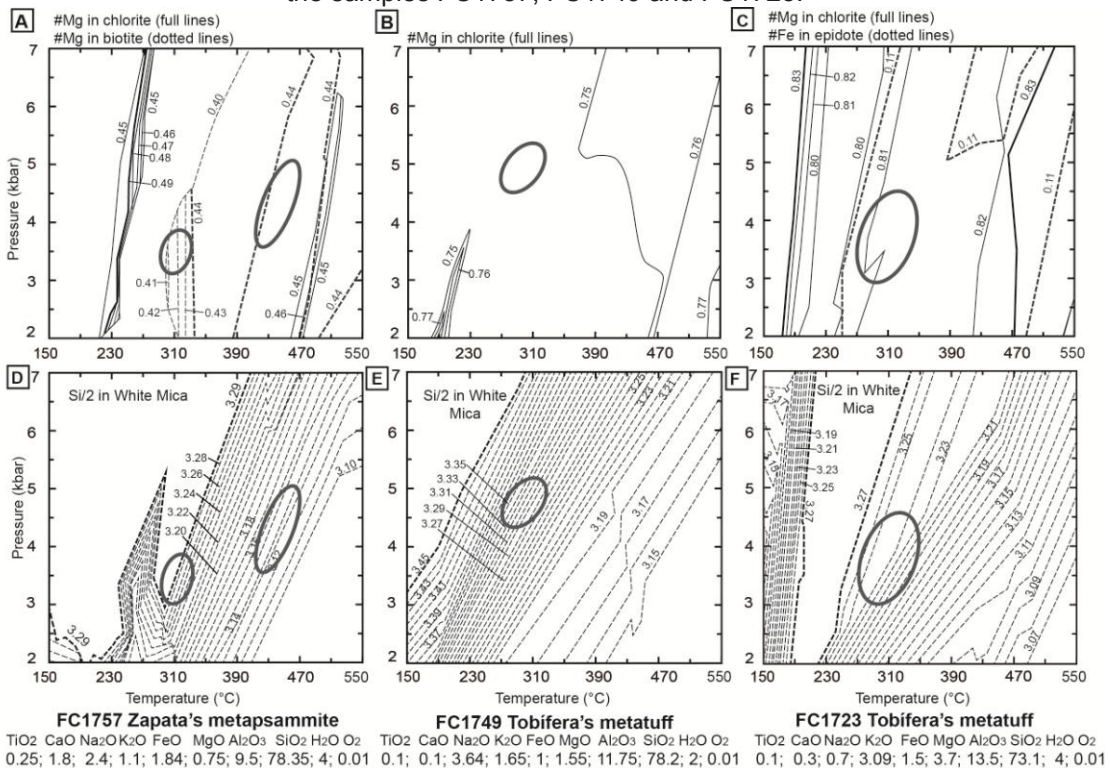

Sample FC1723 is a very fine grained metatuff from the eastern portion of Jeronimo Channel, composed of 3% of faceted porphyroclasts of quartz, feldspars and rhyolitic fragments lacking intracrystalline deformation, but have signals of pressure solution at their rims, where polycrystalline quartz and white mica form asymmetric strain shadows. The 97% of matrix is very fine grained and composed by preferred oriented white mica (40%), chlorite (10%), disperse quartz (40%), feldspar (5%), and radial zoisite (5%) with asymmetric and symmetric strain shadows of white mica. The best P-T constraints of metamorphism are 3.5-4.5 kbar and 300°C (Fig. 12 c,f), from intersection between isopleths of #Mg in chlorite (0.8-0.84, average: 0.82), Si in phengite (3.05-3.29, average: 3.21) and pistacite number in epidote (Fe/(Fe+Al) of ca. 0.1). The predicted stable mineral assemblage is quartz (54.9%), white mica (30.7%), chlorite (10.4%), epidote (0.5%), clinopyroxene (0.3%), titanite (0.2%) and water (3%). The amount of epidote seems underestimated, but the overall composition is in accordance with the modal composition. The small amount of clinopyroxene was not found in the thin section, and could be converted in

chlorite during retrograde metamorphism. The 3% of free water is plausible considering a LOI of 3.8%.

Figure 13: Calculated P-T pseudosections for the metatuff of Tobífera Fm. (sample FC1727). Mineral abbreviations: Wm: white mica; Ch: chlorite; Kf: alkali feldspar; Pl: plagioclase; Cp: clinopyroxene; St: stilpnomelane; Tt: titanite; Gt: garnet; Q: quartz; Law: lawsonite; Stb: stilbite; Anl: analcite; Ilm: ilmenite; Mt: magnetite; Hm: hematite; Lmt: laumontite; Ru: rutile; An: annite; Pnt: pyrophanite; Pxm: pyroxmangite.

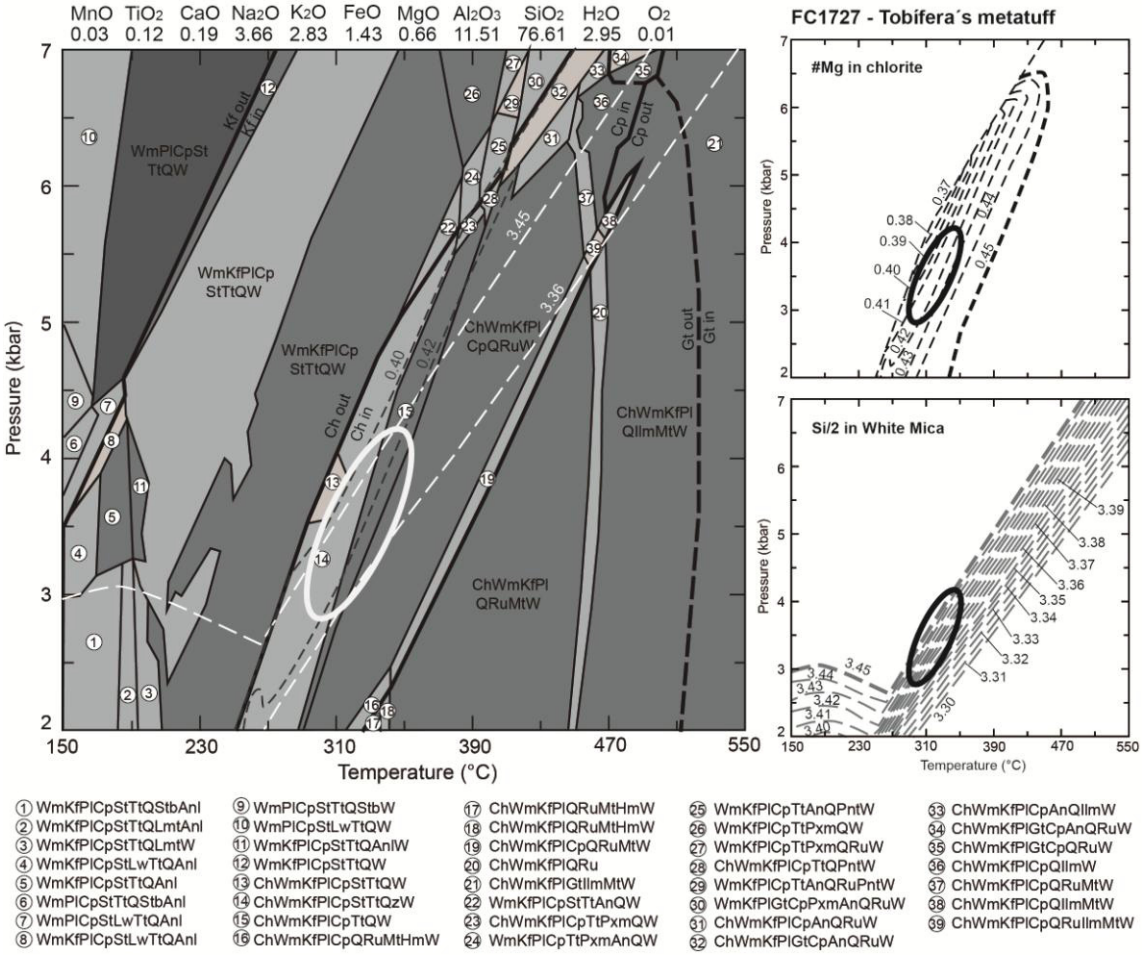

Sample FC1727 is a protomylonite derived from a fine grained metatuff from Estero Wickam, composed approximately of 15% of porphyroclasts of alkali feldspars and plagioclase, normally fractured and faulted and in perfect bonding with the matrix, but some of them have a discrete reaction rim of feldspars and quartz (Fig. 5 e). The porphyroclasts have eroded borders truncated by the anastomosed cleavage domains rich in white mica (15% of whole rock), chlorite (2% of whole rock) opaques (2% of whole rock), iron oxides (1% of whole rock) and traces of titanite. The matrix is composed by very fine grained quartz (45% of whole rock) and feldspar (20%). The pseudosection is presented on figure 13, considered representative of the overall metatuffs of Tobífera Fm. The best intersection field between the compositional isopleths of

#Mg in chlorite (0.35-0.45, average: 0.4) and Si content in phengite (3.30-3.45, average: 3.38) is near 3.5 kbar and 320°. At these conditions, the predicted stable mineral assemblage is quartz (41.6%), plagioclase (30.1%), white mica (11.9%), alkali-feldspar (7.9%), chlorite (2.3%), clinopyroxene (0.4%), titanite (0.2%) and water (5.7%).

8 DISCUSSION

The results of field work coupled to metamorphic and geochronologic constraints on the region of Otway and Skyring sounds present a good correlation with prior interpretations of closure of the RVB with a west-directed subduction of que quasi-oceanic floor and continentward structural development of the MFTB (Harambour, 2002; Hervé et al., 2007a; Calderón et al., 2012). The RVB metavolcanic and metasedimentary units seem to have deformed during Late Cretaceous by a thin-skinned tectonics of thrusts and folds, experiencing medium to high pressure and low temperature conditions of metamorphism, lately overprinted by medium temperature contact metamorphism near intrusive plutons of Campanian age. The non-coaxial deformation occur in strained corridors where S-C-type foliations develop in rocks belonging to Tobífera Fm., Zapata Fm. and Sarmiento Ophiolitic Complex, but the straining seems to have been controlled by the rheology of rocks, acting more plastically in metasedimentary rocks and metabasalts, whereas the felsic metatuffs have a britlle-plastic behavior. These mylonitic corridors have a N-S to NW-SE trending, dipping in low to high angle to SW or to NE. The kinematic indicators presented in this work show vergence with top to the N or NE, but additional structures with vergence to the SW near the Sarmiento ophiolites were described before by Calderón et al. (2006, 2012), and Harambour (2002) as a result of backfolding and backthrusting due to uplift of the belt. Here, the mylonitic foliations dipping to northeast could be associated to this phase of deformation as well. This mylonitic zone on the region of Skyring and Otway sound (52-54°S) have a good correlation with the Canal de las Montañas Shear Zone (Calderón et al., 2012) in the northern portion of the belt (51-52°), and probably represent an extension of this shear zone, which is considered the metamorphic sole of emplacement of Sarmiento ophiolites (Calderón et al., 2012).

The contact with pre-Jurassic units interpreted from seismic cross-sections appears like a detachment level, which could be allowed a decoupling of the Cretaceous RVB units from the metamorphic pre-Jurassic basement. However, in some locations slices of the pre-Jurassic basement crop out, suggesting thrusting of these units in an Andean phase of deformation as well (Forsythe and Allen, 1980; Allen, 1982; Betka et al., 2015). The normal faults from the rift phase had an important role for the shortening of the RVB, since they appear to have been reactived and converted in thrust zones, as discussed before by Fosdick et al. (2011) in the Ultima Experanza region, Rapalini et al. (2008) in the Cordillera Sarmiento, and Betka et al. (2015) for the southernmost region of Otway sound.

In any case, the thrusts and folds are consequence of progressive deformation and the metamorphic conditions point out to a growing accretionary wedge environment from west to east, that made possible the emplacement of Sarmiento ophiolites when the inception of Andean orogenesis in Southernmost Patagonia. The tectonic environment of emplacement of the Sarmiento ophiolites and the collision of the drifted magmatic arc with the South American continental margin will be discussed in the light of the metamorphic constraints from pseudosection modeling, which suggest a fast subduction of Zapata and Tobífera layers, causing the characteristic high pressure peak of subductions still in low temperatures (Bucher and Grapes, 2011; Ernst, 1999, van Staal et al., 2001; Aoki et al., 2008). The upper age limit for the ophiolite emplacement is proposed from the metamorphic $^{40}Ar/^{39}Ar$ dating in the strained metatuffs and the relative dating of non-deformed intrusive plutons.

8.1 Shear Zones and the emplacement of Sarmiento ophiolites in the MFTB

Shear zones accumulate strain and displacement of rocks; they grow by connecting faults that accommodate deformation by a combination of coaxial and non-coaxial deformation (Fossen and Cavalcante, 2017). In progressive deformation, networks of shear zones form with variations in orientation, length, thickness, strain geometry, deformation mechanisms and coaxiality along rocks, forming complex patterns of deformation (Ramsay and Graham, 1970; Sibson, 1977; Simpson and De Paor, 1993; Ramsay, 1980; Fossen and Cavalcante, 2017). Shear Zones also may be classified as plastic, brittle or brittle-plastic by

their dominant micro-scale deformation mechanism, which is controlled by the mineralogy, pressure, temperature, presence of fluids, strain rate and grain size (Fossen and Cavalcante, 2017). In the narrow westernmost part of the MFTB the RVB metamafic, metarhyolitic and metasedimentary rocks present zones where the primary mineral assemblages and structures are preserved, however, zones where these rocks are totally or partially recrystallized by pressure solution and dislocation creep mechanisms prevail. One characteristic (proto)mylonitic foliation S1 is developed in these rocks but the deformational patterns depends on the lithotype and the location in the belt, defining plastic and brittle-platic shear zones.

Generally, the metabasalts belonging to the Sarmiento Ophiolitic Complex are metamorphosed in greenschist facies but non-deformed plastically, they are only fractured with carbonate and quartz veins filling the cavities, attesting CO_2-rich fluids percoling the rocks, and the recrystallization to metamorphic minerals such as actinolite, chlorite, albite, titanite and epidote are result of ocean-floor metamorphism (Stern et al., 1976; Elthon and Stern, 1978). Nevertheless, in the western boundary of the ophiolitic stack, the same mineral assemblage of metabasalts is plastically deformed, an anastomosed foliation weakly crenulated defines the S1 trending NNW-SSE and dipping to the southwest, following the general pattern of imbrications in the MFTB (Allen, 1982; Fosdick et al., 2011). The kinematic indicators in the metabasalts, which are sigma shaped porphyroblasts of actinolite, show vergence to the north and northeast, and it is suggested as the vergence of thrusts during ophiolite emplacement. These rocks are structurally between metapelites, metapsammites and metatuffs of Tobífera and Zapata formations and, to the west, metasedimentary rocks are highly strained presenting the NNW-SSE trending S-C-type plastic foliation (S1) crenulated; the dipping angles vary from low-to-medium angles to southwest, to steep angles to the northeast. These contraty dip-angles in the innermost part of the belt were identified before by Harambour (2002) and Calderón et al. (2012), and the foliations dipping steeply to northeast were associated to backfolds and backthrusts formed during the uplift of the MFTB, in a late phase of deformation “D2” after the continent directed thrusting “D1”, which formed the S1 foliations dipping to the southwest. In the field it was difficult to separate texturally the foliations belonging to D1 and D2, but from petrographic observations we note that when S1 is strongly

crenulated, a crenulation foliation S2 forms, but it was only observed on this innermost part of the MFTB near the contact with the ophiolites.

The metamorphic constraints on a highly strained metapelite of Zapata Fm. of this portion of the belt record blueschist metamorphism (SHP141), typical of metamorphism in subduction zones (*e.g.* Ernst, 1999, Bucher and Grapes, 2011), in an estimated temperature of 270°C and 14 kbar of pressure. This HP-LT metamorphic condition is significantly different from another metapelitic rock analysed, that present a MP-LT mineral assemblage overprinted by MP-MT metamorphic minerals near intrusive bodies. This HP-LT metamorphic signature attest the subduction environment of deformation for the metapelites near the contact with the ophiolites and support the model of an accretionary wedge formation for the closure of the RVB (Harambour, 2002; Hervé et al., 2007a; Calderón et al., 2012). The phengite and chlorite analysed by the electron probe micro-analyser are stretched and preferred oriented in the S1 general NNS-SSE trend and dip to southwest, this is considered a shear zone that accommodated deformation during the tectonic burial of ophiolites and metasedimentary rocks of the RVB, and because of this represent the metamorphic sole of ophiolite emplacement (concept of Wakabayashi and Dilek, 2003). This share zone was lately exhumed by the second deformational phase of uplift of the belt, causing the crenulations and the contrary-dipping foliation S2, in spite of the necessity of greater investigation about the backfolds and backthrusts in this part of the MFTB.

To the east and structurally below of the metabasalts of Sarmiento Ophiolitic Complex metatuffs of Tobífera Fm. crop-out with a well developed S1 foliation with brittle-plastic behavior, the sigma shaped porphyroclasts of quartz present dynamic recrystallization microstructures formed by dislocation creep, while the porphyroclasts of feldspars are broken and displaced by the flux, with eroded borders by pressure solution. By definition “mylonites” are formed dominantly by ductile flow (Bell and Etheridge 1973; Tullis et al. 1982), and quartz porphyroclasts often are lost by the recrystallization mechanism of grain boundary reduction and grain boundary migration (Passchier and Trouw, 2005), because of this we avoid to use therm mylonites for the metatuffs, prefering to use the prefix “proto” to implicit the brittle-plastic character of deformation. The metapsammites of Zapata Fm., on the other hand, are highly plastic strained, the recystallization is complete forming microlithons of quartz and cleavage

domains of phengite and chlorite, that are tightly folded and ruptured by a S-C-type foliation. This difference mean a rheologic control on the deformation, where the less competent rocks of Zapata Fm. have a more plastic deformation than the competent rocks of Tobífera Fm.

Figure 14: Synthesis of the tectonic evolution of the hinternland of the Magallanes fold and thrust belt.

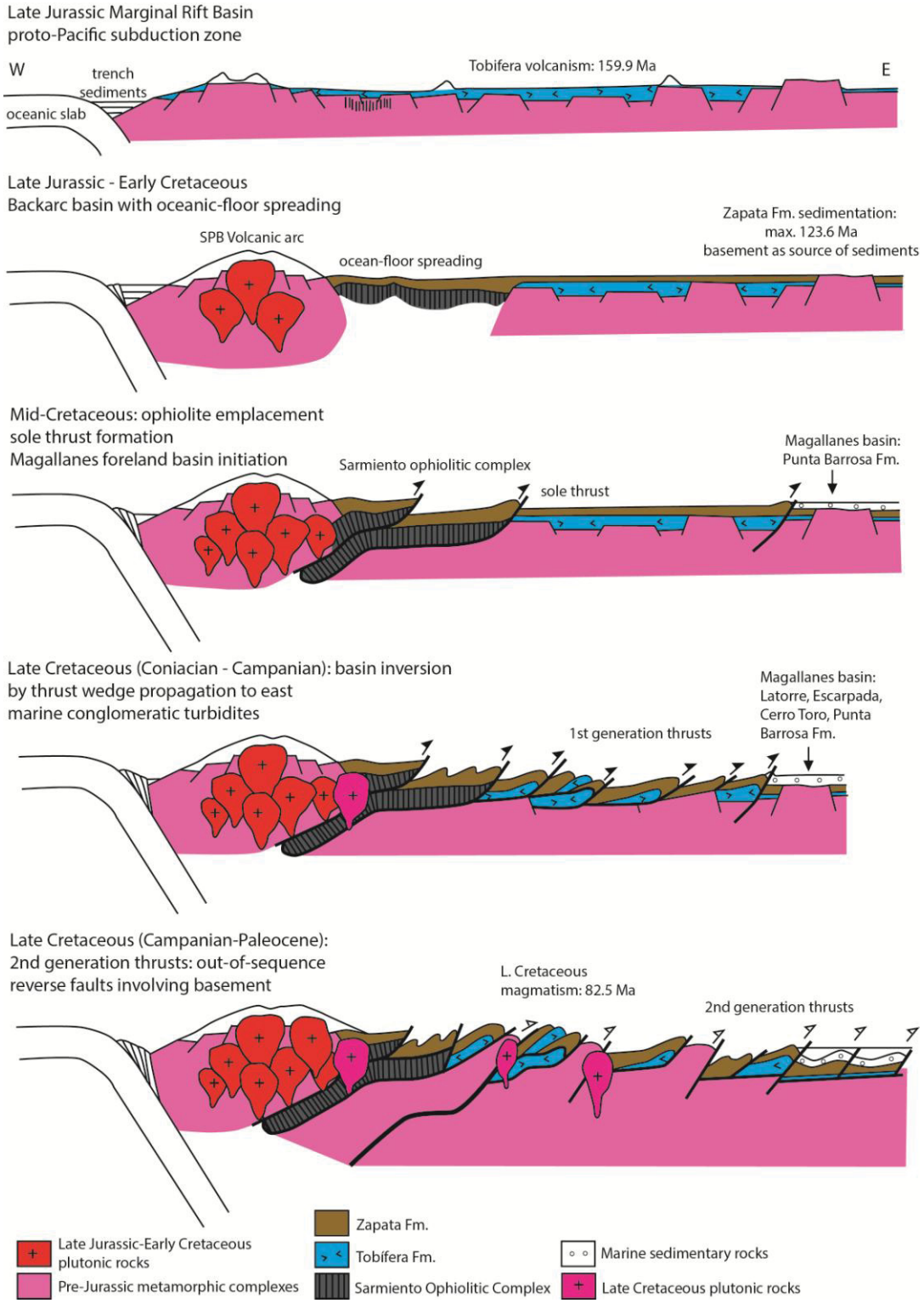

Thrust zones were interpreted in the geologic cross section of figure 7 and in the tectonic scheme of figure 14 from contacts between the Tobífera and Zapata formations, but the shearing is pervasive in the area with the S1 foliation, boudinage, and associated subhorizontal folds developed in the whole width of the hinterland of the MFTB, until the easternmost contact of Zapata Fm. and Latorre Fm. The differences in dipping of the S1 foliation could reflect the westward tilting of the shear zones due to tectonic inversion of normal listric faults, argumented by Rapalini et al. (2008) from magnetic remanence directions of the S1 foliation. Besides, the regional folds of subhorizontal axes, which also generate the L2 lineations in crenulations of S1, also disturb the orientation of the S1 foliations, causing a variation in the dip angles. These folds are ubiquituous in the hanginwall of the thrusts and are interpreted as a result of progressive deformation in thin-skinned tectonics of imbrications of thrust sheets.

In spite of the different structural behavior of metatuffs and metapelites in the MFTB, from brittle-plastic to plastic, the metamorphic signatures presented in the pseudosection modeling suggest a wide zone of common MP-LT condition of metamorphism, in temperatures close to 300±30°C and pressures between 3.5 and 5 kbar. This greenschist facies of metamorphism in both metatuffs and metapsammites, also supports the model of accretionary wedge for the closure of the RVB (Harambour, 2002; Calderón et al., 2012), where several thrust zones trending NNW-SSE and dipping SW accommodate the deformation and juxtapose the units by imbrications verging to the east and northeast. The depth of deformation until these rocks were buried could be estimated from the micro-scale deformational mechanisms and from the metamorphic conditions as well. The approximated crustal boundary between brittle to plastic deformational mechanisms for quartz recrystallization in a shear zone is near 15 km of depth (Fossen and Cavalcante, 2017), where bulging and subgrain rotation occur at quartz grains while feldspars keep brittle behavior, like occur in Tobífera metatuffs. Accordingly, thermal gradients in subduction environments are normally low, between 10 and 18°C per km in vertical depth (*e.g.* Aoki et al., 2008; van Staal et al., 2001), thus, the protomylonitic metatuffs and metapsammites recording 300° ± 30°C of metamorphism might be reached 16 km of depth, using the higher thermal gradient (18°C/km). Thus the approximated 16 km is considered the minimum depth of burial for the

metavolcanic and metasedimentary rocks of the RVB structurally below the Sarmiento ophiolites, where brittle-plastic to plastic shear zones were active, accompaining underthrusting in an accretionary environment with vergence to the east and northeast. On the other hand, the maximum depth of burial in the MFTB near the Otway and Skyring sounds is recorded in a blueschist facies metapelite of Zapata Fm., on the westernmost domain of the belt, which attained 14 kbar of pressure and because of this we assume a lower themal gradient of ca. 8°C/km (Ernst, 1999) for the HP-LT metamorphism, resulting in 33 km of depth in the subduction channel directed to the west, below the ancient magmatic arc in the drifted microplate to the west (Hervé et al., 2007a; Kramer, 2003; Cunningham, 1995; Gealey, 1980), representing a remnant of the metamorphic sole of the emplacement of Sarmiento ophiolites (figure 14).

The exhumation of subducted rocks often occurs by buoyancy of decoupled crustal sheets of sialic rocks at the subduction channel to mid crustal levels. Normal and reverse faults accommodate the decompression, and it is in this phase when the backthrusts tend to develop (Wakabayashi and Dilek, 2003; Dilek and Whitney, 1997; Ernst, 1999). In this context, the contraty-dipping S2 foliation that occur rarely in crenulated metapelites would be a record of the the exhumation phase of the metamorphic sole and the ophiolites in the hinterland of the MFTB. Normally, thin sheets of subducted sialic crust lose its heat in this process, but thickest sheets can preserve their higher temperatures of subduction (Ernst, 1999) when the process is fast enough to occur adiabatically. The blueschist facies metapelite of Zapata Fm. have a temperature record (270°C, 14 kbar) similar to the other samples that record medium pressures (~300°C, 3.5-5 kbar). This temperature is low comparing to profund subduction, where the T can reach 700°C, and is thus possible that new mineral assemblages had overprinted the earlier during the exhumation, for example the decomposition of carpholite and lawsonite to chlorite and albite. Similarly, the MP-LT metatuffs and metasedimantary rocks of the thrust sheets to the east of the ophiolites can be experienced subduction at shallower and/or slower rates of descent, or even can be buried to higher depths but had these mineral assemblages overprinted by the new conditions of exhumation in a slower rate, generating the characteristic assemblage of Pheng+Chl+Ab (Bucher and Grapes, 2011).

In the pre-Jurassic basement Paleozoic phases of deformation and metamorphism between the greenschist and amphibolites facies are well described (Nelson et al., 1980; Kohn et al., 1993; Hervé et al., 2003b; Hervé et al., 2010b; Klepeis et al., 2010; Maloney et al., 2011). The overprinting by a Late Cretaceous Andean phase of deformation is being proposed (Forsythe and Allen, 1980; Allen, 1982; Betka et al., 2015), and the coincidence of orientations between the S1 in the RVB units and the S1/S2 subparallel schistosities of the pre-Jurassic basement rocks is in agreement with a common Andean deformation. As showed in the seismic cross-section (Fig. 3), the contac of basement and the Cretaceous units of the RVB seems to has acted as a detachment level, allowing thin-skinned tectonics in the upper layers, however, the thrust zones also cause perturbation in the pre-Jurassic basement. It is probable that they also were partially underthrusted below the magmatic arc to the west, when a new metamorphic and deformational phase affected these metasedimentary rocks. Due to its higher depth, the pre-Jurassic basement could be deformed with a more plastic behavior, affected by the shear zones of the acretionarry wedge, and after juxtaposed to the units of RVB by thusts and backthrusts of the uplift phase. The involvement of the pre-Jurassic basement in the process leads to a thick accretionary wedge, and thus supports the exhumation of slices with preservation of HP mineral assemblages. The decoupling of RVB cover from the basement generates different mechanical environments and deformational rates, allowing different times for accommodation of shortening and thickening during the same compressive interval.

8.2 Geochronologic constraints

The zircon U-Pb analysis (SHRIMP) in a metatuff of Tobífera Fm. (FC1727) gave the mean crystallization age of 159.9 ± 1 Ma, corresponding to Oxfordian at the Late Jurassic. This age is at least 10 Ma older than the crystallization ages of Tobífera metatuffs in Cordillera Sarmiento, to the north of the study area, that are ca. 142 to ca. 148 Ma (Calderón et al., 2007). However, the mean crystallization age is closer to the ages of ca. 154 Ma of El Quemado Complex (50°S) and ca. 153 Ma of Ibañez Fm. (46°S) (Pankhurst et al., 2000), which also comprise felsic volcanic rocks correlative to Tobífera Fm. to the

north. Thus, we correlate the volcanism of Tobífera Fm. in the Seno Otway with the volcanism in El Quemado Complex and Ibañez Fm., and propose a wider range for the V1 volcanic interval proposed by Pankhurst et al. (2000), and diacronism in felsic magmatic activity of Southern Patagonia during Late Cretaceous, from Oxfordian to Berriasian, evolving from the south to the north, in accordance with the northward unzipping of opening of the RVB (Stern and De Wit, 2003).

The detrital ages of a schistose metapsammite of Zapata Fm. (FC1754) span from Early Cretaceous to Neoproterozoic, giving the 123.6 ± 0.9 Ma as the maximum sedimentation age of Zapata Fm. in Seno Skyring region. The greatest peak of provenance is Early Cretaceous, pointing to the magmatic arc to the west (Hervé et al., 2007b) and the correlative volcanic rocks of Tobífera Fm. (Calderón et al., 2007) as the main sediment sources for Zapata Fm. The maximum crystallization age obtained is ca. 10 Ma younger than the 132 Ma maximum crystallization age of the upper section of Zapata Fm. in Cordillera Sarmiento (Calderón et al., 2007), and ca. 30 Ma younger than the 152 Ma maximum depositional age of a quartzite of Yaghan Fm. (Klepeis et al., 2010), the equivalent of Zapata Fm. in Cordillera Darwin. It also suggest a diachronic sedimentation of Zapata Fm. in the RVB, that was propably partitioned by the horsts and grabbens of pre-Jurassic basement, and also suggest a northward unzipping of RVB, with younger detrital zircons to the north of the Cordillera Darwin.

Secondary peaks of detrital zircons in the metapsammite of Zapata Fm. are are Permian, Devonian and Ordovician, and some grains have Cambrian and pre-Cambrian ages, suggesting the pre-Jurassic basement as another important source of sediments to Zapata Fm., like the Eastern Andes Metamorphic Complex, which have its sources from Proterozoic cratons of Gondwana and the Paleozoic Gondwanide mountain belts (Hervé et al., 2003b, 2008). The pre-Jurassic basement was faulted during the rifting episodes os opening of the basin, forming horsts that could have remained as topographic highs until the deposition of Zapata Fm. (Fildani and Hessler, 2005). Breccias with basement clasts at Tobífera Fm., found in the Eastern Jeronimo Channel and cited by other authors (Calderón et al., 2007), also are evidence of the basement as source of sediments to RVB. The lack of zircons of Late Devonian and Carboniferous ages might be a positive argument for the correlation with

the Eastern Andes Metamorphic Complex as the source, since the detrital zircon age patterns of this metamorphic complex have not very pronunciated peaks in Devonian and Carboniferous, what is also nill in some samples (Hervé et al., 2003b).

The mean crystallization age of the diorite that intrudes the metapsammites of Zapata Fm. (FC1759) at the middle portion of Gajardo Channel, and consequently the Tobífera Fm. and the Sarmiento Ophiolitic Complex, according to stratigraphic relationships (Fig. 7), is 82.5 ± 1.7 Ma. This age could be considered as the upper age limit of the ophiolite emplacement and thrust imbrications in the MFTB, since the intrusive body cross-cut the structures of the belt. This Campanian age corresponds to the Cretaceous 3 generation plutons of the Southern Patagonian Batholith (Hervé et al., 2007b), which are the late phase in Cretaceous arc plutonism. Simmilarly, in Cordillera Sarmiento plutonic and hypabissal rocks within the Sarmiento ophiolitic stack provided the U-Pb ages interval from 78 to 81 Ma as the upper age limit of ohpiolite emplacement (Calderón et al., 2012). When compared with the Aptian maximum sedimentation age in Zapata Fm. (ca. 123 Ma), the upper age limit of deformation (ca. 82 Ma) imply in a maximum time span of 40 Ma for the end of sedimentation in the RVB and development of the MFTB due to the thrust imbrications among the units in the hinterland.

However, when this upper age limit of deformation is compared with the $^{40}Ar/^{39}Ar$ age in syn-tectonic phengite of Zapata Fm. (SHP141) of the westernmost part of the MFTB, they seem inconsistent, since the mean metamorphic age is 71.4 ± 1.1 Ma, suggesting a metamorphic event ca. 10 Ma younger than the ophiolite emplacement, right in the zone considered the metamorphic sole of subduction, which record the HP-LT meatmorphic peak. A possible explanation for the younger age of syn-tectonic phengite is that it is recordeding the cooling age of the metapelite, since the closure temperature of $^{40}Ar/^{39}Ar$ in white mica is near 250°C (Peyton and Carrapa, 2013), and from the P-T pseudosection modeling this sample attained 270°C during metamorphism. Another alternative is that the syn-tectonic phengite is really younger than the plutonic body located to the east, and the upper age limit for the ophiolite emplacement is ca. 71 Ma. Thus, the western part of the belt would have a late mylontic development compared to the eastern part of the belt, and it favors the Maastrichian out-of sequence thrusts formed during the late-stage of the MFTB

hinterland growing (Betka et al., 2015), causing the extrusion of the orogenic wedge, in the transition from an accretionary to a collisional environment between the magmatic arc and the continental margin.

8.3 Uplift and sedimentation in the foreland

The D2 deformational phase discussed by Harambour (2002) and Calderón et al. (2012) must be responsible for the late uplift and exhumation of the hinterland of MFTB, with backfolding and backthrusting. Towards the foreland of the study area, at conglomerates of Escarpada Fm., and graywackes of Bertrand Fm., the clasts are mainly composed of metabasalts, rhyolites, shales, which might be provenientes from the exhumed RVB, and and schists that might be provenients from the pre-Jurassic basement. Previous studies about the subsidence in foreland (Fildani et al., 2008, 2003; Fildani and Hessler, 2005; Romans et al., 2011, Fosdick et al., 2011, 2014) points to a flexural subsidence induced by shortening and thickening in the hinterland of the MFTB, which would have worked as source of sediments to the foreland during Late Cretaceous, from Cenomanian to early Paleocene (Fosdick et al., 2011, 2014; Romans et al., 2011). Fildani and Hessler (2005) studied the origin of clasts of Punta Barrosa Fm., known as the first deep water sequence of Magallanes Basin, and highlight the important presence of clasts derived from the metamorphic pre-Jurassic basement, beyond clasts derived from the magmatic arc and from units of the RVB, and suggest early uplift of the hinterland units, including basement-involved thrust zones, as source of sediments. Here, we could not distinguish between schist clasts derived from the pre-Jurassic basement or from the highly strained rocks of Zapata Fm., and thus the presence of schist clasts not necessarily date the basement-involved thrusts as earlier than the marine sedimentary feed of the Magallanes Basin from Cenomanian (ca. 100 Ma, Fosdick et al., 2011).

9 CONCLUSIONS

The Rocas Verdes ophiolites in the region of Otway and Skyring sounds (52-54°S) were emplaced in the South American continental margin due to accretionary mechanisms, they are associated with a west-directed subduction of the quasi-oceanic basin units, represented by the felsic volcanic rocks of Tobífera Fm. of Oxfordian age, metabasalts of the Sarmiento ophiolites, and metapsammopelitic rocks of the Zapata Fm. with a maximum depositional age regarding the Aptian. The subduction environment is evident in foliated metapelitic rocks of Zapata Fm. recording blueschist (HP-LT) metamorphism in a shear zone with complex mylonitic deformation that is considered the metamorphic sole of the ophiolite emplacement and a prolongation of the Canal de las Montañas Shear Zone to the south. This mylonitic metapelites attained 270°C and 14 kbar of pressure in an estimated depth of 33 km in the subduction channel, contrasting with greenschist (MP-LT) metamorphism in foliated metatuffs and metapsammites to the east of the Sarmiento ophiolites, which attained 300 ± 30°C of pressure and 3.5 to 5 kbar of pressure in a eastward growing accretionary wedge buried until 16 km of depth. Nowadays, the units belonging to the Rocas Verdes Basin are imbricated by thrust sheets with (proto)mylonitic corridors trending NNW-SSE and dipping to the southwest in low to high dip angles, and intruded by undeformed plutonic bodies of Campanian age that caused contact metamorphism at greenschist (MP-MT) conditions, overprinting of the metamorphic assemblages in the neighbourhood of intrusions.

The NNW-SSE trending and SW dipping foliation S1 is a S-C-type mylonitic foliation developed widely in the RVB units during the MFTB development, with a brittle-plastic behavior in more competent rocks like the metatuffs of Tobífera Fm., and with a plastic behavior in less competent rocks like the metapelites and metapsammites of Zapata Fm. In the metabasalts of Sarmiento Ophiolitic Complex, the S1 foliation is restricted to the contact with the metamorphic sole to the east, near the contact with the magmatic arc in the drifted microplate to the west. This deformational phase of Andean deformation is considered the phirst phase of closure of the Rocas Verdes Basin and also affected the pre-Jurassic metamorphic rocks of the basement, which present similar orientations of between their foliations and the S1 in the RVB units.

Additionaly, the contact between the Late Jurassic-Early Cretaceous units of the RVB and the pre-Jurassic basement seem to have acted as a detachment level separating the upper rocks defomed by thin-skinned tectonics, from the lower rocks less affected by horizontal displacements, but the inherited normal faults from the rift phase were important zones of reactivation for the thrusts. A contraty-dipping crenulation foliation in metapelites of Zapata Fm. in the westernmost part of the belt suggest backfolding and backthrusts associated to the uplift of the metamorphic sole and the ophiolites, and the Maastrichian age of syn-tectonic phengite in this part of the belt may be associated to this event of uplift in the late development of the belt, by out-of-sequence thrusts. However, greater investigation would be necessary to elucidate the uplift phase and exhumation of the MFTB on this region.

10 ACKNOWLEDGEMENTS

This work was supported by the Fondecyt Project Nº 1161818 in Chile and by LAMIR/UFPR/PETROBRAS Research Project Nº 2016/00141-1 in Brazil. Special thanks to geologists Andrea Goddard, Fernanda Torres and Diego Rojo by the helping during the field work and to the crew of the Marypaz II that made possible the campaign through the Patagonian fjords on October, 2017. I also thank to all LAMIR team by the technical, financial and intellectual attendance to this research.

5 COMPLEMENTARY RESULTS

5.1 PETROGRAPHIC ANALYSIS

Four thin sections of the pre-Jurassic basement were analyzed (one sample in SEM-EDS) and the main mineral assemblages of the schist and quartzites are: quartz, white mica (phengite), biotite, chlorite, ilmenite, pyrite, plagioclase (albite), and zircon and apatite as accessory phases. Quartz can present undulose extintion, bulging, and matle-and-core texture (Fig. 5.1.1 a, c). Biotite is subhedric to euhedric and can present undulose extiontion (Fig. 5.1.1 a). Minerals are preferred oriented defining a schistosity, micaceous and opaque minerals define the cleavage domains. The paragenesis is characteristic of upper greenschist facies, under biotite isograde (Fig. 5.1.1 d) (Bucher and Grapes, 2011). The calc-silicate lithologies are main composed by: carbonate, quartz, plagioclase, opaque minerals, epidote, white mica and titanite (Fig. 5.1.1 b). Carbonate is well crystallized and often of larger granulation than the other minerals. The crystals are preferred oriented and opaque minerals can concentrate in cleavage domains. The paragenesis of calc-silicate rocks also is compatible with upper greenschist facies (Fig. 5.1.1 e) (Bucher and Grapes, 2011).

Figure 5.1.1: Photomicrographs of the pre-Jurassic basement taken under polarized light: a) biotite-schist (FC1704); b) calc-silicate rock (FC1721); c) schist with wihte mica and quartz with subgrain rotation (FC1718); d) metamorphic facies diagrams for metapelitic rocks on the system KFMASH, and e) for calc-silicate rocks in prograde metamorphism at low X_{CO2} system, from Bucher and Grapes, 2011. The green spaces are the suggestion of metamorphic grade for the basement rocks, according to mineral assemblages.

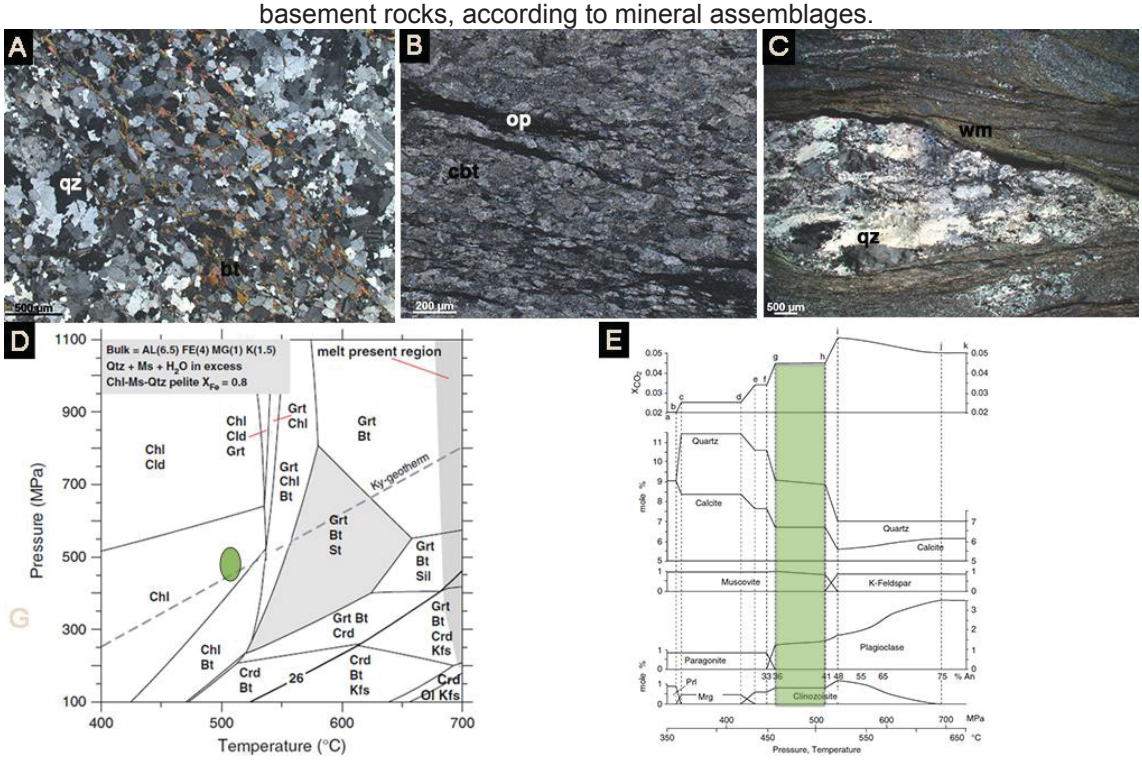

Petrographic analysis was done in fifteen thin sections of Tobífera Fm., and two samples in the SEM. Rhyolites main composition is plagioclase (albite), alkali feldspar, quartz and white mica; chlorite, apatite (high Y), barite, zircon, ilmenite and Ti-magnetite (high Nb) are accessory phases. The quartz-feldspathic matrix presents granophyric texture in very small grained crystals (Fig. 5.1.2 a, b, c). Alkali-feldspars and plagioclase are phenocrystals up to 1 mm, and can be crystallization germens to fast cooling spherulites (Fig. 5.1.2 b). Plagioclase can be zoned and deformed (kind of kink, Fig. 5.1.2 c), are little altered to sericite. White mica origin can be hydrothermal, it´s concentrated in interstitial domains. Breccias characterized by basement angular fragments (schists and quartzites) up to 2 cm (Fig. 5.1.2 d, e, f), welded by a matrix of fine grained quartz with undulose extiontion and bulging, very fractured.

Figure 5.1.2: Tobífera Fm. rocks: a) rhyolite (FC1755) and b, c) correspondent photomicrograph of spherullites and granophyric matrix; d) breccia (FC1722) and e, f) correspondent photomicrographs of clasts of schist.

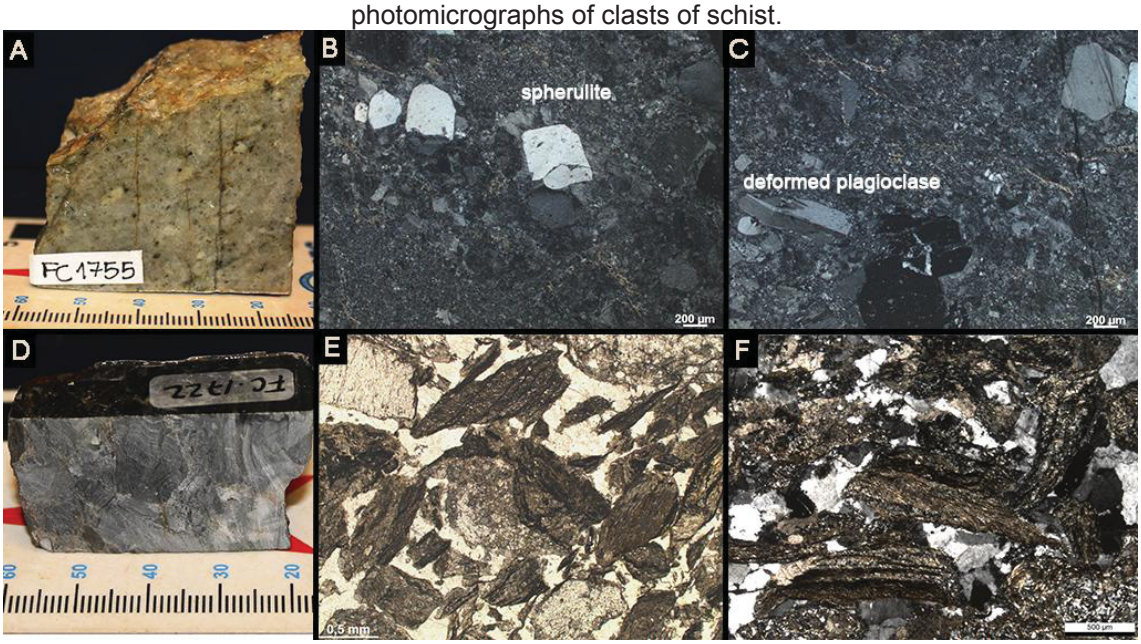

Metatuffs, the main lithotype of Tobífera Fm. (Fig. 5.1.3 a, d, g) is composed by quartz, alkali feldspar, plagioclase, white mica (phengite), zoisite, chlorite, epidote and stilpnomelane; zircon is an accessory phase. Quartz, plagioclase, alkali-feldspars and rhyolitic fragments can be angular porphyroclasts up to 2 mm, which can be factured (Fig. 5.1.3 e), disrupted by cleavage domains (Fig. 5.1.3 e, h), rotated and with strain shadows (Fig. 5.1.3 b, h). Micaceous minerals are concentrated in cleavage domains (Fig. 5.1.3 c, h, f). Zoisite is fibrous-radial very fine grained often occurring at white mica domains (Fig. 5.1.3 i; Fig. 5.1.4 a, b, c). Fall structures can be preserved, as fine grained layers deformed by the clasts (Fig. 5.1.3 b). Other igneous structure that can be preserved is crystaloclasts engulfing the matrix (Fig. 5.1.3 c), related to very ductile relations between crystals and matrix in effusive lavas (McPhie, 1993). Metamorphism range from subgreenschist to lower greenschist facies (Fig. 5.1.4 d) (Bucher and Grapes), and the recrystalized grains coexist with primary crystals and structures.

Figure 5.1.3: Tobífera´s metatuffs a) sample FC1762 and b) correspondent photomicrographs with fall structures, and c) crystaloclasts engulfing the matrix; d) sample FC1723 and e) correspondent photomicrograph with fractured feldspar in mylonite, and f) cleavage domain of a mylonite with chlorite and stilpnomelane; g) sample FC1749 and h) correspondent photomicrograph of porphyroclasts of quartz and feldspars and white mica cleavage domains in a mylonite, and i) zoisite crystals in the white mica and quartz-feldspatic matrix.

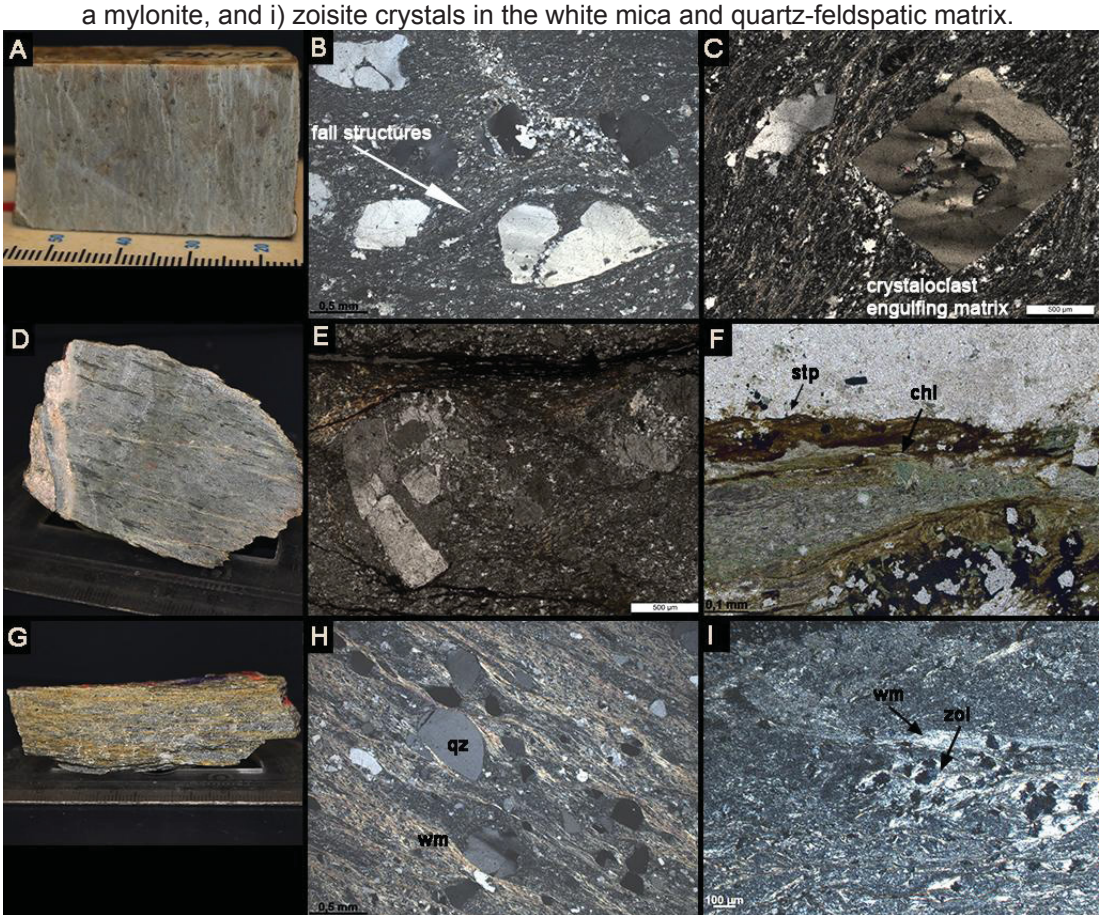

Figure 5.1.4: SEM images of Tobífera´s metatuff: a, c) crystals of zoisite and phengite with b) spots of EDS analysis; d) metamorphic facies diagram for quartz-feldspatic rocks, the green space is the estimated for Tobífera´s metatuffs, from Bucher and Grapes, 2011.

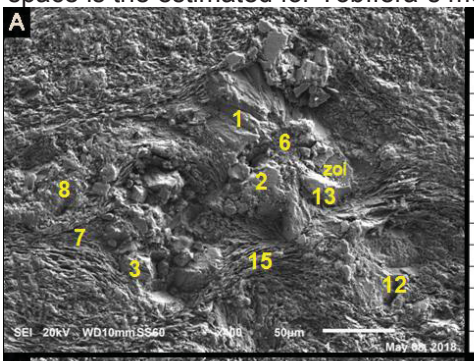

B

	CaO	Na2O	MgO	Al2O3	Si02	K2O	FeO
1	26.38			27.45	46.17		
2	62.47		3.31	14.08	20.15		
3	53.12			19.24	27.64		
4	39.65		1.96	20.78	32.95		4.66
5	16.00		11.42	26.72	39.69		6.17
6	34.65			23.87	41.48		
7			5.46	28.57	52.28	13.69	
8		18.60	2.24	17.92	61.24		
9			4.49	28.16	50.82	16.53	
10			9.46	27.72	48.38	14.43	
11	25.14			27.12	47.74		
12	23.57			25.43	51.00		
13	19.96		2.96	24.03	49.60	3.45	
14	5.02		28.87	20.75	34.57	2.63	8.17
15			5.48	24.97	44.51	25.03	

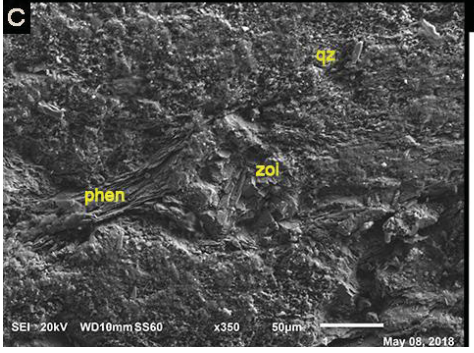

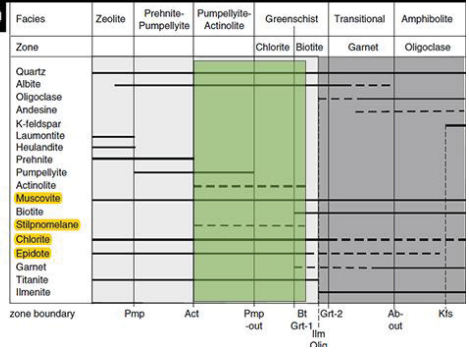

Petrographic analysis was done in four thin sections of the COS, and one samples in the SEM. Metabasalts are the main lithology in the complex and their composition is plagioclase (albite), quartz, actinolite, opaque minerals, chlorite, white mica, titanite, carbonate, epidote and zoisite. On the SEM, an indeterminate aluminous-silicate of Na and Mg was found. These phases are associated due to reactions of ocean-floor metamorphism. The actinolite occur as porphyroblasts and is in contact with chlorite by diffuse contacts (Fig. 5.1.5 f), the porphyroblasts' rims are very corroded (Fig. 5.1.5 g, i), or can be totally substituted by chlorite that is usually fribrous-radial (Fig. 5.1.5 e). Zoisite can be fibrous-radial and very fine grained (Fig. 5.1.5 c). Plagioclase can be saussuritized, but in many samples white mica, epidote and carbonate are well crystallized and don´t show reaction relations with plagioclase (Fig. 5.1.5. d, e), suggesting grow by metamorphism and stability. Titanite is anhedral, fine grained and disperses in relative abundance at all the matrix (Fig. 5.1.5. b, f). The rocks are often much fractured, and fractures are filled by quartz, chlorite, carbonate, epidote and actinolite (Fig. 5.1.5. f, h). When the metabasalts present pillow structures, zones with greater concentration of carbonates occur (Fig. 5.1.5. a, b), pointing to percolation of fluids rich in CO2 on the interface of pillows. This mineral assemblage is typical of low-grade metamorphism of mafic rocks and is probably related to ocean floor hydration (figure 5.1.8 e, f) (Bucher and Grapes, 2011).

Figure 5.1.5: SOC metabasalts: a) pillow basalt (FC1760) and b) correspondet photomicrograph with inter photomicrographs of metabasalt -pillow carbonates, and c) zoisite crystals; d, e) photomicrographs of metabasalt (FC1763) with epidote, carbonate, chlorite, titanite and f) veins filled by quartz, chlorite and actinolite; g) photomicrographs of metabasalt (FC1765) with actinolite porphyroblasts, h) veins filled by chlorite and epidote; and i)photomicrographs od metabasalt (FC1766) with deformed actinolite.

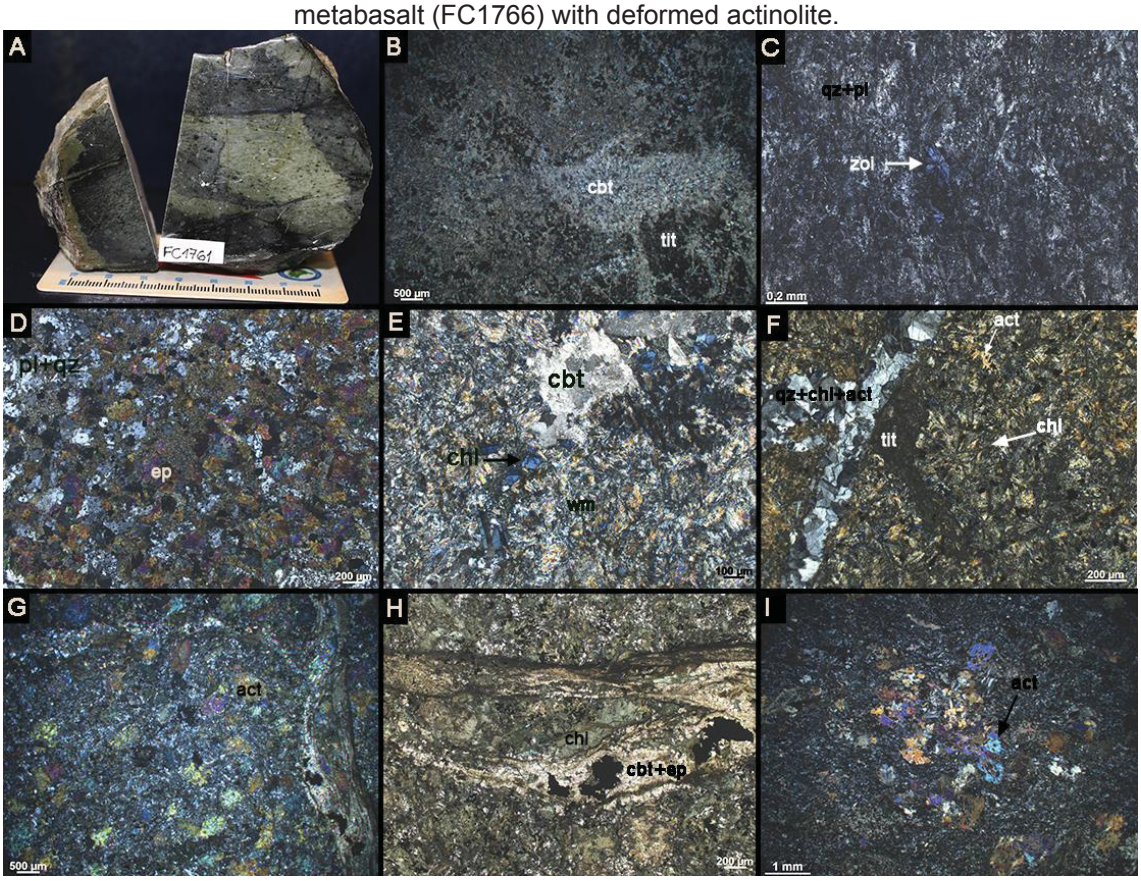

Some metabasalts have a well developed schistosity, the mineral assemblage is the same for non-foliated metabasalts (quartz + chlorite + carbonate + titanite + white mica + epidote + plagioclase + actinolite + opaque minerals) (Fig. 5.1.8 b, d), but with less amount of plagioclase and actinolite (Fig. 5.1.6 a-f). The foliation is defined by preferred oriented chlorite in cleavage domains, and by carbonate, quartz, plagioclase, actinolite and titanite (Fig. 5.1.6 b-e). This rock experienced subgreenschist to greenshcist metamorphism, associated with shear zones in the base of hangingwalls of obducted ophiolites (Bucher and Grapes, 2011).

Figure 5.1.6: Foliated metabasalts of SOC with crenulations: a) foliated metabasalt (FC1768) and b) correspondent photomicrograph with crenulated foliation; c) preferred oriented actinolite (FC1763); d, e) cleavage domains of chlorite and carbonate (FC1765); f) actinolite porphyroblasts folded (FC1766).

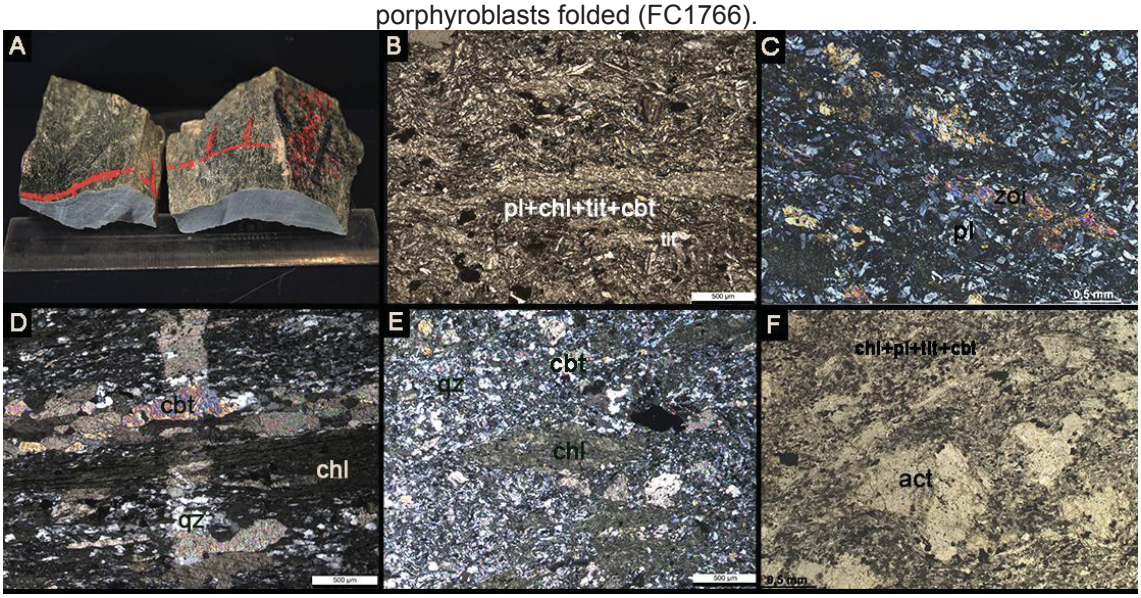

Indiferentiate mafic rocks in Jeronimo Channel were classified as distinct from the SOC due to their different petrographic features, specially tha absence of deformation, and different lithogeochemistry, which will be explained in the next section (5.2. Lithogeochemistry). These rocks were grouped in a Miocene Indiferentiate volcanosedimentary unit due to their association with sedimentary pelitic rocks of Miocene. The volcanic lithotypes are andesites in apparent intrusive contact with lappili-tuffs (Fig. 5.1.7 a, e), the andesite is composed of euhedric phenocrystals of plagioclase, zoned and saussuritized (Fig. 5.1.7 b, d); euhedric crystals of actinolite with inclusions of Ti-magnetite and ilmenite (Fig. 5.1.7 b, c, d); pseudomorphs of pyroxene totally substuted to chlorite, with opaque minerals on the rims (Fig. 5.1.7 c); subhedric Ti-magnetite and ilmenite (Fig. 5.1.7 b); anhedral quartz; well crystallized carbonate; the matrix is very fine grained and composed by saussuritized plagioclase, titanite, chlorite, white mica and opaque minerals (Fig. 5.1.8 a, c). The magmatic texture is apparently preserved, and characterized as blastogranular in metamorphic therms, and the assemblage is characteristic of transition for greenschist facies (Bucher and Grapes, 2011). Lapilli-tuffs are composed by angular fragments of basaltic, andesitic and granophyric rocks, as well as quartz and plagioclase, which can be altered to epidote, chlorite, carbonate and white mica (Fig. 5.1.7 e-f). The matrix is very fine grained and composed by opaque minerals, probably resultant of recrystallization of volcanic glass, with disperse chlorite

and epidote. Veins are filled by epidote (Fig. 5.1.7 f). Hydorthermalism is suggested for the alteration, considering that the secondary minerals are very sparse and the volcanic texture is preserved, but a subgreenschist facies metamorphism also can be the cause of this mineral generation (Bucher and Grapes, 2011).

Figure 5.1.7: indiferentiate mafic rocks of Jeronimo Channel: a) andesite (FC1711) and b) correspondet photomicrograph with phenocrystals of actinolite, plagioclase, and ilmenite, c) chlorite over pseudomorph of pyroxene or amphibole with Ti-magnetite on the rims, d) plagioclase saussuritized and actinolite phenocrystal;e) lapilli-tuff (FC1710)and f) correspondent photomicrographs with mafic clasts, veins filled by epidote, g) alteration to epidote and carbonate and h) lapilli of andesitic rocks.

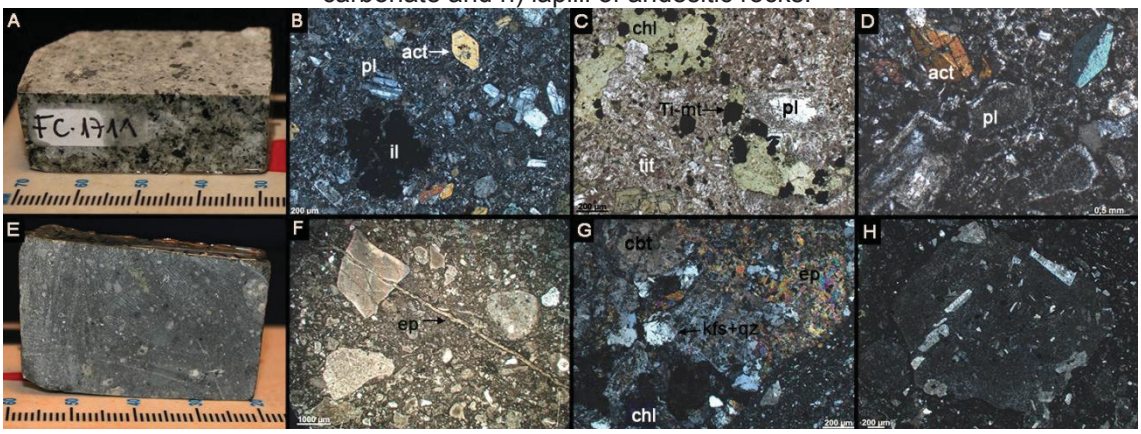

Figure 5.1.8: a) SEM image with EDS spots of indiferentiate andesite and c) correspondent chemistry for the sports and inferred minerals; b) SEM image and EDS spots for SOC foliated metabasalt and d) correspondent chemistry for the sports and inferred minerals.

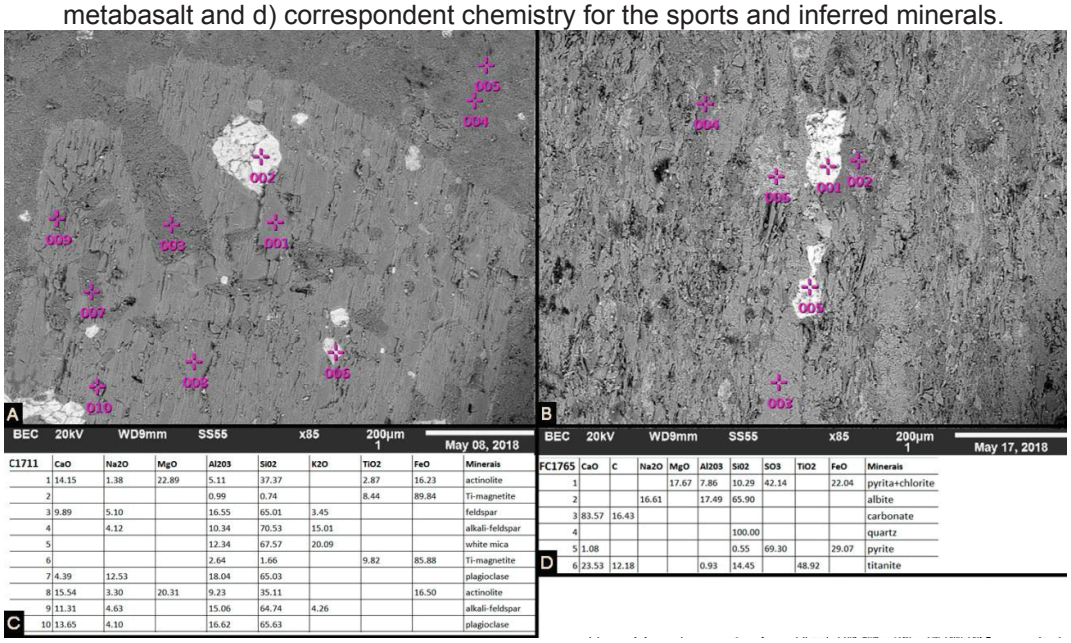

C1711	CaO	Na2O	MgO	Al2O3	SiO2	K2O	TiO2	FeO	Minerals
1	14.15	1.38	22.89	5.11	37.37		2.87	16.23	actinolite
2				0.99	0.74		8.44	89.84	Ti-magnetite
3	9.89	5.10		16.55	65.01	3.45			feldspar
4		4.12		10.34	70.53	15.01			alkali-feldspar
5				12.34	67.57	20.09			white mica
6				2.64	1.66		9.82	85.88	Ti-magnetite
7	4.39	12.53		18.04	65.03				plagioclase
8	15.54	3.30	20.31	9.23	35.11			16.50	actinolite
9	11.31	4.63		15.06	64.74	4.26			alkali-feldspar
10	13.65	4.10		16.62	65.63				plagioclase

C

FC1765	CaO	C	Na2O	MgO	Al2O3	SiO2	SO3	TiO2	FeO	Minerals
1				17.67	7.86	10.29	42.14		22.04	pyrita+chlorite
2			16.61		17.49	65.90				albite
3	83.57	16.43								carbonate
4						100.00				quartz
5	1.08					0.55	69.30		29.07	pyrite
6	23.53	12.18			0.93	14.45		48.92		titanite

D

Five thin sections of Zapata Fm. were described. The metapelitic rocks are composed of clay minerals, quartz, white mica, opaque minerals, chlorite, carbonate, plagioclase and alkali-feldspar (Fig. 5.1.9 a, d, f). The minerals are very fine grained, quartz and feldspars can be platy and the contacts are curved

to indented, with undulose extinction. Preferred oriented chlorite, white mica and clay minerals define the slaty cleavage. Metapsammites are composed of quartz, feldspars, white mica, chlorite, biotite and opaque minerals, fine grained (Fig. 5.1.9 b, c, e). The mineral assemblage characterizes low grade metamorphism in subgreenschist to greenschsit facies (Bucher and Grapes, 2011).

Figure 5.1.9: Photomicrographs of Zapatas rock samples: a) metapelite of Estero Wickham (FC1728) with a main foliation S1; b) metapsammite of Estero Wickham (FC1729) with euhedric pyrite and preferred oriented chlorite; c) metapsammite of Gajardo Channel (FC1753) with domains of opaque minerals defining the S2 foliation; d) metapelite of Gajardo Channel (FC1754) with domains of preferred oriented white mica in conjugated planes S-C, of the foliation S1; e) metapsammite of Gajardo Channel (FC1757) with folded domains of quartz with subgrain rotation and biotite with no preferred orientation; f) metapelite of Gajardo Channel (SHP141) with preferred oriented white mica and quartz.

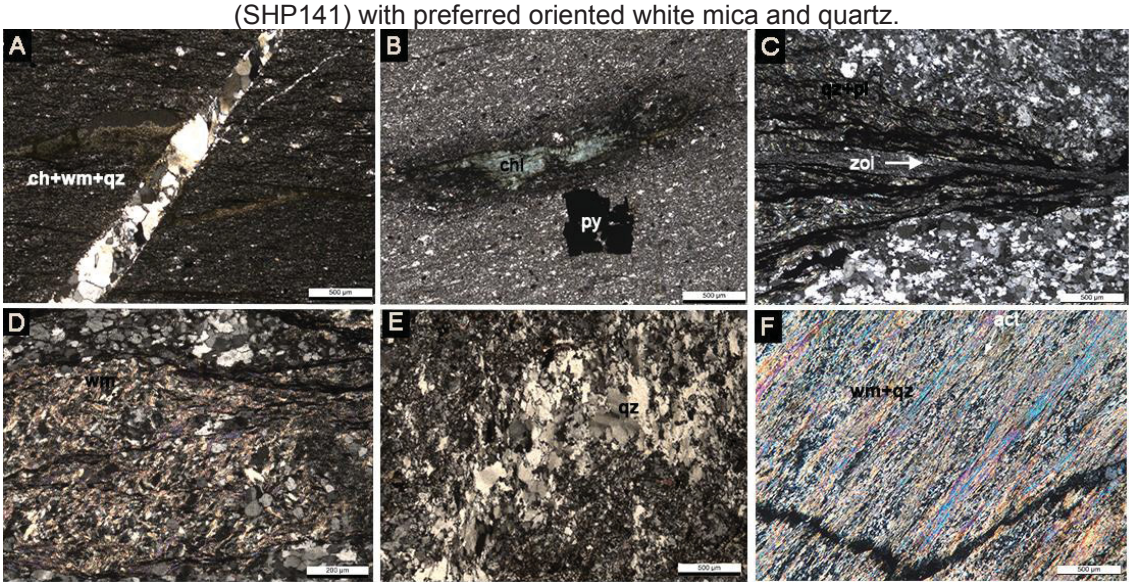

Five thin sections of South Patagonian Batholith were described. The granodiorite is composed by plagioclase, alkali feldspar, quartz, biotite, hornblende, opaque minerals and white mica, with a weak grade of alteration, crystals are anhedral to euhedral, and a magmatic foliation occur (Fig. 5.1.10 a, b). Xenoliths of basement schist can be inside of granodiorites (Fig. 5.1.10 c, d), in the contact with that, the felsic rock present intracrystalline deformation, as undulose extinction and bulging, that is probably syn-magmatic. Gabbros are composed by hornblende, plagioclase, epidote, White mica, opaque minerals, titanite and chlorite (Fig. 5.1.10 e, f). The crystals are euhedral and medium grained. Some porphyritic basalts were labeled as SPB, in spite of their volcanic origin, and is not probable that they are related to the COS because their very weak grade of alteration and deformation (Fig. 5.1.10 h-i). They are probably a

subvolcanic unit of SPB. Their composition is plagioclase, actinolite, epidote, hornblende, biotite, opaque minerals, white mica, and volcanic glass (Fig. 5.1.10 g). Plagioclase and actinolite occur as euhedral phenocrystals up to 3 mm (Fig. 5.1.10 e-i).

Figure 5.1.10: Photomicrographs of SPB: a, b) granodiorite, c, d) basement xenoliths inside granodiorite; e, f) hornblende-gabbro with phenocrystals of hornblende; g, h, i) pohpyritic basalts with phenocrystals of plagioclase.

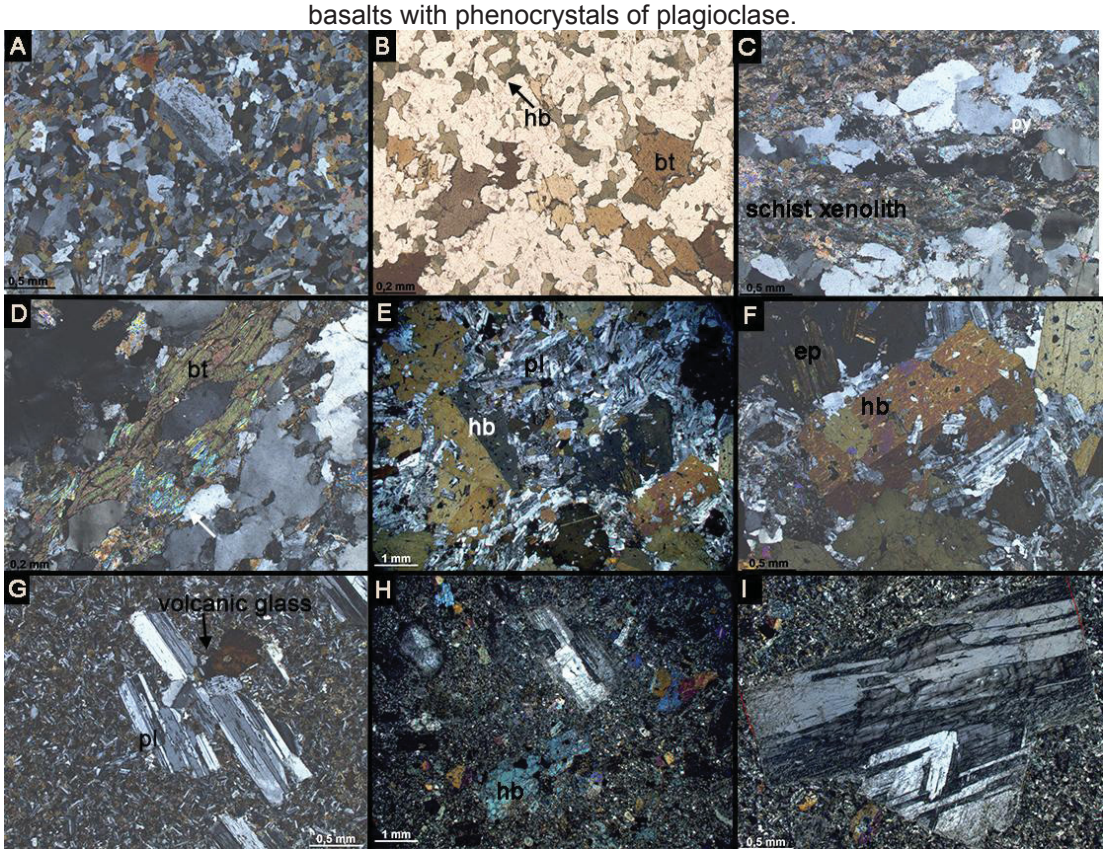

Thirteen thin section of units of Magallanes Basin were described, they are conglomerates and lithic sandstones of Escarpada Fm. and Bertrand Fm (Fig. 5.1.11 a-f), wackestones of Rocallosa Fm. (Fig. 5.1.11 g) and volcanic sandstones of La Pera Complex (Fig. 5.1.11 h). The conglomerates and lithic sandstones are clasts sustained, is interesting to note the lithic types: slate, rhyolite, andesite, basalt, schist and quartzite (Fig. 5.1.11 a-c). By the composition of these samples, the probable origin is from the RVB units, which were uplifted during the closure, and eroded when the Magallanes Basin became active (Fildani et al., 2003). The clasts are well preserved, as well as carbonatic fossils (Fig. 5.1.11 d-f), including slate or shale ones, proving a short transportation. A weak recrystallization occurs in the matrix, composed mainly by quartz, white mica and carbonate, whats was probably a diagenetic reaction.

The wackestone of Rocallosa Fm. presented many microfossils or fragments of them in a micritic matriz (Fig. 5.1.11 g), but they are not conclusive to infer a specific sedimentary environment. Plagioclase clasts also occur and can be deposited by the wind, taking into account that the micritic matrix leads to a calm and warm environment, as discussed in the section 7.1.

Shales of Estero Condor were grouped in a Miocene Indiferentiate unit, due to petrographic features different from Zapata Fm. and recent dating (Calderón, verbal information). These shales are composed by clay minerals, quartz, carbonate, white mica, opaque minerals and chlorite, and a cleavage is oblique to the foliation, defined by clay and opaque minerals (Fig. 5.1.11 i).

Sandstones of La Pera Complex are composed of quartz, plagioclase, white mica, chlorite, biotite, epidote, opaque minerals, actinolite and clay minerals. The texture is similar to poor selected lithic sandstones, but opaque aggregates can be recrystallized volcanic glass (Fig. 5.1.11 h), and suggest a volcanic origin. They were collected from the basis of a turbiditic sequence.

Figure 5.1.11: Photomicrographs of Magallanes basin units: a, b) conglomerates of Escarpada Fm.; c) lithic sandstone of Escarpada Fm.; d, e, f) conglomerates with fossils of Bertrand Fm.; g) wackestone of Rocallosa Fm. with variated fossis; h) lithic sandstone of La Pera Complex with opaque aggregates, it can has volcanic origin; i) shale of Miocene indiferentiate unit with indeterminate clayey features, can be root marks.

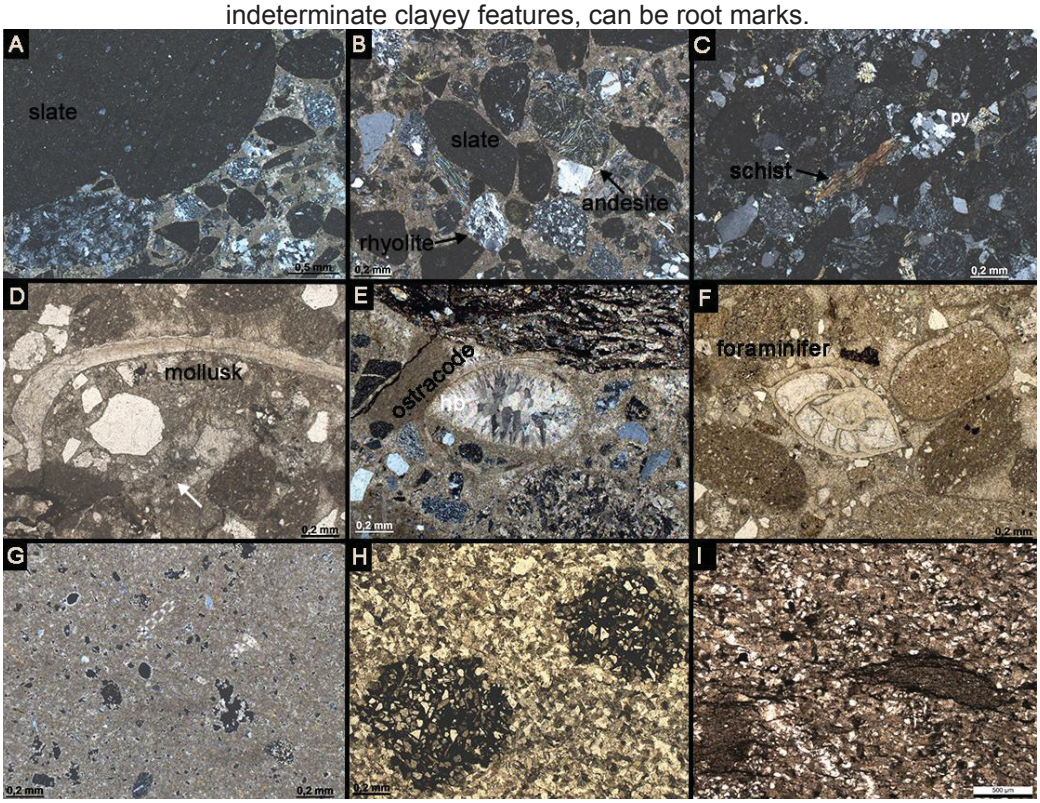

7.2 LITHOGEOCHEMISTRY

Twenty five samples were chemically analyzed by XRF and ICP-MS to obtain the whole rock composition for major and trace elements (including rare earth elements), allowing correlating lithotypes and making inferences about the origin of the rock, for both magmatic and metasedimentary. The results are presented on the table 5.2.1 for oxides, 5.2.2 for REE, and 5.2.3 for trace elements. Geochemical digrams and explanations are in the following text.

The figure 5.2.1 present the classification diagrams for the volcanic rocks of RVB, including eight rock samples of Tobífera Fm. and ten rock samples of the SOC. The weight of the oxides was recalculed to 100% in anhydrous base. The rock samples of the SOC were divided in mafic rocks of Jeronimo channel, which actually are two lapilli-tuffs with basaltic and andesitic clasts in aphanitic matrix; one porphyritic andesite, one breccia with fine-grained mafic clasts and one metabasalt; and mafic rocks of the Gajardo channel, which also can be subdivided in two pillow basalts and three foliated metabasalts. The rock samples of Tobífera Fm. are mainly metatuffs, but one is a breccia with clasts of schists in a quartzose matrix, one is a rhyolite with granophyric texture, and one is a metapelite with stretched porphyroclasts of quartz. The classification diagrams of figure 5.2.1 a, b, c and d are in agreement for the classification of Tobífera rock samples as rhyolites for the metatuffs and the granophyric rhyolite, the two samples classified as dacites or andesites are the metasedimentary rocks, with a minor content of SiO_2, and because of this, its classification must be disconsidered. For the SOC, the foliated metabasalts of Gajardo channel were classified as basalts (Fig. 5.2.1 a-c), while the pillow basalts are distinct, one is a picro basalts with very small amount of SiO_2 (Fig. 5.2.1 a), and the other is in the field of andesitic basalt, mainly due to higher content of SiO_2 (Fig. 5.2.1 a, c). The diagram of Jensen (Fig. 5.2.1 d) shows these basalts as high-Mg basalts to basalt. On the other hand, the mafic rocks of the Jeronimo were mainly classified as dacites or andesites, showing a greater enrichment in SiO_2 and consequently a higher differentitation grade (Fig. 5.2.1 a-d).

Table 5.2.1. Whole rock major elements composition in weight %.

Sample	Lithotype	Unit	SiO2	Al2O3	Fe2O3	MgO	CaO	Na2O	K2O	TiO2	P2O5	MnO	Cr2O3	LOI	Sum	C Total	S total
FC1704	Metapsamite	pJ basement	69.57	14.53	3.1	1.52	3.61	4.38	0.93	0.49	0.14	0.04	0.007	1.4	99.83	0.09	0.14
FC1726	Calc silicate schist	Tobífera Fm.	59.47	17.42	7.34	2.34	3.21	4.12	1.63	0.96	0.19	0.16	0.008	2.9	99.9	0.14	<0,02
FC1753	Schist	Zapata Fm.	55.72	19.15	8.08	4.27	0.43	1.63	4.01	0.97	0.23	0.11	0.012	5.1	99.83	0.62	0.06
FC1767	Schist	Tobífera Fm.	79.33	7.24	4.48	3.57	0.09	0.14	1.69	0.1	0.06	0.07	0.005	3	99.84	0.03	0.84
FC1770	Schist	Tobífera Fm.	63.66	6.87	9.01	5.52	4.24	0.19	0.28	0.26	2.9	0.14	0.033	6.7	99.8	0.77	1.28
FC1710	Lapilli-tuff	Indiferentiate	62.42	15.74	6.14	2.03	4.37	4.14	1.78	0.99	0.3	0.14	0.002	1.7	99.77	0.03	<0,02
FC1711	Porphyritic andesite	Indiferentiate	61.56	16.54	5.06	2.45	4.65	4	2.11	0.63	0.15	0.09	0.005	2.5	99.78	0.12	<0,02
FC1714	Lapilli-tuff	Indiferentiate	60.01	16.16	5.96	2.33	4.83	3.35	2.24	0.82	0.21	0.14	0.004	3.7	99.8	0.2	0.62
FC1715	Metabasalt	Indiferentiate	64.09	14.16	7.55	1.6	5.9	0.43	2.68	0.78	0.26	0.15	<0,002	2.2	99.81	0.04	0.05
FC1717	Breccia	Indiferentiate	60.35	17.11	6.67	2.1	3.3	5.12	0.74	0.66	0.25	0.24	0.002	3	99.56	0.07	0.1
FC1760	Pillow basalt	SOC	49.37	12.64	5.49	5.85	16.25	0.6	0.74	0.51	0.04	0.13	0.034	8.1	99.81	1.8	<0,02
FC1761	Pillow basalt	SOC	36.47	18.35	17.01	12.68	5.07	1.06	0.06	0.66	0.07	0.3	0.053	7.9	99.7	0.28	0.04
FC1763	Metabasalt	SOC	43.7	18.13	12.05	9.56	5.43	3.69	0.05	1.58	0.21	0.31	0.043	4.8	99.59	0.02	<0,02
FC1765	Metabasalt	SOC	44.33	15.42	10.88	8.2	7.33	2.13	0.93	1.27	0.14	0.24	0.041	8.8	99.74	1.16	0.05
FC1768	Metabasalt	SOC	43.86	15.58	10.39	10.35	6.67	1.68	2.47	1.03	0.19	0.24	0.055	7.1	99.75	0.75	0.06
FC1722	Breccia	Tobífera Fm.	60.96	8.56	16.85	1.53	0.19	0.07	1.37	0.32	0.1	0.58	0.005	9.3	99.82	2.03	1.56
FC1723	Metatuff	Tobífera Fm.	73.07	12.65	1.97	4.49	0.45	0.3	2.91	0.09	0.01	0.02	<0,002	3.8	99.82	0.1	<0,02
FC1727	Metatuff	Tobífera Fm.	77.85	11.7	1.61	0.67	0.2	3.72	2.88	0.12	<0,01	0.03	<0,002	1	99.85	0.05	0.04
FC1749	Metatuff	Tobífera Fm.	78.1	11.84	1.14	1.58	0.06	3.84	1.65	0.06	<0,01	0.03	<0,002	1.6	99.88	0.04	0.1
FC1750	Metapelite	Tobífera Fm.	63.77	16.36	4.8	3.26	0.12	0.68	4.69	0.45	0.1	0.06	0.006	5.3	99.68	0.86	0.09
FC1751	Metatuff	Tobífera Fm.	77.92	12.75	0.87	0.76	0.04	2.7	2.9	0.05	0.01	<0,01	<0,002	1.8	99.88	0.1	0.02
FC1755	Rhyolite	Tobífera Fm.	76.44	12.58	0.66	0.23	0.04	2.77	6.36	0.06	<0,01	0.01	<0,002	0.5	99.84	0.02	<0,02
FC1762	Metatuff	Tobífera Fm.	81.02	10.29	0.6	0.15	0.09	2.12	4.75	0.1	0.02	<0,01	<0,002	0.6	99.82	0.03	<0,02
FC1720	Shale	Zapata	69.14	12.8	6.17	1.83	1.97	1.12	1.24	0.52	0.06	0.07	0.008	4.9	99.9	0.96	1.47
FC1757	Metapsamite	Zapata Fm.	69.19	15	3.43	1.5	1.87	2.92	3.23	0.5	0.14	0.05	0.008	1.9	99.87	0.06	0.02

Table 5.2.2. Whole rock REE elements composition in ppm.

Sample	Lithotype	Unit	La	Ce	Pr	Nd	Sm	Eu	Gd	Tb	Dy	Ho	Er	Tm	Yb	Lu
FC1710	Lapilli-tuff	Indiferentiate	31.1	67.7	8.61	34.1	7.21	1.82	6.63	1.06	6.03	1.30	3.77	0.54	3.48	0.55
FC1711	Porphyritic andesite	Indiferentiate	18.8	39.2	4.74	18.5	3.70	0.94	3.39	0.51	2.87	0.58	1.84	0.27	1.67	0.26
FC1714	Lapilli-tuff	S Indiferentiate	24.5	50.6	6.52	24.7	5.44	1.38	5.07	0.82	4.83	1.06	2.98	0.43	2.85	0.45
FC1715	Metabasalt	Indiferentiate	23.4	52.7	7.03	29.5	6.98	1.85	7.67	1.31	8.01	1.87	5.68	0.83	5.60	0.87
FC1717	Breccia	Indiferentiate	10.1	19.6	2.60	11.3	2.88	1.14	3.39	0.59	3.74	0.94	2.71	0.39	2.61	0.43
FC1760	Pillow basalt	SOC	1.7	4.2	0.69	4.0	1.22	0.49	1.77	0.33	2.28	0.50	1.52	0.23	1.47	0.21
FC1761	Pillow basalt	SOC	1.9	4.8	0.79	4.2	1.49	0.59	2.30	0.45	2.98	0.67	1.99	0.29	1.74	0.27
FC1763	Metabasalt	SOC	7.6	20.0	2.98	14.3	3.84	1.33	4.91	0.90	6.21	1.52	4.59	0.70	4.66	0.72
FC1765	Metabasalt	SOC	7.3	17.1	2.55	12.3	3.55	1.35	4.53	0.80	5.16	1.10	3.20	0.47	2.96	0.47
FC1722	Breccia	Tobífera Fm.	34.9	68.9	7.89	28.0	5.34	1.18	4.00	0.47	2.24	0.43	1.31	0.20	1.34	0.21
FC1723	Metatuff	Tobífera Fm.	32.4	65.2	7.65	27.6	5.60	0.50	5.78	0.96	5.69	1.31	3.90	0.61	4.11	0.62
FC1727	Metatuff	Tobífera Fm.	25.0	54.2	6.93	27.3	6.27	1.11	6.76	1.24	7.30	1.56	5.05	0.72	4.70	0.70
FC1749	Metatuff	Tobífera Fm.	11.0	25.1	3.05	12.1	3.23	0.31	3.53	0.73	4.73	1.12	3.40	0.52	3.38	0.53
FC1750	Metapelite	Tobífera Fm.	37.5	84.7	9.84	37.7	8.33	0.90	8.23	1.33	7.92	1.73	5.00	0.72	4.64	0.70
FC1751	Metatuff	Tobífera Fm.	13.3	31.9	4.34	17.6	5.24	0.29	5.70	1.18	7.95	1.76	5.70	0.84	5.55	0.80
FC1755	Rhyolite	Tobífera Fm.	16.5	49.2	4.92	20.1	5.38	0.37	5.74	1.01	6.35	1.41	4.14	0.61	3.96	0.61
FC1762	Metatuff	Tobífera Fm.	34.0	65.4	7.71	28.2	5.67	0.64	5.68	0.92	5.55	1.23	3.57	0.51	3.23	0.50

Table 5.2.3. Whole rock trace elements composition in ppm.

Sample	Lithotype	Unit	Ba	Ni	Sc	Be	Co	Cs	Ga	Hf	Nb	Rb	Sn	Sr	Ta	Th	U	V	W	Zr	Y	K	P	Ti
FC1704	Metapsamite	pJ basement	213	21	9						14			2						245	22	9300	1400	4900
FC1726	Calc silicate schist	Tobífera Fm.	538	<20	19						16			242						271	37	16300	1900	9600
FC1753	Schist	Zapata Fm.	668	29	19						22			291						261	24	40100	2300	9700
FC1767	Schist	Tobífera Fm.	608	26	5						8			251						96	32	16900	600	1000
FC1770	Schist	Tobífera Fm.	77	63	12						6			94						60	42	2800	29000	2600
FC1710	Lapilli-tuff	Indiferentiate	473	<20	19	2	79.1	0.8	17.5	5.4	9.9	43.4	2	81	0.7	9.5	2.3	115	326.5	212.3	33.8	17800	3000	9900
FC1711	Porphyritic andesite	Indiferentiate	368	<20	12	1	76.1	0.8	16.9	3.7	4.8	63.7	1	511.7	0.4	8.2	1.8	100	333.6	133.4	16.1	21100	1500	6300
FC1714	Lapilli-tuff	Indiferentiate	464	<20	18	<1	51.3	1.3	16.1	4.7	7.3	69.2	2	325.9	0.6	7.8	1.9	120	223.8	170.5	27.5	22400	2100	8200
FC1715	Metabasalt	Indiferentiate	302	<20	17	<1	69.6	1	17.8	7.8	9.5	79.4	2	174.5	0.6	7.2	1.6	16	421.3	297.9	47.9	26800	2600	7800
FC1717	Breccia	Indiferentiate	165	27	28	2	276	0.7	16	2.1	2.3	14.5	<1	208	0.5	2.7	0.8	111	2288.4	64.9	23.6	7400	2500	6600
FC1760	Pillow basalt	SOC	57	151	23	<1	70	1.3	10.7	0.9	0.4	23.2	<1	156.3	<0,1	0.3	0.6	140	242.5	32.6	12.7	7400	400	5100
FC1761	Pillow basalt	SOC	13	296	25	<1	77.4	0.3	15.2	1	0.5	1.1	<1	95.3	<0,1	0.3	2.2	191	33.5	32.1	16.8	600	700	6600
FC1763	Metabasalt	SOC	25	105	46	<1	164.4	<0,1	17.8	3.3	3.5	<0,1	<1	116.9	0.3	1.8	0.3	283	946.5	121.5	38.3	500	2100	15800
FC1765	Metabasalt	SOC	454	71	41	<1	61.9	0.4	15.1	2.3	2.2	15.3	<1	151.4	0.2	1.1	0.2	278	154.6	88	29.3	9300	1400	12700
FC1768	Metabasalt	SOC	628	123	39						7			6						85	18	24700	1900	10300
FC1722	Breccia	Tobífera	216	<20	8	2	89.1	1.8	19.2	2.2	5.5	51.5	14	13.8	0.5	6.6	1.7	65	569.8	76.5	12	13700	1000	3200
FC1723	Metatuff	Tobífera	690	<20	6	4	46.7	2.9	15.2	5.1	8.1	104.3	4	56.9	0.9	18.7	3.4	<8	298.6	138.4	30.9	29100	100	900
FC1727	Metatuff	Tobífera	762	<20	8	1	89.5	1.3	12.8	5.3	9.1	97.5	3	55.7	0.8	13.5	3.3	<8	501.4	168.6	43	28800		1200
FC1749	Metatuff	Tobífera	220	<20	5	2	60.6	1.1	11.4	3.4	7	76.4	5	52.3	0.9	15.3	4.1	<8	372.2	71.2	30.6	16500		600
FC1750	Metapelite	Tobífera	769	<20	14	4	123.1	4.6	19.1	5.4	11.7	218.2	4	21.2	1.1	17.1	5.5	85	1093.8	159.8	54.8	46900	1000	4500
FC1751	Metatuff	Tobífera	367	<20	5	3	58.5	2.5	15.3	4.3	8.9	130	6	36.1	1.3	21.4	5.6	<8	359.3	91.6	48.9	29000	100	500
FC1755	Rhyolite	Tobífera	1606	<20	8	4	110.2	0.8	12.8	3.5	7.8	152.7	2	107.9	1.1	16.1	2.9	<8	681.1	84.5	37.6	63600		600
FC1762	Metatuff	Tobífera	773	<20	5	<1	111.9	0.9	9.2	4.4	6.4	89.9	2	129.7	0.8	13.6	3.3	<8	714	139.3	31.9	47500	200	1000
FC1720	Shale	Zapata	381	30	20						5			497						81	19	12400	600	5200
FC1757	Metapsamite	Zapata	657	20	9						11			58						244	23	32300	1400	5000

The figure 5.2.1 e is the classification of alkalinity of the rocks by Shand (1943). The Tobífera rocks are peraluminous, the mafic indiferentiate rocks of Jeronimo channel are metaluminous and the mafic rocks of SOC in Gajardo channel are divided in two groups, peraluminous and metaluminous. The foliated metabasalts of SOC are metaluminous to peraluminous. In the AFM diagram of Irvine and Baragar (1971) the Tobífera rock samples are in the calc-alkaline series, while the mafic rocks of SOC in Gajardo channel are in the tholeitic series. The anomalous rock sample of Tobífera with high amount of FeOt is the breccia. The mafic indiferentiate rocks of Jeronimo channel are in the calc-alkaline series, but the metabasalt (FC1715) is tholeitic.

In the Harkers diagram of variation (figure 5.2.2) all the rock samples including the pre-Jurassic basement and the Zapata rock samples were plotted to make correlations between the units. As expected, the metabasalts of SOC are the more primitive rocks, with small amounts of SiO_2 and are plotted on the left of the diagrams. A sequence of magmatic differentiation can be seen in the group of metabasalts of Gajardo channel, the pillow picro-basalt is the most primitive, evolving to the foliated metabasalts, and then to the pillow basalt, by a consumption of TiO_2, Al_2O_3, MgO, CaO, and FeOt (a-d, h) forming a negative alignment. The digrams for Na2O and K2O (Fig. 5.2.2 d-f) are has a high dispersion of the data, but a positive tendence can be slightly traced due to the magmatic enrichment in alkalis. The mafic rocks of Jeronimo channel forms another group, more differentiated than the metabasalts of Gajardo channel, and they can have different magmatic sources, due to the gap between these two groups besides geochemical differences in the most of the classifications. However, the tendence lines of magmatic evolution are the same that Gajardo channel, negative for Ti-Fe-Mg-Ca-Al-P and positive for Na-K. The Tobífera felsic rocks are the most differentiate among the volcanic, grouped on the right side of the Herker diagrams. The tendence lines are negative for Ti-Fe-Mg-Ca-Al-P and disperse for Na-K, but slightly positive.

Figure 5.2.1: Geochemical classification diagrams for 18 volcanic rocks of RVB: a) TAS (Middlemost, 1994); b) R1-R2 (De la Roche et al., 1980); c) Nb/Y – Zr/TiO_2 (Winchester and Floyd, 1977; d) Jensen (1976); e) A/CNK [$Al_2O_3/(CaO+Na_2O+K_2O)$] – A/NK [Al2O3/(Na_2O+K_2O)](Shand, 1943); f) AFM (Na_2O+K_2O, FeOt, MgO).

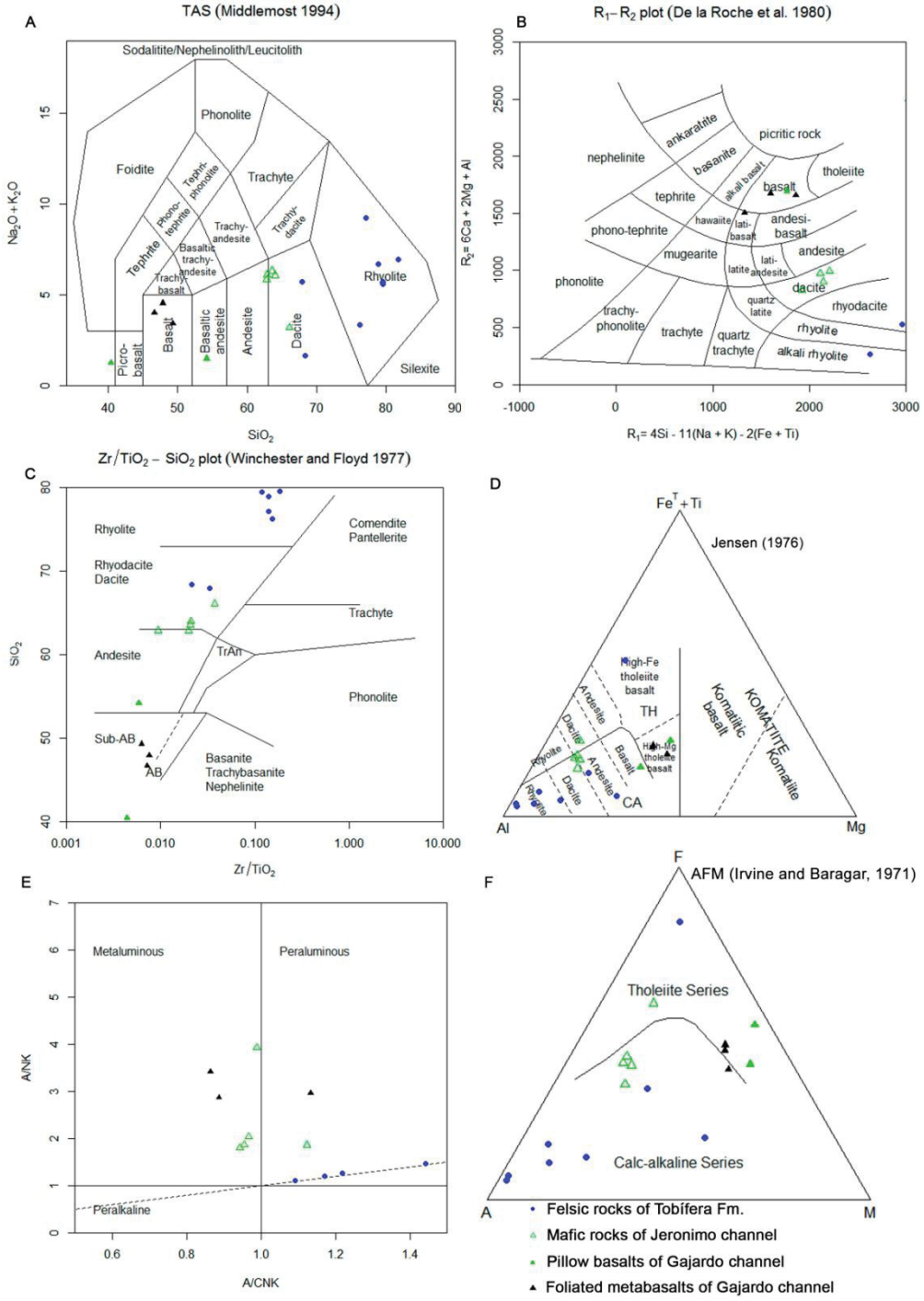

The metasedimentary rocks of the pre-Jurassic basement and Zapata Fm. are dispersed in the diagrams. Lines of tendence can be traced, although the dispersion, and are negative for Ti-Fe-Mg-Ca-Al-P, for Na-K the dispersion is very high. Normally these metasedimentary rocks are close to the group of the mafic rocks of Jeronimo channel, but probably it is due to similar amounts of

SiO_2 but they can not be directly correlated, the basement must be older than the mafic rocks and a crustal contamination during mafic magmatism could be occurred, but is not certain.

Figure 5.2.2: Harker variation diagrams for the 18 volcanic rock samples of RVB, 6 metasedimentary rocks of Pre-Jurassic basement and 1 of metasedimentary rock of Zapata Fm., using the oxides a) TiO_2, b) Al_2O_3, c) MgO, d) CaO, e) Na_2O, f) K_2O, g) P_2O_5, h) FeOt versus SiO_2.

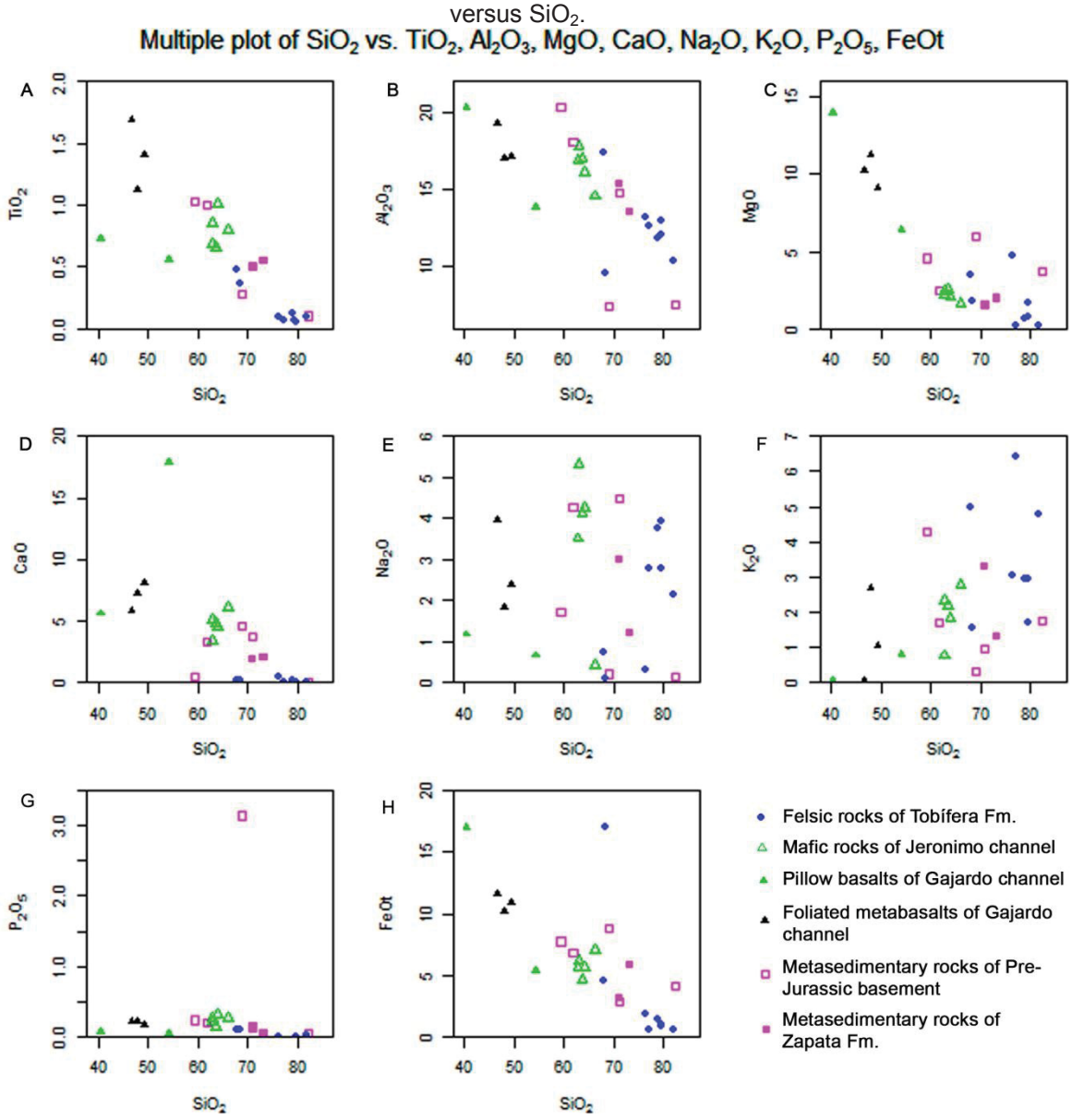

The figure 5.2.3 show the spider diagrams for the volcanic rock samples of RVB. In the REE spidergram (Fig. 5.2.3 a) the Tobífera felsic rocks are depleted in heavy REE (HREE) and present a strong negative anomaly of Eu, what occurs due to plagioclase retention in the source and these rocks are result of fractional crystallization (Rollinson, 1993). The depletion of the HREE

relative to light REE (LREE) may be due to hornblende retention in the source, but zircon also retains HREE and could have caused fractionation in the melt. The only sample that slightly leaves the pattern of Tobífera Fm. is the sedimentary breccia, and because of this cannot be correlated to the other magmatic samples.

The mafic rocks of the indiferentiate unit and SOC show strong differences in two groups of REE patterns, besides, the metabasalts of SOC in Gajardo channel can be subdivided in two groups. For the SOC rock samples, both the pair of foliated metabasalts and the pair of pillow basalts present a flat REE pattern, typical of mafic rocks similar to the primitive mantle, but the foliated metabasalts are more enriched in REE. It can prove differences in magmatic generation or modifications due to metamorphism, considering that foliated metabasalts must have experienced a metamorphism accompanied of deformation and secondary fluids must have interacted with the rocks. However, REE often are inmobile during low-grade metamorphism or hydrothermalism (Rollinson, 1993). Even so, the enrichment in REE on the foliated metabasalts probably show that they are less evolved than the pillow basalts that are more differentiate. The mafic indiferentiate rocks of Jeronimo channel are enriched in REE in relation to the Gajardo channel metabasalts. The REE pattern is depleted in HREE, and they have a weak negative anomaly of Eu, showing a higher degree of fractional crystallization. These mafic rocks of Jeronimo channel show patterns more similar to the felsic rocks of Tobífera Fm. than the mafic rocks of Gajardo channel, this evidence, coupled to the other geochemical data presented before show that their affinity is more calc-alkaline and they are more differentiate than the mafics of Gajardo channel.

In the spidergrams for the incompatible elements (Fig. 5.2.3 b) the patterns are very similar for all the rocks, felsic and mafic, but the mafic of Gajardo channel are lesser enriched in the incompatible elements, proving one more time the minor degree of differentiation from the primitive mantle. The mafic indiferentiate rocks of Jeronimo channel and the felsic rocks of Tobífera Fm. are very similar on the incompatible pattern and it has a correlation with the lower continental crust, where the positive anomaly of K and Zr are characteristic due to feldspars and zircon in the composition of the differentiate rocks (Rollinson, 1993). The mafic rocks are more enriched in Sr and Ti

compared to the felsic rocks, what is expected because Ti is present in mafic minerals and Sr in plagioclase.

Figure 5.2.3: Spidergrams for a) REE elements normalized to chondrite (Nakamura, 1974) and b) for the trace elements normalized to the Chondrite (Sun and McDonough, 1989). Abbreviations: l.t. – lapilli-tuff; and. – andesite, m.b. – mafic breccias; p.b. – pillow basalt; f.b. – foliated basalt.

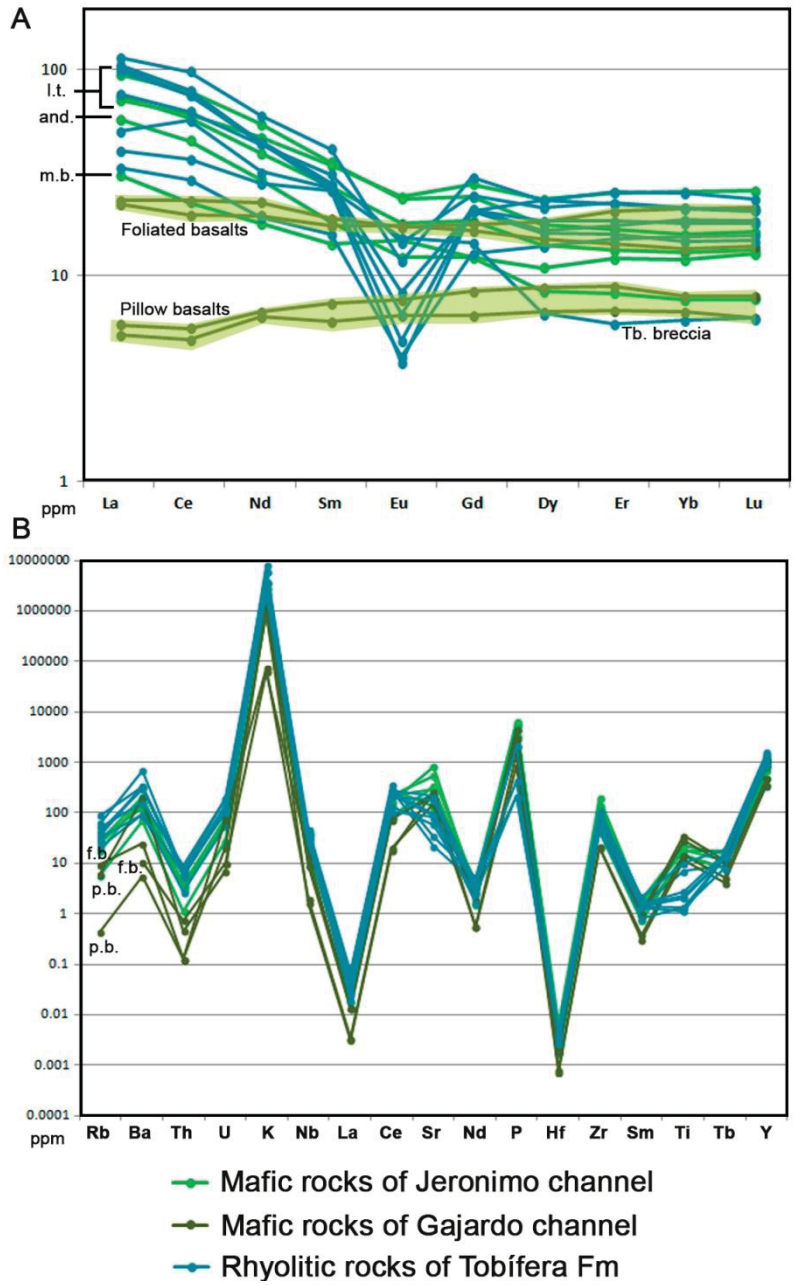

In the geotetonic digrams of figure 5.2.4 the volcanic rock samples are classified in tectonic environments. The Fig. 5.2.4 a show that the mafic rocks of SOC in Gajardo channel are in the volcanic arc array but closer to the MORB-type basalts, the pillow basalts are similar to normal ocean ridge-type and the

foliated metabasalts are more similar to the anomalous ocean ridge-type. The mafic indiferentiate rocks of Jeronimo channel have tendencies of volcanic arc or island arc, as well as the Tobífera volcanic that are volcanic-arc-type. The Fig. 5.2.4 b show the classification of the metabasalts of Gajardo channel as Ocean ridge and floor, in accordance with the correlation with the SOC ophiolites, on the other hand, the mafic rocks of the Jeronimo channelare in the Spreading center island field and closer to the orogenic field, showing that they have a greater influence of subduction. In the Fig. 5.2.4 c, the foliated metabasalts are clearly plotted in the MORB field, while the pillow basalts as well as the mafic rocks of Gajardo channel are classified as island arc lavas, corroborating the subduction influence. In the diagrams of Pearce et al. (1974) (Fig. 5.2.4 d, e) both the mafics and the felsic rocks are volcanic arc-type, this diagram was idealized for granite classification, but we used here for a better classification of the rhyolites. In the diagrams of Schandl and Gorton (2002) the Tobífera rock samples are plotted as active continental margin and the mafic also, but the metabasalts of Gajardo channel are closer to within plate volcanic zones.

Thus, the geochemical diagrams show at least three groups for the volcanic rocks: the Tobífera felsic rocks, with a rhyolitic composition and calc-alkaline affinity; the Jeronimo channel mafic indiferentiate rocks with andesitic to dacitic composition and calc-alkaline affinity; and the metabasalts of SOC in Gajardo channel with high-Mg basalt to basalt compostions and tholeitic affinity, which can be subdivided in two groups, one more primitive that are the foliated metabasalts, and one more evolved of meta pillow basalts. The geotectonic environment varies, from a mid-ocean ridge of generation of basalts, to an island arc and volcanic arc to the generation of the andesites, dacites and rhyolites. The geochemistry of metasedimentary rocks is not distinctive but has intermediate compositions similar to the dacites and andesites of the Jeronimo channel.

Figure 5.2.4: Diagrams for tectonic classification of the 18 volcanic rock samples of the RVB: a) Th/Yb vs. Nb/Yb (Pearce, 2008); b) FeOt-MgO-Al2O3 (Pearce et al., 1977); Zr vs. Ti (Pearce, 1982); d) Rb vs. Y+Nb and e) Ta vs. Yb (Pearce et al., 1974); f) Th/Ta vs. Yb and g) Ta vs. Yb (Schandl and Gorton, 2002).

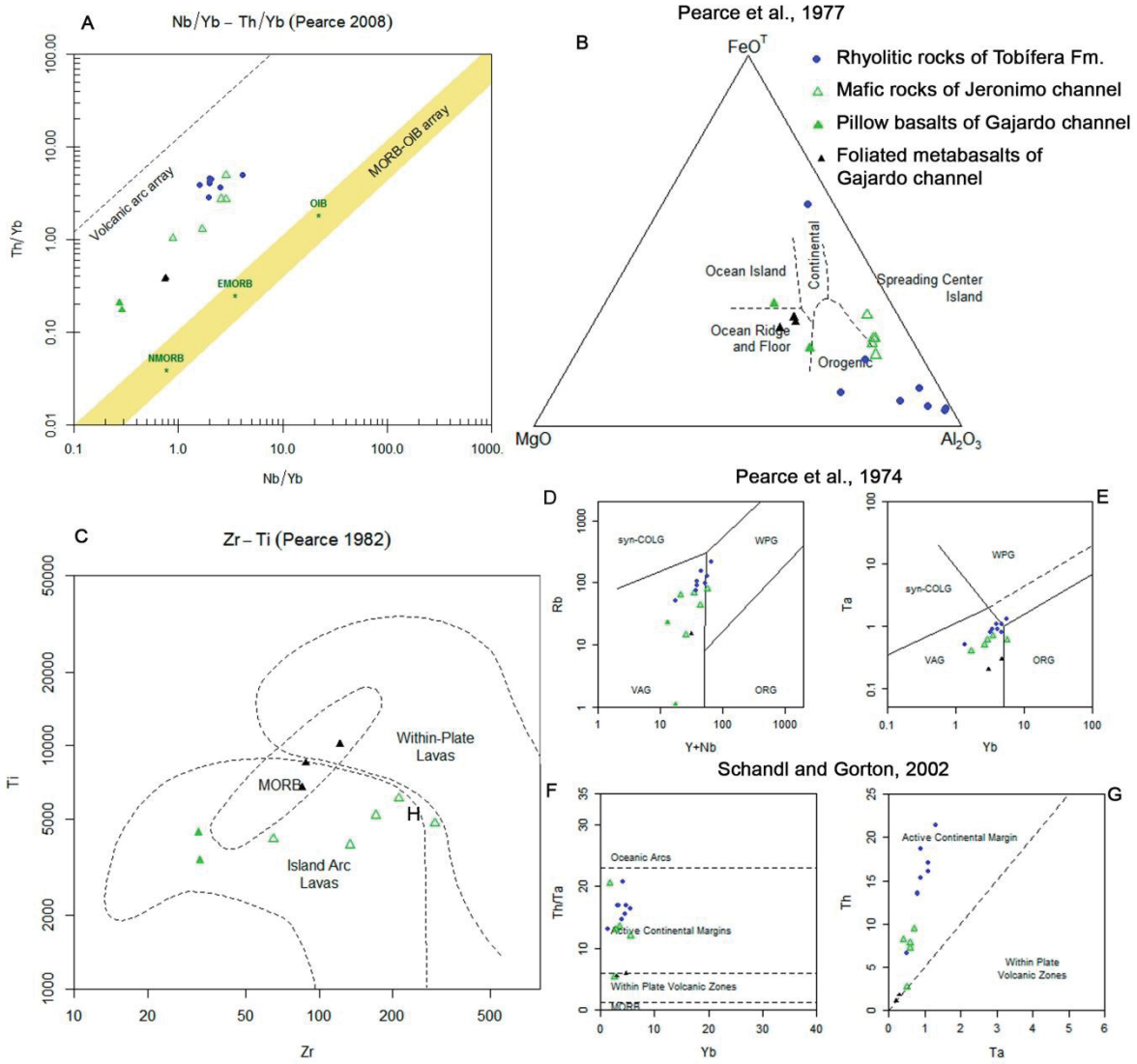

6 DISCUSSION

Discussions about the structural development of the Magallanes fold and thrust belt, triggered by the emplacement of Rocas Verdes ophiolites over the South American continental margin, were firstly made in the article attached to this dissertation. The formation of an accretionary wedge to the east of the ophiolites, and below the magmatic arc developed on the drifted microplate to the west of the South American continental platform, was proposed due to metamorphic features on the felsic volcanic rocks of Tobífera Fm. and metasedimentary rocks of the Zapata Fm., which must be partially subducted under the Sarmiento ophiolites and the magmatic arc, and record a low grade metamorphism with high-pressure peak, typical of subduction environment. The development of thrust zones of highly strained rocks have formed during this phase and two foliations trending NNW-SSE and dipping normally to the southwest show the vergence of the imbrications with top to the northeast, but they also dip to the northeast due to folds and a possible second phase of backthrusts during the uplift.

The complementary petrographic data of the RVB rock units are in agreement with the structural data and the P-T pseudosections presented in the article in the sense of mineral assemblages showing subgreenschist to lower greenschist facies metamorphism. The metamorphism is orogenic, related to subduction and temperatures are normally near 300°C, and pressures between 3 and 5 kbar, the peak is 14 kbar. However, primary volcanic and sedimentary textures and microstructures often coexist with metamorphic textures and deformation, showing deformation at upper crustal levels.

In the metabasalts of SOC identified in the western Gajardo channel, a previous ocean-floor metamorphism acted during and after the oceanic spreading, resulting in the characterist mineral assemblage: actinolite-chlorite-plagioclase-epidote-titanite-carbonate of upper greenschist facies, without modification of the primary structures like the pillows. The ocean floor metamorphism generate fracturing filled by hydrothermal phases, and pillow structures also worked as conduits for percolation of fluids, the filling with carbonate suggest enrichment of CO2 in the fluids. However, some of these metabasalts are strongly foliated with stretched porphyroblasts of actinolite, cleavage domains of chlorite and preferred oriented plagioclase, titanite and

carbonate. The foliation development is probably related to the emplacement of the metabasalts over the continental crust, generating shearing by thrusts with top to the northeast. The geochemistry of these metabasalts is similar to the mid-ocean ridge basalts derived from the primitive mantle, and thus they seems to be part of the Sarmiento ophiolitic complex, generate by spreading centers of the Rocas Verdes backarc basin (Calderón et al., 2007b; Stern and De Wit, 2003). However, the multielementar pattern on the spidergram of figure 7.2.3 b is similar to the patterns of the lower continental crust, showing that a subduction component also can be involved, and pointing for a suprasubduction zone environment for the generation of the ophiolites, in accordance with the models proposed by Calderón et al. (2007b) and early by Stern and De Wit (2003).

The mafic indiferentiate rocks of Jeronimo channel have clearly differences from the mafic rocks of Gajardo channel, petrographically and geochemically. The rocks in Jeronimo channel have not signals of deformation and are mainly volcaniclastic rocks as lapilli-tuffs and breccias, some massive metabasalts and one sample of andesite with the porphyritic texture totally preserved, with phenocrystals of plagioclase, hornblende and actinolite. The metamorphism is very low or just a hydrothermalism that generate epidote, chlorite and carbonate. The geochemical classification of these rocks is andesites or dacites, and their REE and multielementar patterns show affinities with the lower continental crust. The geotectonic diagrams classify the environment of formation of these rocks as island arc or volcanic arc, what implies in a subduction environment. Currently it´s not possible to prove cogeneticity among the metabasalts of Gajardo channel and the mafic rocks of Jeronimo channel, because their geochemical fingerprints are very different in all the classifications done in this work. However, the previous work of Calderón (2007b) describe dacitic dikes and rhyolitic dikes in the Samiento complex as a result of bimodal magmatism involving crustal contamination, as well as some metatuffs in the upper layer of the Sarmiento complex, like final members of fractional crystallization starting in the upper mantle, and evolving to the upper crust. Thus, the mafic rocks of Jeronimo channel can be part of the Sarmiento Ophiolitic Complex, with higher influence of subduction and crustal contamination. Nevertheless, isotopic studies must be made to a better

correlation between these mafic rocks, and these volcanic rocks have been correlated to Miocenic indiferentiate sedimentary rocks due to their intercalation.

The Tobífera felsic rocks are calc-alkaline and have signatures of volcanic arc. In the extensive bibliography (Calderón et al., 2007a, 2007b; Hervé et al., 2007a, Hervé et al., 2007b; Stern and De Wit, 2003; Pankhurst et al., 2000; Dalziel, 1981; Allen, 1982) the Tobífera Fm. are described as felsic volcanism related to the rifts during the early break-up of Gondwana, but the proto-Pacific convergent margin influenced the magmatism resulting in the volcanic arc geochemical fingerpring. However, Calderón et al. (2007a, 2007b) also describes a bimodal magmatism in the Sarmiento Ophiolitic complex, with felsic metatuffs and granophyres in the intermediate layers of the complex, with similar petrological and geochemical features. Therefore, is difficult to differentiate felsic rocks of Tobífera Fm. from the felsic rocks of Sarmiento Complex, and isotopic studies must be indicate to this understanding, as Calderón et al. (2007b) make with Nd isotopy. In the geochemical diagrams, the felsic samples have similar REE and multielementar patterns with the mafic rocks of the Jeronimo channel, and a higher degree of fractional crystallization from the same source is a possible explanation. Anyway, the andesites and dacites of Jeronimo channel, and the felsic rocks accredited to Tobífera Fm. have formed in an active convergent margin, and the subduction had important contribution in magma generation. Correlations among the felsic magmatism in the Tobífera Fm. and the first phase of magmatism in the volcanic arc growing in the drifted microplate to the west also are done by other authors (Hervé et al., 2007b; Stern and De Wit, 2003; Pankhurst et al., 2000).

Dating of the mafic rocks of the Jeronimo channel and Gajardo channel must help to understand the genesis of this mafic volcanism and make correlations with the Tobífera Fm., which is dated in this study in 159.9 ± 1 Ma. Nd, Sr and Ar isotopes also should have provide important constraints in the timing and evolution of the units of RVB in this area, which remains poorly explored comparing to the Cordillera Darwin and Cordillera Sarmiento regions.

The origin and evolution of the pre-Jurassic basement in the region is another topic of interest for the tectonic reconstructions of the Southwesternmost Gondwana. In this study, we recognized metassedimentary rocks, mainly metapelites and metapsamites, but also calc-silicate rocks not

described before, deformed in at least two deformational phases, including defomation during the Cretaceous Andean deformation in lower crustal levels, after exhumed and imbricated with RVB units. A metamorphism at upper greenschist facies is clearly identified by the mineral assemblages, but is uncertain the timing of its occurrence and overprinting of older metamorphic events must be studied. A Cretaceous metamorphism is described for the Cordillera Darwin Metamorphic Complex, considering that it have been correlated to the Eastern Andes Metamorphic Complex, a Cretaceous metamorphism in the rocks of the study area may be occurred and not only the Permian and/or Jurassic metamorphic episodes must be affected these rocks.

Besides that, many discussions can be raised studying the origin of sediments of the pre-Jurassic basement, starting from the environment of deposition and its role for the Andean Orogeny development, and finally comparing the detrital sedimentary patterns with the metasedimentary rocks of Tobífera and Zapata Fm. to differentiate them and reconstruct the early environment of opening of the basin. In the Gajardo channel, the metasedimentary rocks were first accredited to pre-Jurassic basement due to the polyphasic deformation and greenschist metamorphism in metapelites. However, the detrital zircons presented in this study for a rock sample in the middle of Gajardo channel proved to be Zapata Fm. due to the main population of Cretaceous zircons, together with Paleozoic and Proterozoic populations of zircons. It implies in two new discoverings: the degree of deformation and metamorphism in Zapata Fm. may be much higher than accredited to it, and the imbrications with Pre-Jurassic basement slices can be fewer than mapped before.

7 CONCLUSIONS

This work have contributed for the understanding of the evolution of the Rocas Verdes Basin in Southern Patagonia in many ways, from its opening to its closure, with new constraints about magmatic generation, depositional ages, paleogeography and sedimentary sources, metamorphic conditions for the emplacement of ophiolites, deformational events and tectonic setting for the Magallanes fold and thrust belt formation and exhumation. Some of the new data and its importance are the following:

1- The maximum age of deformation and exhumation of the hinternland of the Magallanes fold and thrust belt is between 82.5 ± 1.7 Ma and 71.4 ± 1.1 Ma, dated by an intrusive body of the thrid magmatic phase of the South Patagonian Batholith.

2- The metamorphism in highly strained felsic volcanic rocks of the Tobífera Fm. and metasedimentary rocks of the Zapata attained equilibrium at 300 ± 30°C and the pressures recorded are from 3.5 to 5 kbar, with a peak of 14 kbar, attesting a subduction environment and formation of an accretionary wedge subducted until 33 km depth below the emplaced ohpiolites and the magmatic arc to the west.

3- The formation of the accretionary wedge was accommodated by thrust faults with top to the northeast forming protomylonites and phyllonites dipping to southwest in rocks of Tobífera Fm., Zapata Fm. and Sarmiento ophiolites. The detachment levels seem to be the horizon of contact with the Pre-Jurassic basement.

4- Two Andean phases of deformation were responsible for the development of the Magallanes fold and thrust belt, first the initiation of the subduction of the ophiolites and the accretionary wedge formation progressing during the shortening of the RVB untis by folds and thrusts, and second the exhumation of the hinternland by backthrust verging to the west.

5- The latter foliation of the pre-Jurassic basement is correlative to the foliations developed in the RVB units, and it attest for a Late Cretaceous deformation in the basement in lower crustal levels, while the RVB units deformed at upper crustal levels in a brittle-ductile environment. A Cretaceous metamorphism in the Pre-Jurassic basement also is thought.

6- The Tobífera magmatism is dated 159.9 ± 1 Ma, older than expected and leads to a diachronous felsic magmatism during the RVB opening from south to north. The geochemical fingerprints are calc-alkaline and must be highly influenced by the subduction in the active convergent margin on the Patagonian Andes.

7- The maximum age of deposition of the Zapata Fm. is dated 123.6 ± 0.9 Ma, younger than expected, and Paleozoic and Proterozoic populations of detrital zircons, similar to basement detrital zircon patterns, prove that the Pre-Jurassic basement was source of sediments for Zapata Fm, probably like horsts exposed to erosion .

8- The sedimentation in the deep marine Magallanes foreland basin includes clasts derived from the RVB and the Pre-Jurassic basement, showing that exhumation of the basement by the latter phase of thrusts was prior or synchronous to the foreland basin development (Cenomanian).

9- The mafic rocks of the Seno Otway and Seno Skyring region can be divided in two groups, one of metabasalts with MORB-signature of the Sarmiento Ophiolitic Complex, found at the western Gajardo channel, and one group of andesitic-dacitic volcanic rocks with calc-alkaline signature and island arc basalt affinity, found at Jeronimo channel, and their correlation with the Sarmiento ophiolites is uncertain, they were grouped in a Miocene Indiferentiate unit together with metasedimentary intercalled rocks.

REFERENCES

Allen, R.B., 1982. Geología de la Cordillera Sarmiento, Andes Patagónicos, entre los 51º00' y 52º15' Lat. S, Magallanes, Chile. Servicio Nacional de Geología y Minería. Boletín 38, 1–46.

Ambrosio, Ghiglione, Orts, 2010. Estructura Bloque Otway. Unpublished, Universidad de Buenos Aires and Geopark.

Anonymous, 1972. Penrose field conference on ophiolites. Geotimes 17, 24–25.

Aoki, K., Itaya, T., Shibuya, T., Masago, H., Kon, Y., Terabayashi, M., Kaneko, Y., Kawai, T., Maruyama, S., 2008. The youngest blueschist belt in SW Japan: implications for the exhumation of the Cretaceous Sanbagawa high-P/T metamorphic belt. Journal of Metamorphic Geology 26, 583–602.

Avendaño, V., Calderón, M., Hervé, F., Simonetti, A., 2008. Aptian seafloor metamorphic event in the Rocas Verdes basin: titanite U-Pb dating of microbial-like structures in the Tortuga Ophiolite, Fuegian Andes. 33rd International Geological Congress, Symposium MRD-14 Ophiolites, greenstone belts and ore deposits, Oslo, Norway.

Bell, T.H., Etheridge, M.A. 1973. Microstructure of mylonites and their descriptive terminology. Lithos, 6 (4), 337–348.

Bernhardt, A., Jobe, Z.R., Lowe, D.R., 2011. Stratigraphic evolution of a submarine channel-lobe complex system in a narrow fairway within the Magallanes foreland basin, Cerro Toro Formation, southern Chile. Mar. Pet. Geol. 28, 785-806. https://doi.org/10.1016/j.marpetgeo.2010.05.013

Betka, P., Klepeis, K., Mosher, S., 2015. Along-strike variation in crustal shortening and kinematic evolution of the base of a retroarc fold-and-thrust belt: Magallanes, Chile 53°S–54°S. Geological Society of America Bulletin, 127 (7–8), 1108–1134. doi:10.1130/B31130.1

Betka, P.M., 2013. Plate 1: Geologic map and cross-sections of the Patagonian fold-thrust belt, Magallanes, Chile 1:100,000. In: Betka, P. M., 2013. Structure of the Patagonian fold-thrust belt in the Magallanes region of Chile, 53°-55° S Lat. Unpublished PhD thesis, The University of Texas at Austin.

Bruhn, R.L., Stern, C.R., de Wit, M.J., 1978. Field and geochemical data bearing on the development of a Mesozoic volcano-tectonic rift zone and back-arc basin in southernmost South America. Earth and Planetary Science Letters 41 (1), 32–46.

Bucher, K., Grapes, R., 2011. Petrogenesis of metamorphic rocks. Springer Science and Business Media.

Calderón, M., Fildani, A., Hervé, F., Fanning, C.M., 2007a. Late Jurassic bimodal magmatism in the northern sea-floor remnant of the Rocas Verdes

basin, southern Patagonian Andes. Journal of the Geological Society of London, 164, 1011–1022.

Calderón, M., Fosdick, J.C., Warren, C., Massonne, H.J., Fanning, C.M., Cury, L.F., Schwanethal, J., Fonseca, P.E., Galaz, G., Gaytán, D., Hervé, F., 2012. The low-grade Canal de las Montañas Shear Zone and its role in the tectonic emplacement of the Sarmiento Ophiolitic Complex and Late Cretaceous Patagonian Andes orogeny, Chile. Tectonophysics, 524–525, 165–185. doi.org/10.1016/j.tecto.2011.12.034

Calderón, M., Galaz, G., Tascón, G., Ramírez, C., Luca, R., Massonne, H.-J., Brandelik, A., Hervé, F., 2005. Metamorphic P-T constraints for non-coaxial ductile flow of Jurassic pyroclastic deposits: key evidence for the closure of the Rocas Verdes basin in southern Chile. 6th International Symposium on Andean Geodynamics. ISAG, Barcelona, 138–141.

Calderón, M., Hervé, F., Cordani, U., Massonne, H.-J., 2007b. Crust-mantle interactions and generation of silicic melts: insights from the Sarmiento Complex, southern Patagonian Andes. Rev. Geológica Chile 34 (2), 249–275.

Calderon, M., Prades, C. F., Herve, F., Avendaño, V., Fanning, C. M., Massonne, H. J., Theye, T., Simonetti, A., 2013. Petrological vestiges of the Late Jurassic-Early Cretaceous transition from rift to back-arc basin in southernmost Chile: New age and geochemical data from the Capitán Aracena, Carlos III, and Tortuga ophiolitic complexes. Geochemical Journal, 47 (2), 201–217.

Coleman, R.G. 2014. The ophiolites concept evolves. Elements, 10, 2, 82-84. DOI:10.2113/gelements.10.2.82

Coloma, F., Avendaño, V., Calderón, M., Astudillo, N., Rapalini, A., 2011. Petrologic and paleomagnetic structure of the Upper Mesozoic Tortuga Ophiolite, Fuegian Andes. Latinmag Letters, 1, 1–7.

Connolly, J.A.D., 1990. Multivariable phase diagrams; an algorithm based on generalized thermodynamics. American Journal of Science 290 (6), 666–718.

Cunningham, W. D., 1995. Orogenesis at the southern tip of the Americas: the structural evolution of the Cordillera Darwin metamorphic complex, southernmost Chile. Tectonophysics, 244, 197–229.

Dalziel, I.W.D., 1981. Back-arc extension in the southern Andes: A review and critical reappraisal. Royal Society of London Philosophical Transactions A, 300, 319–335.

Dalziel, I.W.D., 1986. Collision and Cordilleran orogenesis: an Andean perspective. In: Coward, M.P., Ries, A. C. (Eds.), Collision Tectonics. Geological Society of London Special publications, 19, 389–404.

De La Roche, H., Leterrier, J. T., Grandclaude, P., and Marchal, M. 1980. A classification of volcanic and plutonic rocks using R1R2-diagram and major-element analyses—its relationships with current nomenclature. Chemical geology, 29(1-4), 183-210.

Dilek, Y., Furnes, H., 2011. Ophiolite genesis and global tectonics: Geochemical and tectonic fingerprinting of ancient oceanic lithosphere. Geological Society of America Bulletin, 123, 387–411.

Dilek, Y., Furnes, H., 2014. Ophiolites and their origins. Elements 10, 93–100. doi.org/10.2113/gselements.10.2.93

Dilek, Y., Furnes, H., Shallo, M., 2007. Suprasubduction zone ophiolite formation along the periphery of Mesozoic Gondwana. Gondwana Research, 11, 453–475.

Dilek, Y., Polat, A., 2008. Suprasubduction zone ophiolites and Archean tectonics. Geology, Geol. Soc. Am., 36, 5, 431-432.

Dilek, Y., Whitney, D.L., 1997. Conterclockwise P-T-t trajectory from the metamorphic sole of a Neo-Tethyan ophiolite (Turkey). Tectonophysics, 280, 295–310.

Elthon, D., Stern, C.R., 1978. Metamorphic petrology of the Sarmiento Ophiolite Complex, Chile. Geology, 6 (8), 464–468.

Ernst, W.G., 1999. Metamorphism, partial preservation, and exhumation of ultrahigh-pressure belts. The Island Arc, 8, 125–153.

Fildani, A., Cope, T.D., Graham, S.A., Wooden, J.L., 2003. Initiation of the Magallanes foreland basin: Timing of the southernmost Patagonian Andes orogeny revised by detrital zircon provenance analysis. Geology 31, 1081–1084. https://doi.org/10.1130/G20016.1

Fildani, A., Hessler, A.M., 2005. Stratigraphic record across a retroarc basin inversion: Rocas Verdes-Magallanes Basin, Patagonian Andes, Chile. Bull. Geol. Soc. Am. 117, 1596–1614. https://doi.org/10.1130/B25708.1

Fildani, A., Romans, B.W., Fosdick, J.C., Crane, W.H., Hubbard, S.M., 2008. Orogenesis of the Patagonian Andes as reflected by basin evolution in southernmost South America. Arizona Geological Society Digest,22, 259–268.

Forsythe, R., Allen, R.B., 1980. The basement rocks of Península Staines, Región XII, Province of Última Esperanza, Chile. Revista Geológica de Chile, 10, 3–15. http://dx.doi.org/10.5027/andgeoV7n2-a01

Fosdick, J.C., Graham, S.A., Hilley, G.E., 2014. Influence of attenuated lithosphere and sedimentloading onflexure of the deep-water Magallanesretroarc foreland basin, Southern Andes. Tectonics, 33, 2505–2525. doi:10.1002/2014TC003684

Fosdick, J.C., Romans, B.W., Fildani, A., Bernhardt, A., Calderón, M., Graham, S.A., 2011. Kinematic evolution of the Patagonian retroarc fold-and-thrust belt and Magallanes foreland basin, Chile and Argentina, 51°30's. Bull. Geol. Soc. Am. 123, 1679–1698. https://doi.org/10.1130/B30242.1

Fossen, H., 2010. Structural Geology. First ed., Cambridge University Press., Cambridge. https://doi.org/10.1017/CBO9780511777806

Fossen, H., Cavalcante, G.C.G., 2017. Shear zones – A review. Earth-Science Rev. 171, 434–455. https://doi.org/10.1016/j.earscirev.2017.05.002

Fuenzalida, R., Covacevich, V., 1988. Volcanismo y bioestratigrafía del Jurásico y Cretácico Inferior en la Cordillera Patagónica, Región de Magallanes, Chile. In: V Congreso Geológico Chileno 3, H159–H183.

Galaz, G., Hervé, F., Calderón, M., 2005. Metamorfismo y deformación de la Formación Tobífera en la Cordillera Riesco, Región de Magallanes, Chile. Revista de la Asociación Geológica Argentina, 60 (4), 762–774.

Gealey, W.K., 1980. Ophiolite obduction mechanism. In: Panayiotou, A. (Ed.), Ophiolites. Proceedings International Ophiolite Symposium, Cyprus. Cyprus Geological Survey, Nicosia, 228–243.

Gomes, C.B., Dutra, C.V., 1984. A Fluorescência de Raios X na Geologia. In: Gomes, C. B. (Coord.). *Técnicas analíticas instrumentais aplicadas à Geologia.* First Ed., Edgard Blücher ltda., Pró-Minério, São Paulo.

Harambour, S., 2002. Deep seated thrusts in the frontal part of the Magallanes fold and thrust belt, Ultima Esperanza, Chile. XV Congreso Geológico Argentino, 3. El Calafate, Argentina, p. 230. CD ROM.

Hervé, F, Calderón, M., Faúndez, V., 2008. The metamorphic complexes of the Patagonian and Fuegian Andes. Geological Acta, 6, 43–53.

Herve, F., Calderon, M., Fanning, C. M., Kraus, S., and Pankhurst, R. J., 2010b. SHRIMP chronology of the Magallanes Basin basement, Tierra del Fuego: Cambrian plutonism and Permian high-grade metamorphism. Andean Geology, 37(2), 253–275.

Herve, F., Fanning, C. M., Pankhurst, R. J., Mpodozis, C., Klepeis, K., Calderón, M., Thomson, S. N., 2010a. Detrital zircon SHRIMP U–Pb age study of the Cordillera Darwin Metamorphic Complex of Tierra del Fuego: sedimentary sources and implications for the evolution of the Pacific margin of Gondwana. Journal of the Geological Society, 167(3), 555–568.

Hervé, F., Fanning, C.M., 2003a. Early Cretaceous subduction of continental crust at the Diego de Alamgro archipelago, southern Chile. Episodes 26, 285–289.

Hervé, F., Fanning, C.M., Pankhurst, R.J., 2003b. Detrital zircon age patterns and provenance of the metamorphic complexes of southern Chile. J. South Am. Earth Sci. 16, 107–123. doi.org/10.1016/S0895-9811(03)00022-1

Hervé, F., Massonne, H.-J., Calderón, M., Theye, T., 2007a. Metamorphic P-T conditions of Late Jurassic rhyolites in the Magallanes fold and thrust belt, Patagonian Andes, Chile. Journal of Iberian Geology 33, 5–16. ISSN (online): 1886-7995.

Hervé, F., Pankhurst, R.J., Fanning, C.M., Calderón, M., Yaxley, G.M., 2007b. The South Patagonian batholith: 150 my of granite magmatism on a plate margin. Lithos 97, 373–394. doi:10.1016/j.lithos.2007.01.007

Holland, T.J.B., Powell, R., 1998. An internally consistent thermodynamic data set for phases of petrological interest. Journal of Metamorphic Geology 16, 309–343.

INFORME DE TERRENO PROYECTO FONDECYT Nº 1161818, 2017. Calderón, M., Cristóbal, R. A., Fosdick, J., Goddard, A., Ghiglione, M., Muller, V., Rojo, D, Torres, F.

Irvine, T. N. J., Baragar, W. R. A. 1971. A guide to the chemical classification of the common volcanic rocks. Canadian journal of earth sciences, 8(5), 523-548.
Jensen, L. S. 1976. A new cation plot for classifying subalkalic volcanic rocks; Ont dep. Mines Misc Pap67 87–95.

Jolivet, L., Faccenna, C., D'Agostino, N., Fournier, M., Worrall, D., 1999. The kinematics of back-arc basins, examples from the Tyrrhenian, Aegean and Japan Seas. In: Mac Niocaill, C., Ryan, P.D. (Eds), Continental Tectonics, Geological Society, London, Special Publications, 164, pp. 21-53. https://doi.org/10.1144/GSL.SP.1999.164.01.04

Katz, H.R., 1964. Some new concepts on geosynclinal development and mountain building at the southern end of South America. 22nd International Geological Congress, India, Proceedings. New Delhi 4, 242–255.

Klepeis, K., Betka, P., Clarke, G., Fanning, M., Hervé, F., Rojas, L., Mpodozis, C., Thomson, S.N., 2010. Continental underthrusting and obduction during the Cretaceous closure of the Rocas Verdes rift basin, Cordillera Darwin, Patagonian Andes. Tectonics, 29 (3), TC3014. doi:10.1029/2009TC002610.

Kley, J., Monaldi, C. R., Salfity, J. A., 1999. Along-strike segmentation of the Andean foreland: causes and consequences. Tectonophysics, 301(1-2), 75-94.

Kohn, M.J., Spear, F.S., and Dalziel, I.D., 1993, Metamorphic P-T paths from Cordillera Darwin, a core complex in Tierra del Fuego, Chile: Journal of Petrology, 34, 519–542. doi: 10.1093 /petrology /34 .3 .519.

Kohn, M.J., Spear, F.S., Harrison, T.M., Dalziel, I.W.D., 1995. 40Ar/39Ar geochronology and P-T-t paths from the Cordillera Darwin metamorphic

complex, Tierra del Fuego, Chile. Journal of Metamorphic Geolology 13, 251–270.

Kraemer, P.E., 2003. Orogenic shortening and the origin of the Patagonian orocline (56°S.Lat). Journal of South American Earth Sciences 15, 731–748.

Ludwig, K.R., 2000. SQUID 1.00, A User's Manual. Berkeley Geochronology Center Special Publication, 2, 2455.

Maloney, K.T., Clarke, G.L., Klepeis, K.A., Fanning, C.M., and Wang, W., 2011. Crustal growth during back-arc closure: Cretaceous exhumation history of Cordillera Darwin, southern Patagonia. Journal of Metamorphic Geology, 29 (6), 649–672. doi: 10 .1111 /j.1525-1314 .2011 .00934 .x .

Massonne, H.J., Willner, A., 2008. Dehydration behaviour of metapelites and mid-ocean ridge basalt at very-low to low grade metamorphic conditions. European Journal of Mineralogy 20, 867–879.

McAtamney, J., Klepeis, K., Mehrtens, C., Thomson, S., Betka, P., Rojas, L., Snyder, S., 2011. Along-strike variability of back-arc basin collapse and the initiation of sedimentation in the Magallanes foreland basin, southernmost Andes (53–54.5°S). Tectonics, 30 (5), TC5001. doi: 10 .1029 /2010TC002826

McPhie, J., Doyle, M., Allen, R., 1993. Volcanic Textures – A guide to the interpretation of textures in volcanic rocks. First ed., Centre for Ore Deposit and Exploration Studies, University of Tasmania.

Middlemost, E. A. 1994. Naming materials in the magma/igneous rock system. Earth-Science Reviews, 37 (3-4), 215-224.

Mpodozis, C., Alvarez, P., Elgueta, S., Mella, P., Hervé, F., and Fanning, M., 2007. Revised Cretaceous stratigraphy of the Magallanes foreland basin at Seno Skyring: Regional implications of new SHRIMP age data on detrital zircon populations. In GEOSUR 2007 International Congress on the Geology and Geophysics of the Southern Hemisphere: Santiago, Chile, Pontificia Universidad Católica de Chile, abstract (p. 106).

Nakamura, N. 1974. Determination of REE, Ba, Fe, Mg, Na and K in carbonaceous and ordinary chondrites. Geochimica et Cosmochimica Acta, 38(5), 757-775.

Nelson, E.P., Dalziel, I.W.D., and Milnes, A.G., 1980. Structural geology of the Cordillera Darwin; collisional style orogenesis in the southernmost Chilean Andes. Eclogae Geologie Helvetica, 73 (3), 727–751.

Pankhurst, R.J., Riley, T.R., Fanning, C.M., Kelley, S.P., 2000. Episodic silicic volcanism in Patagonia and the Antarctic Peninsula: Chronology of magmatism associated with the break-up of Gondwana. Journal of Petrology, 41, 605–625. doi.org/10.1093/petrology/41.5.605

Passchier, C. W., Trouw, R. A. J., 2005. *Microtectonics*. Second ed., Springer, New York.

Pearce, G. W., Strangway, D. W., Gose, W. A. 1974. Magnetic properties of Apollo samples and implications for regolith formation. In Lunar and Planetary Science Conference Proceedings (Vol. 5, pp. 2815-2826).

Pearce, J. A. 1982. Trace element characteristics of lavas from destructive plate boundaries. Andesites, 8, 525-548.

Pearce, J. A. 2008. Geochemical fingerprinting of oceanic basalts with applications to ophiolite classification and the search for Archean oceanic crust. Lithos, 100(1-4), 14-48.

Pearce, T. H., Gorman, B. E., Birkett, T. C. 1977. The relationship between major element chemistry and tectonic environment of basic and intermediate volcanic rocks. Earth and Planetary Science Letters, 36(1), 121-132.]

Ramos, V.A., 1989. Andean Foothills structures in northern Magallanes Basin, Argentina. American Association of Petroleum Geologists Bulletin, 73 (7): 887–903.

Ramsay, J. G., 1980. Shear zone geometry: a review. Journal of structural geology, 2 (1-2), 83–99.

Ramsay, J.G., Graham, R.H., 1970. Strain variation in shear belts. Canadian Journal of Earth Sciences, 7, 786–813.

Rapalini, A.E., Calderón, M., Singer, S., Hervé, F., Cordani, U., 2008. Tectonic implications of a paleomagnetic study of the Sarmiento Ophiolitic Complex, southern Chile. Tectonophysics 452, 29–41. doi.org/10.1016/j.tecto.2008.01.005

Rollinson, H., 1993. Using Geochemical Data: Evaluation, Presentation, Interpretation. First ed., Pearson Education Limited, London.

Romans, B.W., Fildani, A., Hubbard, S.M., Covault, J.A., Fosdick, J.C., Graham, S.A., 2011. Evolution of deep-water stratigraphic architecture, Magallanes Basin, Chile. Mar. Pet. Geol. 28, 612–628. doi.org/10.1016/j.marpetgeo.2010.05.002

Schandl, E. S., Gorton, M. P. 2002. Application of high field strength elements to discriminate tectonic settings in VMS environments. Economic geology, 97(3), 629-642.

Schellart, W.P., Lister, G.S., 2005. The role of the East Asian active margin in widespread extensional and strike-slip deformation in East Asia. J. Geol. Soc. London. 162, 959–972. https://doi.org/10.1144/0016-764904-112

SERNAGEOMIN, 2003. Mapa Geológico de Chile: digital version. Geological Base scale 1:1.000.000. Chile Government, Servicio Nacional de Geología y Minería.

Sibson, R. H., 1977. Fault rocks and fault mechanisms. Journal of the Geological Society, 133(3), 191–213.

Simpson, C., De Paor, D. G., 1993. Strain and kinematic analysis in general shear zones. Journal of Structural Geology, 15(1), 1–20.

Stern, C.R., De Wit, M.J., 2003. Rocas Verdes ophiolites, southernmost South America: remnants of progressive stages of development of oceanic-type crust in a continental margin back-arc basin. Geol. Soc. London, Spec. Publ. 218, 665–683. https://doi.org/10.1144/GSL.SP.2003.218.01.32

Stern, C.R., de Wit, M.J., Lawrence, J.R., 1976. Igneous and metamorphic processes associated with the formation of Chilean ophiolites and their implications for ocean floor metamorphism, seismic layering, and magnetism. Journal of Geophysical Research 81 (23), 4370–4380.

Stewart, J., Cruzat, A., Page, B., Suárez, M., Stambuk, V., 1971. Estudio geológico economico de la Cordillera Patagónica entre los paralelos 51º00' y 53º30' Lat. S, Provincia de Magallanes. Instituto de Investigación Geológica, unpublished, 174 p.

Sun, S. S., McDonough, W. F. 1989. Chemical and isotopic systematics of oceanic basalts: implications for mantle composition and processes. Geological Society, London, Special Publications, 42(1), 313-345.

Tera, F., Wasserburg, G., 1972. U-Th-Pb systematics in three Apollo 14 basalts and the problem of initial Pb in lunar rocks. Earth and Planetary Science Letters 14, 281–304.

Thomson, S.N., Hervé, F., Fanning, C.M., 2000. Combining fission-track and U–Pb SHRIMP zircon ages to establish stratigraphic and metamorphic ages in basement sedimentary rocks in southern Chile. Resumenes Expandidos, IX Congreso Geológico Chileno, 2, 769–773.

Tullis, J., Snoke, A.W., Todd, V.R., 1982. Significance and petrogenesis of mylonitic rocks. Geology, 10, 227–230.

Van Staal, C. R., Rogers, N., Taylor, B. E., 2001. Formation of low-temperature mylonites and phyllonites by alkali-metasomatic weakening of felsic volcanic rocks during progressive, subduction-related deformation. Journal of Structural Geology, 23(6-7), 903–921.

Wakabayashi, J., Dilek, Y., 2003. What constitutes 'emplacement' of an ophiolite?: Mechanism and relationship to subduction initiation and formation of metamorphic soles. In: Dilek, Y., Robinson, P.T. (Eds.), Ophiolites in Earth History: Geological Society, London, Special Publications, 218, pp. 427–447.

Will, T.M., 1998. Phase Diagrams and their Application to Determine Pressure-Temperature Paths of Metamorphic Rocks. Neues Jahrb. für Mineral. - Abhandlungen 103–130. doi.org/10.1127/njma/174/1998/103

Williams, I.S., 1998. U-Th-Pb geochronology by ion microprobe. In: McKibben, M.A., Shanks III, W.C., Ridley, W.I. (Eds.), Applications of Microanalytical Techniques to Understanding Mineralizing Processes: Reviews in Economic Geology, 107, 1–35.

Wilson, T.J., 1991. Transition from back-arc to foreland basin development in southernmost Andes: Stratigraphic record from the Ultima Esperanza District, Chile. Geological Society of America Bulletin 103, 98–1

Winchester, J. A., Floyd, P. A. 1977. Geochemical discrimination of different magma series and their differentiation products using immobile elements. Chemical geology, 20, 325-343.